Inorganic Chemistry

pubs.acs.org/IC Article

Separation of ^{44m}Sc/^{44g}Sc Nuclear Isomers Based on After-Effects

Elena Sergeevna Kurakina,* Luke Wharton, Jurabek Khushvaktov, Eldar Parpachevich Magomedbekov, Valery Radchenko, and Dmitry Filosofov

Cite This: https://doi.org/10.1021/acs.inorgchem.3c01495 Read Online

ACCESS | Metrics & More | Article Recommendations

ABSTRACT: ^{44g}Sc presents a particular interest for application in nuclear medicine for positron emission tomography (PET) due to its favorable nuclear decay properties ($t_{1/2}$ = 3.97 h, E_{max} = 1.47 MeV, branching ratio 94.3% β^+). Its nuclear isomer ^{44m}Sc ($t_{1/2}$ = 58.61 h) decays by isomeric transition (IT) into ^{44g}Sc, accompanied by ≈12% of conversion electron emission, which can cause a partial release of the daughter ^{44g}Sc from the chelate complex. A 13 MeV cyclotron at TRIUMF was used to produce both ^{44m}Sc and ^{44g}Sc via the ^{nat}Ca(p,n)^{44m,g}Sc reaction. A ^{44m}Sc/^{44g}Sc generator was designed by using a Strata C-18E cartridge. After several tested systems, a successful separation method was developed using DOTATOC as a chelator, a Strata C-18E cartridge as a generator column, and an elution solution of 0.1 M NH_4-α-HIB. The yield of the generator with the daughter ^{44g}Sc release was equal to 9.8 ± 1.0% (or ≈80% per portion of conversion). This result shows the important role of after-effects in the design of radionuclide generators. Nuclear cross-section calculations were applied using the TALYS code to allow for the determination of the most promising alternative routes for ^{44m}Sc production, which will enable the development of a full-scale ^{44m}Sc/^{44g}Sc radionuclide generator based on after-effects.

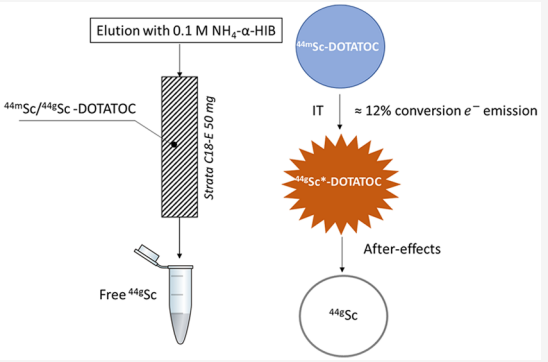

INTRODUCTION

The separation of isomeric pairs has been studied since the late 1930s. Among the first isotopes under investigation were ^{127m}Te, ^{129m}Te, and ^{80m}Br isomers.[1−3] Later, in the 1950s, the chemical separation of nuclear isomers (e.g., ^{58m}Co, ^{104m}Rh, and ^{114m}In) involved organic molecules, including chelating agents.[4−6] However, these works were mostly aimed at qualitative detection and the prospect of isomeric separation rather than quantitative evaluation. Indeed, the after-effects of radioactive decay were the main principle for the separation, or more precisely the emission, of conversion electrons, which create a vacancy in the inner shells (K, L) followed by the Auger process and other relaxation processes. The chemical separation scheme for the aforementioned elements was mainly based on covalent compounds formed with organic molecules or basic chelators. After-effects typically lead to bond rupture and the formation of new forms of the daughter radionuclide, which are then separated from the organic molecule of the parent radionuclide with negligible retention of the daughter.

Later studies involving macrocyclic chelators (e.g., 1,4,7,10-tetraazacyclododecane-1,4,7,10-tetraacetic acid (DOTA)) which exhibit slow reaction kinetics allowed for the separation of most metal ions.[7−9] It should be noted that such separations were carried out for acyclic chelators (e.g., DTPA) earlier as well; however, their kinetics are not as slow as for macrocyclic chelators, therefore leading to difficulties in the separation (except the radionuclides with short half-lives of less than 1 min). Based on the principle of after-effects and DOTA-based chemical separations, the following generators were recently designed: the ^{177m}Lu(IT)/^{177g}Lu isomeric pair[10,11] and the ^{140}Nd(EC)/^{140}Pr pair.[12] In the latter case, a vacancy is created as a result of electron capture (EC).

It should be noted that a detailed mechanism (at the micro level) of the initial complex disintegration caused by after-effects is still unknown. Moreover, the literature data on the formation mechanisms of the stable form of the daughter radionuclide are quite lacking. The aforementioned design of the generators describes the distribution of the daughter radionuclide forms over different phases, which allows for the determination of only the macro parameters. However, by choosing the specific chemical form of the parent radionuclide and setting appropriate conditions according to the macro parameters, such processes can be investigated at the micro level (such as in refs 10−12).

Special Issue: Inorganic Chemistry of Radiopharmaceuticals

Received: May 8, 2023

Mossbauer spectroscopy is a useful technique for the investigation of the after-effects in a homogeneous solid-phase medium, while perturbed angular correlation (PAC) is suitable for liquid-phase studies.[13−15] The PAC technique measures the hyperfine interaction between the electric and magnetic moments of the nucleus and the external electric and magnetic fields at the nuclear site and is sensitive to the local environment of the probe nucleus.[15−17] However, these two methods allow for the study of "the fate" of the daughter radionuclide no earlier than 1 ns after radioactive decay, and the measured parameter is still a microparameter, although it has a statistic "detached" ensemble. These two methods can describe the distribution of the daughter radionuclides' forms after 1−10 ns after decay. After-decay processes cannot be investigated by these methods (the Auger process takes 10^{-14} to 10^{-15} s followed by other relaxation processes). However, the information can be extracted even after 1−10 ns after decay in a homogeneous medium, which is valuable for the comprehension of the appropriate models of after-effects at the micro level. Moreover, there are a few other methods that can be useful for the investigation of after-effects. For example, microdosimetry can be applied for the detection of a single- or double-strand breakage in DNA. A study was carried out using [^{125}I]-iododeoxyuridine with the Auger emitter ^{125}I (^{125}I-UdR).[18,19] However, on the micro level, these processes are only described by the appropriate distribution of the DNA breakage.

One of the main parameters which influences the after-relaxation processes after the Auger process is the number of emitted electrons in the cascade. Each of the shells involved in this process roughly duplicates the number of electrons in the cascade. Thus, the greater the *Z*-number of the element, the more significant the destruction in the local environment of the heavier element during the Auger process. Indeed, it is expected that in the case of heavy elements, such a destruction will lead to a rupture of the initial bonds. However, in the case of the elements with low *Z*-numbers, such as Sc, a different picture is observed. Studies by Huclier-Markai et al. demonstrated a relatively low percent of ^{44g}Sc daughter release in the ^{44m}Sc/^{44g}Sc system based on DOTA-[Tyr^3]-octreotate (DOTATATE)[20] and Strata-X. It should be noted that such generators are quite complex systems.[21] Thus, the breakthrough of the parent radionuclide should be negligible, and the transformation of the daughter radionuclide into its parent form should be avoided. Redistribution of the resulting metal complex and its components between different phases is difficult to control with regard to the kinetic parameters of the system. Not taking into account any of the parameters can lead to a wrong interpretation of the after-effect processes on the micro level.

A prototype of the ^{44m}Sc/^{44g}Sc radionuclide generator presented in this work is based on DOTA-[Tyr^3]-octreotide (DOTATOC). ^{44m}Sc ($t_{1/2}$ = 58.61 h) decays 1.20% by EC or β^+ into ^{44}Ca and 98.80% by isomeric transition (IT) into ^{44g}Sc (Figure 1), emitting a 271 keV γ ray accompanied by ≈12% of conversion electron emission, which can cause a partial release of the daughter ^{44g}Sc from the chelate complex. The percentage of electrons produced via IT per decay is given in Table 1. The conversion electrons emitted during the decay of ^{44m}Sc leave an opportunity for the design of a potential generator. Moreover, it is a crucial task for a clear understanding of the fundamental significance of after-effects and their role in the design of some radiopharmaceuticals (e.g., in Auger therapy or *in vivo* generators).

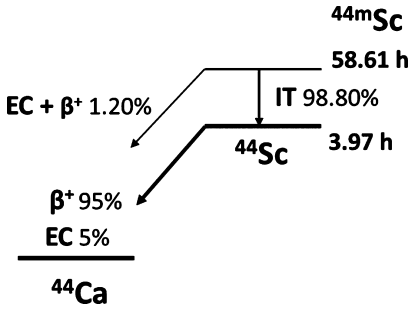

Figure 1. Decay scheme of ^{44m}Sc and ^{44g}Sc. During the ^{44m}Sc IT mode, 88% decays by γ ray emission and 12% by internal conversion.

Table 1. Percentages and Energies of the Conversion Electrons per Decay for ^{44m}Sc[a]

electrons	energy (keV)	intensity (%)
ce K	266.748(10)	10.84
ce L	270.741(10)	1.077
ce M	271.241(10)	0.131
ce N	271.241(10)	0.006

[a]The data indicate that 1.20% of ^{44m}Sc decays to ^{44}Ca. The data are extracted from the NuDat 3 database at Brookhaven National Laboratory.

EXPERIMENTAL SECTION

Chemical Reagents. All solvents and reagents were purchased from commercial suppliers (Sigma-Aldrich, Eichrom, ABX, etc.). Natural calcium turnings 99%, α-hydroxyisobutyric acid (α-HIBA), and the cation-exchange resin Dowex 50Wx8 (200−400 mesh) were purchased from Sigma-Aldrich. All solutions were prepared with 18.2 MΩ cm deionized water. DOTATOC and DOTATATE were purchased from ABX, and DOTA was purchased from Macrocyclics. Ammonium α-hydroxyisobutyrate (NH_4-α-HIB) was prepared by titration of α-HIBA with ammonium hydroxide (VWR) to pH = 4.8, controlled using a pH meter (Orion Star, Thermo Fisher Scientific). Strata-X and Strata C-18E cartridges were purchased from Phenomenex.

Activity Measurements. A Canberra γ spectrometer with a high-purity germanium (HPGe) detector and Genie-2000 software, calibrated with ^{133}Ba and ^{152}Eu at a specific geometry, was used to control the activity of ^{44m}Sc and ^{44g}Sc. The cartridge and appropriate elutions were measured at the same distance from the source. The dead time was kept below 7%. A Capintec (Ramsey, NJ) CRC-15R dose calibrator (setting 938) was used to control the purification process. Radiochemical yields (RCYs) were determined via instant thin-layer chromatography (iTLC) measurements using an AR-2000 TLC imaging scanner and subsequent analysis using WinScan V3_14 software.

Production of ^{44m}Sc and ^{44g}Sc. Irradiation of natural calcium with low-energy protons provides an opportunity to produce both ^{44g}Sc and ^{44m}Sc. ^{44m}Sc/^{44g}Sc was produced via a ^{nat}Ca(p,n)^{44m,g}Sc reaction using a 13 MeV TRIUMF cyclotron (1 h irradiation, current beam of 10 μA). The further radiochemical separation was carried out using a two-step scheme with DGA resin (branched, 50−100 μm) and HCl solutions for the first stage and cation-exchange resin (Dowex 50Wx8, 200−400 mesh) and an NH_4-α-HIB solution for the second stage. The process was described in detail in ref 22. An RCY of the separation scheme applied was 95 ± 3%, which allowed further radiolabeling and a design of the generator without undesirable impurities.

Radiolabeling. Stock solutions of DOTATATE (10^{-3} M) and DOTATOC (10^{-3} M) were prepared in deionized water and used

https://doi.org/10.1021/acs.inorgchem.3c01495
Inorg. Chem. XXXX, XXX, XXX−XXX

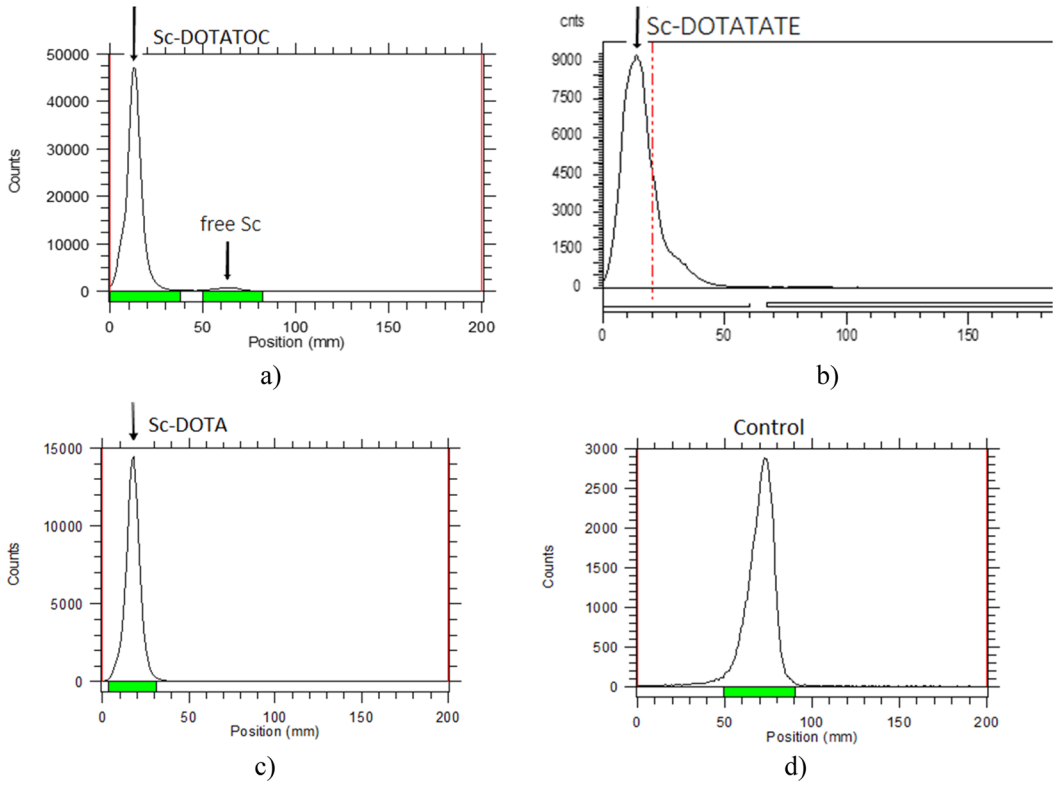

Figure 2. TLC chromatograms for ^{44m}Sc/^{44g}Sc with (a) DOTATOC, (b) DOTATATE, and (c) DOTA at a concentration of 10^{-4} M and a pH = 5 with a 0.1 M NH_4-α-HIB medium (t = 90 °C for 1 h). An internal control (d) without the addition of a chelator was tested under the same conditions.

directly for radiolabeling reactions. Radiolabeling studies were performed by the addition of a [^{44m}/^{44g}Sc]Sc^{3+} fraction (200 μL) to solutions of DOTATOC (25 μL, 25 nmol) or DOTATATE (25 μL, 25 nmol) in 0.1 M NH_4-α-HIB (pH = 4.8, 25 μL), for a total volume of 250 μL (≈450 kBq of ^{44m}Sc). Radiolabeling reactions were heated at 90 °C, and radiochemical yields (RCYs) were determined at 1 h via iTLC using Si on Al TLC plates (Agilent Technologies) and Na citrate (0.4 M, pH = 4.0) as the eluent. Under these conditions, ^{44m}Sc/^{44g}Sc-labeled DOTATOC/DOTATATE remains on the baseline (R_f = 0.0−0.1) while the free activity migrates with the solvent front (R_f = 0.9−1.0). Separate control reactions without any bioconjugate present were used to monitor the formation of any scandium hydroxo species, which would be observed at the baseline (R_f = 0) and were not observed under the reaction conditions tested.

Generator Development. The generator column (Strata-X or Strata C-18E) was preconditioned with EtOH and H_2O. Afterward, the reaction mixture containing ^{44m}Sc/^{44g}Sc-labeled DOTATOC/DOTATATE (RCY ≈ 98−100%) was loaded onto the generator column. The radiolabeled complex was retained on the column, while free [$^{44m/44g}$Sc]Sc^{3+} was eluted using a 0.1 M NH_4-α-HIB solution. The next day, after an equilibrium between ^{44m}Sc and ^{44g}Sc was achieved, the generator column was first analyzed via γ-spectrometry and then eluted with 0.1 M NH_4-α-HIB (1.5 mL) several times, and fractions were analyzed within 5 min at the same geometry as the generator column. The procedure was repeated daily until the generator activity was negligible. The elutions were performed with single-use syringes for ∼15 s, and the generator column was stored in an 0.1 M NH_4-α-HIB solution to prevent it from drying out.

Table 2. Yields of the Tested System with Strata-X (30 mg) and DOTATATE (10^{-4} M)

elution	^{44g}Sc yield (%)	^{44m}Sc breakthrough (%)
1	0.95	0.10
2	3.24	0.21
3	0.55	0.03
4	0.44	0.02

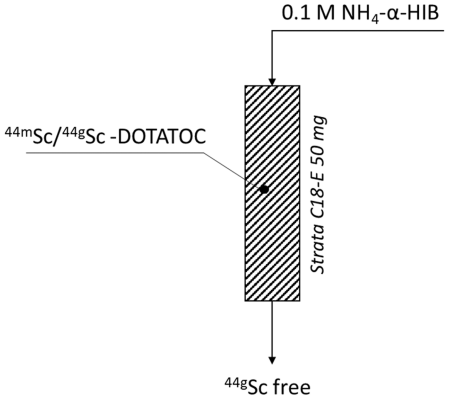

Figure 3. Scheme of the ^{44m}Sc/^{44g}Sc generator (DOTATOC (10^{-4} M) and Strata C-18E (50 mg)).

RESULTS AND DISCUSSION

Production of ^{44m}Sc and ^{44g}Sc. At the end of bombardment (EOB), 100 ± 7 MBq of ^{44g}Sc and 0.61 ± 0.07 MBq of ^{44m}Sc were produced. Despite the relatively low yield of the isomeric state of scandium, ∼500 kBq of ^{44m}Sc was produced at the end of separation (EOS), which was sufficient to design and test a ^{44m}Sc/^{44g}Sc generator.

Radiolabeling with ^{44m}Sc/^{44g}Sc. The final fraction of [$^{44m/44g}$Sc]Sc^{3+} (∼450 kBq of ^{44m}Sc and ∼60 MBq of ^{44g}Sc) at EOS was used for radiolabeling with DOTATOC (2.5 nmol, 10^{-4} M) or DOTATATE (2.5 nmol, 10^{-4} M) at pH = 5 (0.1

https://doi.org/10.1021/acs.inorgchem.3c01495
Inorg. Chem. XXXX, XXX, XXX−XXX

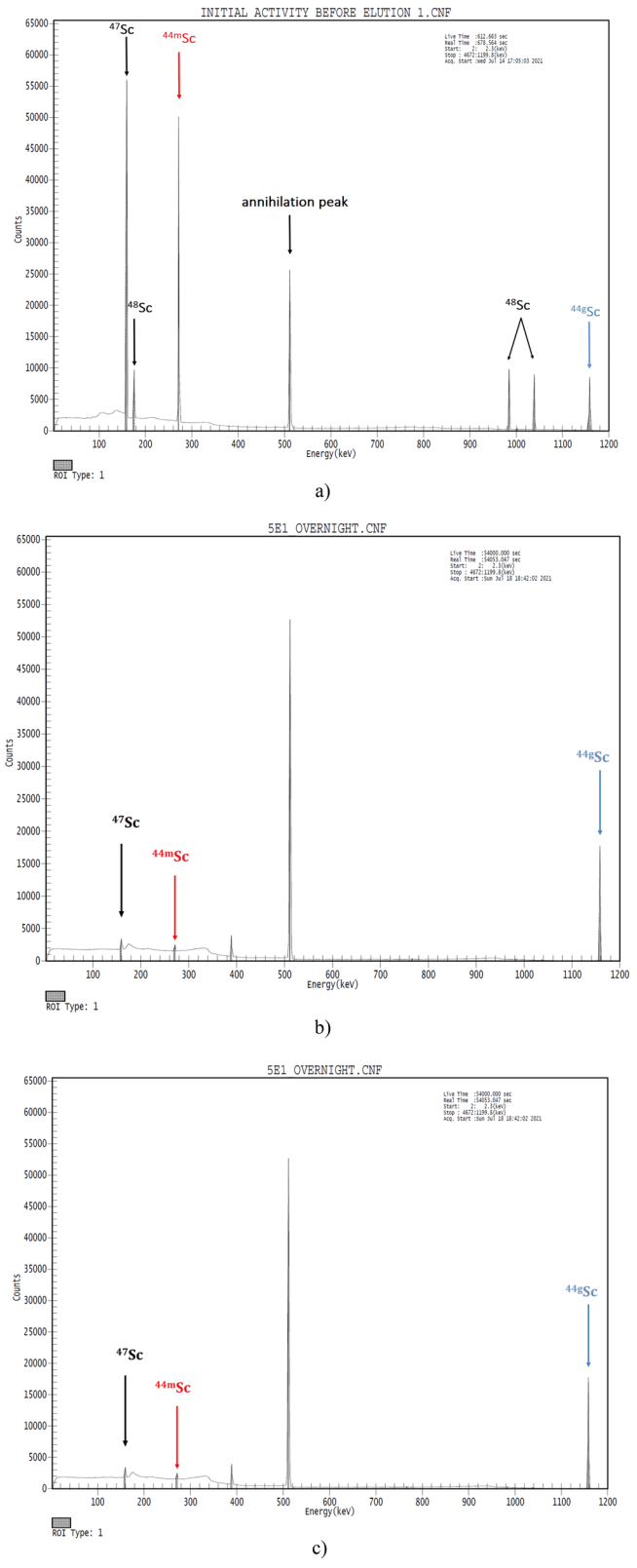

Figure 4. γ spectra of (a) the cartridge, (b) the first elution with 0.1 NH_4-α-HIB, and (c) the last/fifth elution. 1157 and 271 keV peaks stand for the ^{44g}Sc and ^{44m}Sc γ lines, respectively, and the other peaks are attributed to co-produced ^{47}Sc and ^{48}Sc γ lines. The peak at 389 keV corresponds to co-produced ^{87}Y/^{87m}Sr, which is likely associated with Sr impurity in the target material.

Table 3. Yields of ^{44g}Sc from the ^{44m}Sc/^{44g}Sc Generator System (with 10^{-4} M DOTATOC and a Strata C-18E Cartridge) and the Breakthrough of ^{44m}Sc (n = 3)[a]

elution	^{44g}Sc yield (%)	^{44m}Sc breakthrough (%)
1	10.5	3.0
2	10.5	0.5
3	9.7	0.15
4	9.3	0.2
5	8.8	0.03

[a]The generator was eluted with 0.1 M NH_4-α-HIB (V = 5 mL) each day.

M NH_4-α-HIB) for 1 h at 90 °C. Reactions with the free chelate, DOTA (10^{-4} M), were also tested under the same conditions as an internal control. All TLC measurements were determined directly following each radiolabeling reaction, since a short delay time would allow for decay and the release of free ^{44g}Sc. Quantitative radiochemical yields for [$^{44m/44g}$Sc]Sc-DOTATATE and [$^{44m/44g}$Sc]Sc-DOTA were achieved, while reactions involving [$^{44m/44g}$Sc]Sc-DOTATOC were ~98% (Figure 2).

Initial Design of the ^{44m}Sc/^{44g}Sc Generator. First, the following system was investigated: Strata-X (30 mg) with DOTATATE (2.5 nmol, 10^{-4} M). The Strata-X cartridge (preconditioned with EtOH and H_2O) was washed with H_2O and eluted using DTPA (10^{-5} M) daily. However, in this case, a release of the daughter ^{44g}Sc was no greater than 3%, with less than 1% of the breakthrough of ^{44m}Sc (Table 2).

This system did not work as a generator, since the release of the daughter was very low and not constant with every elution. The same result was achieved in the work by Huclier-Markai et al.[20]

A second generator system using cation-exchange resin (Dowex 50Wx8, 200−400 mesh, 200 mg) and DOTATOC (2.5 nmol, 10^{-4} M) was tested. Potentially, this could be a more accessible system for the design of this radionuclide generator; however, in this case, a high breakthrough of ^{44m}Sc was observed (up to 3%).

The aforementioned results showed that a more efficient system still needs to be found.

Design of the ^{44m}Sc/^{44g}Sc Generator. The reaction of ^{44m}Sc/^{44g}Sc with DOTATOC (2.5 nmol, 10^{-4} M) was loaded onto a 50 mg Strata C-18E column (preconditioned with EtOH and H_2O) and eluted with 0.1 M NH_4-α-HIB (~5 mL) to ensure free [$^{44m/44g}$Sc]Sc^{3+} was washed from the column. Afterward, the column was successively eluted with 0.1 M NH_4-α-HIB (3−4 elutions of 1.5 mL) daily until the radionuclide generator reached a negligible activity (Figure 3). The activity of the cartridge before elution, the collected eluent, and the breakthrough of ^{44g}Sc were monitored via γ spectroscopy. The γ spectra of the initial cartridge and the first and fifth elutions are depicted in Figure 4. The yields obtained from the ^{44m}Sc/^{44g}Sc generator and the breakthrough are shown in Table 3. The uncertainty was below 5%, and the average yield of ^{44g}Sc was equal to 9.8%. In Table 3, the breakthrough of ^{44m}Sc reaches ~3% in the first elution, which is likely caused by the residual DOTATOC complex being released, including the presence of colloidal particles in the system. Nevertheless, the breakthrough in each subsequent elution is much lower and reaches 0.03% at the fifth elution.

As already noted, the influence of after-effects on the stability of the chelate complexes is dependent on the Z-

https://doi.org/10.1021/acs.inorgchem.3c01495
Inorg. Chem. XXXX, XXX, XXX−XXX

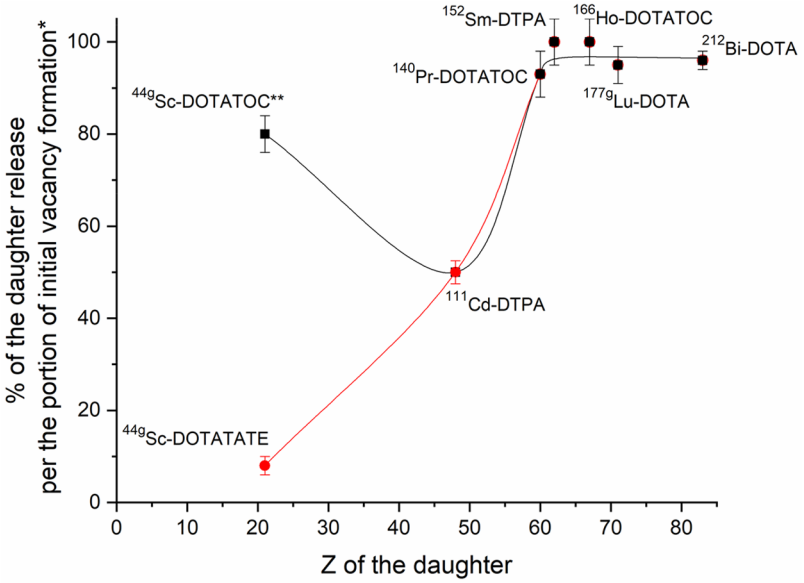

Figure 5. The trend of the percent of the daughter release (*per the portion of conversion, in the cases of IT and β decay, or per the portion of EC) depending on the *Z*-number of the daughter for ^{212}Bi,[23] ^{177g}Lu,[10] ^{152}Sm,[15] ^{166}Ho,[26] ^{140}Pr,[12] ^{111}Cd,[13−15] and ^{44g}Sc. The black curve includes the data on ^{44g}Sc-DOTATOC shown in this work, and the red curve includes the data on ^{44g}Sc-DOTATATE reported by Huclier-Markai et al.,[20] which are in agreement with our data. **Refers to the present work.

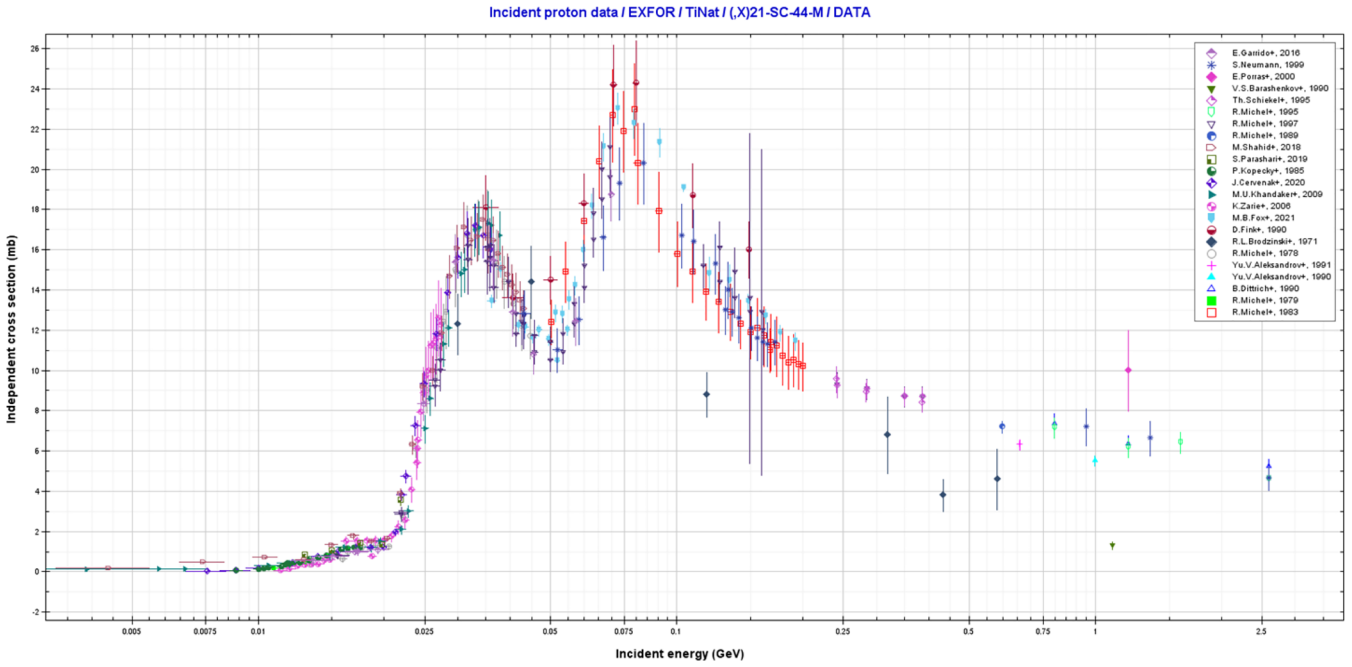

Figure 6. Cross-section (mb) dependence on the incident energy of protons (GeV) via the ^{nat}Ti(p,2pxn)^{44m}Sc reaction.

number of the daughter radionuclide (Figure 5). In the case of [^{212}Pb]Pb-DOTA, a full release (with respect to the portion of internal conversion) of its daughter ^{212}Bi was reported.[23] The authors gave a number of 36 ± 2% for the ^{212}Bi release, while the total conversion was 37.3%. The same case was recorded for [^{152}Eu]Eu-DTPA investigated by PAC; its daughter ^{152}Sm was fully released from the initial complex.[15] Bhardwaj et al. reported the design of a ^{177m}Lu/^{177g}Lu radionuclide generator based on after-effects,[10,24] with a yield of 95 ± 4%.[10] A similar case was noted with the ^{140}Nd/^{140}Pr pair, whereby the daughter ^{140}Pr was released from the initial complex with DOTATOC with a 93 ± 5% release.[12] By contrast, a study on ^{111}In (EC, 100%) complexes with DTPA by PAC showed that only a partial release of its daughter ^{111}Cd is observed, and ≈50% of the complexes remained stable.[13,14] The results of this study are a valuable supplement to the general trend where ^{44g}Sc has the lowest *Z*-number among the aforementioned radionuclides. Previously reported data on [$^{44m/44g}$Sc]Sc-DOTATATE showed a 1% yield for daughter release (≈8% per portion of conversion), which is in agreement with our data when DOTATATE and Strata-X were applied. More likely, the difference in yields of the generator between [$^{44m/44g}$Sc]Sc-DOTATOC and [$^{44m/44g}$Sc]Sc-DOTATATE (Figure 5) is related to the choice of the generator column.

https://doi.org/10.1021/acs.inorgchem.3c01495
Inorg. Chem. XXXX, XXX, XXX−XXX

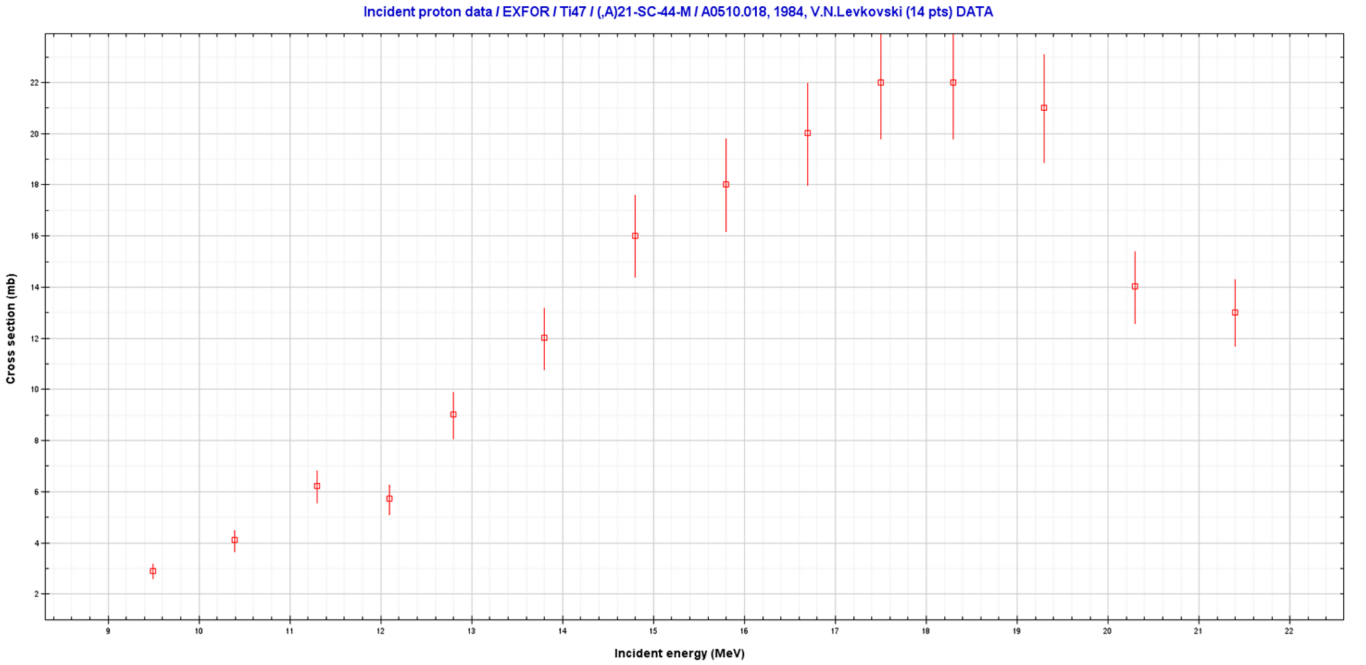

Figure 7. Cross-section (mb) dependence on the incident energy of protons (MeV) via the ^{47}Ti(p,α)^{44m}Sc reaction.

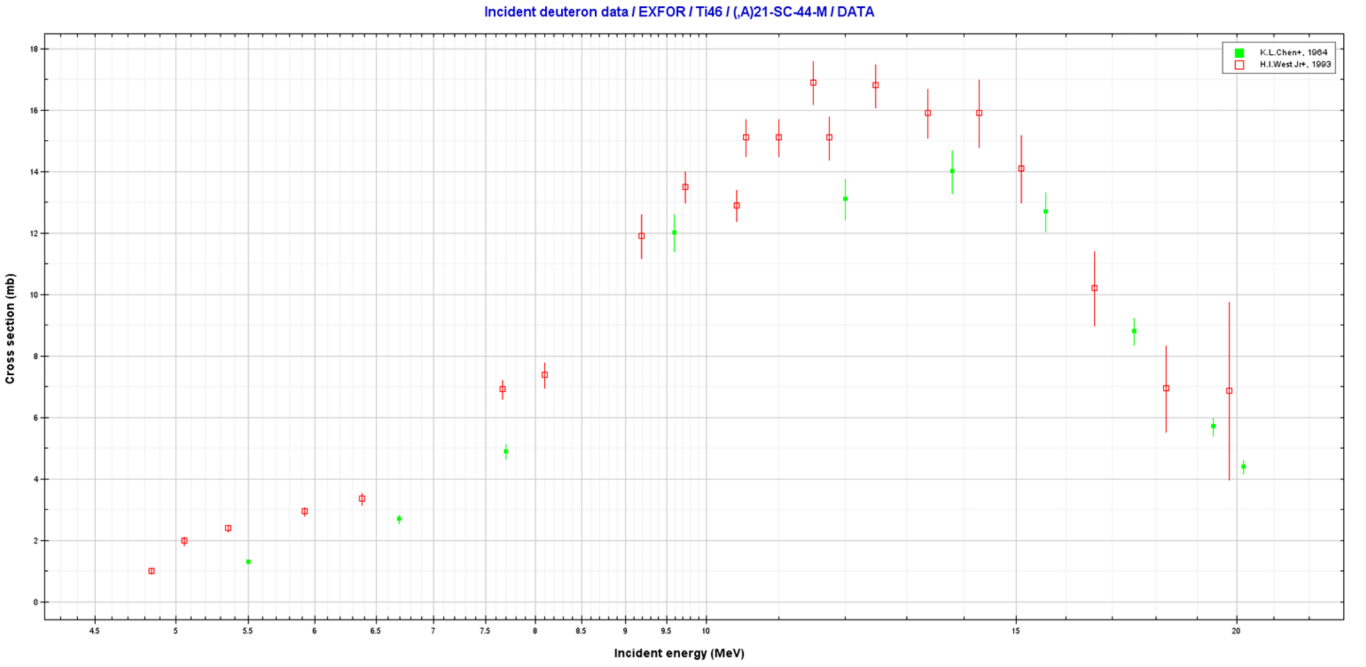

Figure 8. Cross-section (mb) dependence on the incident energy of deutrons (MeV) via the ^{46}Ti(d,α)^{44m}Sc reaction.

It is interesting to mention that the general trend in the percentage of daughter release would be expected to increase with increasing Z due to the additional number of Auger electrons produced with a higher Z,[25] which is shown by the red curve (Figure 5). However, the results of the present study with [$^{44m/44g}$Sc]Sc-DOTATOC suggest that chemical effects and the lifetime of the excited state may have a more significant influence on the initial complex disintegration (black curve in Figure 5).

Alternative Production Routes for ^{44m}Sc. The present study showed the concept for ^{44g}Sc and ^{44m}Sc nuclear isomers separation. However, the ^{44m}Sc production yield is low and equal to 0.06 MBq/μAh, which leaves the practical applicability in question. Therefore, more promising production routes should be considered. We propose that the most attractive production routes are the following: ^{nat}Ti(p,2pxn)^{44m}Sc, Ti(p,α)^{44m}Sc, ^{46}Ti(d,α)^{44m}Sc, ^{42}Ca(α,pn)^{44m}Sc, and ^{41}K(α,n)^{44m}Sc. The cross sections for each reaction are depicted in Figures 6, 7, 8, 9, and 10, respectively, using the TALYS code.[27] Theoretical data on production yields for the aforementioned reactions as well as experimentally determined production yields for ^{42}Ca(α,pn)^{44m}Sc, ^{nat}K(α,n)^{44m}Sc, and ^{44}Ca(d,2n)^{44m}Sc are shown in Table 4.

https://doi.org/10.1021/acs.inorgchem.3c01495
Inorg. Chem. XXXX, XXX, XXX−XXX

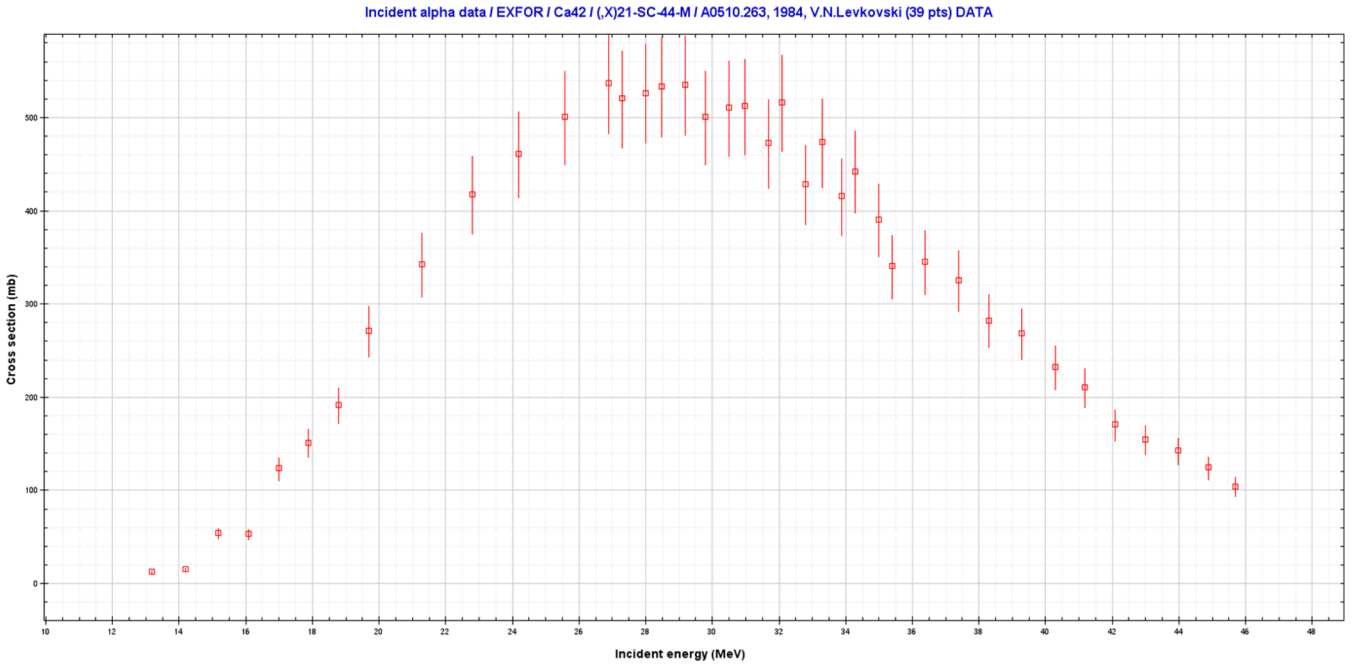

Figure 9. Cross-section (mb) dependence on the incident energy of α-particles (MeV) via the ^{42}Ca(α,pn)^{44m}Sc reaction.

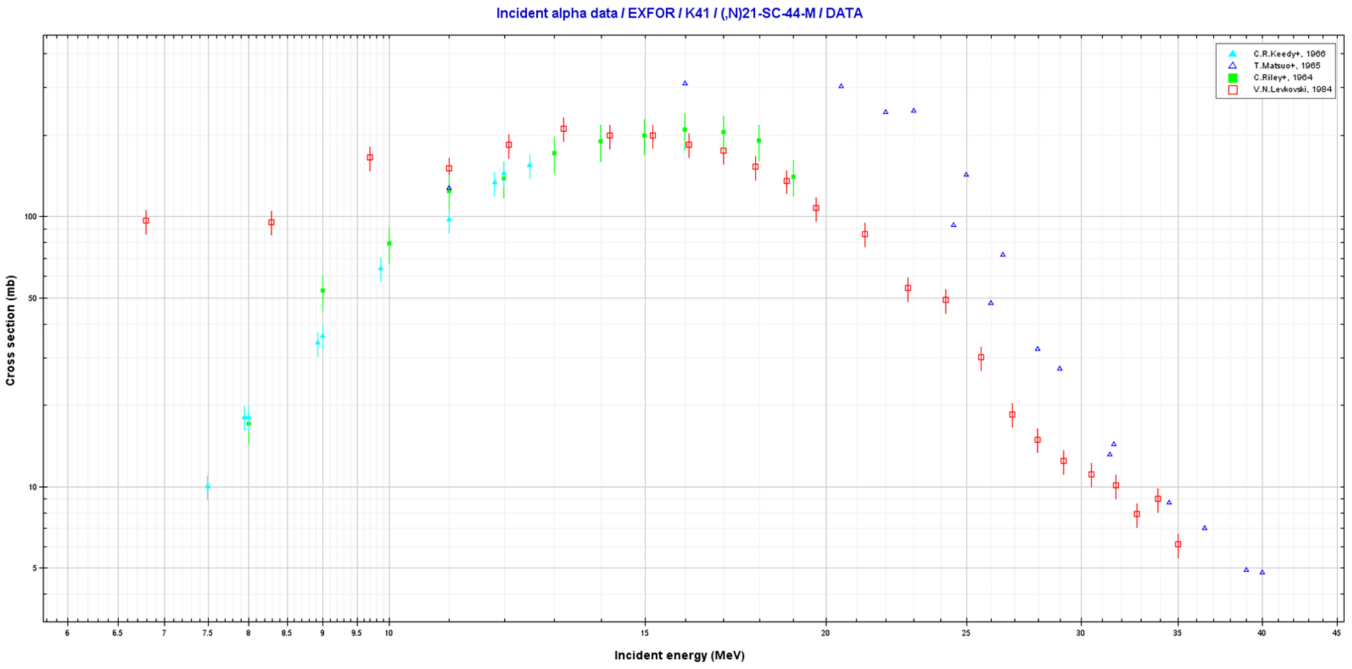

Figure 10. Cross-section (mb) dependence on the incident energy of α-particles (MeV) via the ^{41}K(α,n)^{44m}Sc reaction.

According to Table 4, the most promising reactions are 1, 4 (6), and 8 due to the high production yields. The reactions using enriched targets (2−8) provide higher radionuclidic purity. In these cases, the main contaminants are ^{43}Sc ($t_{1/2}$ = 3.89 h) and excess ^{44g}Sc, which would fully decay within 2 days. It should be mentioned that in reactions 2 and 3, the long-lived ^{46}Sc ($t_{1/2}$ = 83.81 d) is produced, whereas in reactions 4−8, the produced ^{46}Sc is negligible. In the case of reactions 5 and 7, the production yields of the desired ^{44m}Sc are relatively low, which leaves these routes unsuitable for route production. The ^{nat}Ti(p,2pxn)^{44m}Sc in reaction 1 enables the highest production yield among the proposed reactions, which along with the use of a natural target and 70 MeV protons, makes this route attractive. However, in this case, the main contaminant is ^{47}Sc, which has a production yield higher than that of ^{44m}Sc and ^{46}Sc (10% at EOB). Nevertheless, taking into account the cost-effectiveness of the target material, the high production yield, and the relatively soft γ line of ^{47}Sc (150 keV), this route can find applicability in a preclinical setting.

CONCLUSION

After numerous attempts to separate the ^{44m}Sc/^{44g}Sc nuclear isomers based on after-effects, a system consisting of Strata C-18E and DOTATOC resulted in the most effective approach to designing the ^{44m}Sc/^{44g}Sc radionuclide generator. A yield of

https://doi.org/10.1021/acs.inorgchem.3c01495
Inorg. Chem. XXXX, XXX, XXX−XXX

Table 4. Calculated Production Yields (MBq/μAh) per 1 h for the Alternative Routes for ^{44m}Sc[a]

	no.[b]	reaction	incident energy (MeV)	thickness of the target (mg/cm^2)	exit energy (MeV)	production yield (MBq/μAh)
theoretical data	1	^{nat}Ti(p,2pxn)^{44m}Sc	70	5000	25	52
	2	^{47}Ti(p,α)^{44m}Sc	30	1200	7	5.4
	3	^{46}Ti(d,α)^{44m}Sc	16	200	6	2.4
	4	^{42}Ca(α,pn)^{44m}Sc	40	160	12	18
	5	^{41}K(α,n)^{44m}Sc	40	170	9	2.8
experimental data	6	^{42}Ca(α,pn)^{44m}Sc	29	n/a[c]	12	3.3[29]
	7	^{nat}K(α,n)^{44m}Sc	20	n/a[c]	2	0.21[29]
	8	^{44}Ca(d,2n)^{44m}Sc	14.92	800[d]	-	11[30]

[a]The yields were estimated via the IAEA Medical Isotope Browser for the thick targets.[28] Data on reactions 6−8 refer to the experimental studies.[29,30] [b]The data for reactions 1−5 consider the metallic targets. Reactions 6−8 are using a 68% enriched $^{42}CaCO_3$ target, a natural KCl target, and a 96.9% enriched $^{44}CaCO_3$ target, respectively. [c]The authors do not present a precise thickness. For the enriched $^{42}CaCO_3$ target (reaction 6), the authors provide a thickness range of 40−70 mg/cm^2. [d]The authors present the thickness of the $^{44}CaCO_3$ target in μm.

9.8 ± 1.0% was achieved for ^{44g}Sc, which is close to a theoretical yield of ≈12%. The breakthrough of ^{44m}Sc decreased from 3% in the first elution to 0.03% in the final elution. This result not only showed the significant influence of the after-effects on the initial chelate complex stability but also is one of the only examples of the after-effects for radionuclides with low Z-numbers (Z < 48). Thus, ^{44g}Sc is a valuable data point in the overall trend of the influence of after-effects as it helps to evaluate the after-effects in the low Z-number range.

Moreover, the production of the parent ^{44m}Sc would be beneficial using other routes. For instance, ^{nat}Ti(p,2pxn)^{44m}Sc using 70 MeV protons, ^{42}Ca(α,pn)^{44m}Sc using a 40 MeV α-beam, and ^{44}Ca(d,2n)^{44m}Sc using 16 MeV deuterons seem the most promising. This would provide an opportunity for generator sources of ^{44g}Sc to enable transport and kit-labeling synthesis in a medical facility.

AUTHOR INFORMATION

Corresponding Author

Elena Sergeevna Kurakina − *Dzhelepov Laboratory of Nuclear Problems, Joint Institute for Nuclear Research, Dubna 141980, Russian Federation; Department of High-Energy Chemistry and Radioecology, D. Mendeleev University of Chemical Technology of Russia, Moscow 125047, Russian Federation;* orcid.org/0000-0001-5126-1663; Email: kurakina@jinr.ru

Authors

Luke Wharton − *Department of Chemistry, University of British Columbia, Vancouver, British Columbia V6T 1Z1, Canada;* orcid.org/0000-0002-0636-8741

Jurabek Khushvaktov − *Dzhelepov Laboratory of Nuclear Problems, Joint Institute for Nuclear Research, Dubna 141980, Russian Federation*

Eldar Parpachevich Magomedbekov − *Department of High-Energy Chemistry and Radioecology, D. Mendeleev University of Chemical Technology of Russia, Moscow 125047, Russian Federation*

Valery Radchenko − *Department of Chemistry, University of British Columbia, Vancouver, British Columbia V6T 1Z1, Canada*

Dmitry Filosofov − *Dzhelepov Laboratory of Nuclear Problems, Joint Institute for Nuclear Research, Dubna 141980, Russian Federation*

Complete contact information is available at: https://pubs.acs.org/10.1021/acs.inorgchem.3c01495

Notes

The authors declare no competing financial interest.

ACKNOWLEDGMENTS

We would like to thank the TR13 Cyclotron Operations Group, consisting of Toni Epp, Ryley Morgan, and Spencer Staiger and led by David Prevost, for regular irradiations of Ca targets. The authors gratefully acknowledge funding from the National Sciences and Engineering Research Council of Canada (NSERC) discovery programs [Grant RGPIN-2018-04997 (V.R.)]. TRIUMF receives federal funding via a contribution agreement with the National Research Council of Canada.

REFERENCES

(1) Seaborg, G. T.; Livingood, J. J.; Kennedy, J. W. Radioactive Tellurium: Further Production and Separation of Isomers. *J. Am. Phys. Soc.* **1939**, *55*, 794.

(2) Seaborg, G. T.; Kennedy, J. W. Nuclear Isomerism and Chemical Separation of Isomers in Tellurium. *J. Am. Phys. Soc.* **1939**, *55*, 410.

(3) DeVault Don, C.; Libby, W. F. Chemical Separation of Nuclear Isomers. *J. Am. Phys. Soc.* **1939**, *53* (2), 284.

(4) Hoffman, D. C.; Martin, D. S. *Hot Atom Chemistry. Photonuclear Preparation of Cobalt-58, Cobalt-58m* **1952**, *56*, 1097.

(5) Jacobi, E. Der Mechanismus Der Atomisomerentrennung Im Elektrischen Feld Beim 114In. *Helv. Chim. Acta* **1952**, *35* (3), 1480−1495.

(6) Herr, W. Eine Neue Methode Zur Chemischen Trennung von Kernisomeren Mit Cyclischen Komplexverbindungen. *Z. Naturforsch.* **1954**, *9*, 180−181.

(7) Ramogida, C. F.; Orvig, C. Tumour Targeting with Radiometals for Diagnosis and Therapy. *Chem. Commun.* **2013**, *49* (42), 4720−4739.

(8) Price, E. W.; Orvig, C. Matching Chelators to Radiometals for Radiopharmaceuticals. *Chem. Soc. Rev.* **2014**, *43* (1), 260−290.

(9) Stetter, H.; Frank, W. Complex Formation with Tetraazacycloalkane-N, N',N",N"'-Tetraacetic Acids as a Function of Ring Size. *Angew. Chem., Int. Ed. Engl.* **1976**, *15* (11), 686.

(10) Bhardwaj, R.; Wolterbeek, H. T.; Denkova, A. G.; Serra-Crespo, P. Radionuclide Generator-Based Production of Therapeutic 177Lu from Its Long-Lived Isomer 177mLu. *EJNMMI Radiopharm Chem.* **2019**, *4* (1), n/a DOI: 10.1186/s41181-019-0064-5.

(11) Bhardwaj, R.; Wolterbeek, H. T.; Denkova, A. G.; Serra-Crespo, P. Radionuclide Generator-Based Production of Therapeutic 177Lu from Its Long-Lived Isomer 177mLu. *EJNMMI Radiopharm Chem.* **2019**, *4* (1), n/a DOI: 10.1186/s41181-019-0064-5.

(12) Zhernosekov, K. P.; Filosofov, D. V.; Qaim, S. M.; Rosch, F. A 140Nd/140Pr Radionuclide Generator Based on Physico-Chemical

https://doi.org/10.1021/acs.inorgchem.3c01495
Inorg. Chem. XXXX, XXX, XXX−XXX

Transitions in 140Pr Complexes after Electron Capture Decay of 140Nd-DOTA. *Radiochim. Acta* **2007**, *95* (6), 319−327.
(13) Shpinkova, L. G.; Kulakov, V. N.; Sorokin, A. A.; Ryasny, G. K.; Komissarova, B. A.; Nikitin, S. M. Stability of 111In-Ligand Complexes Studied by TDPAC *. *Z. Naturforsch.* **1998**, *53*, 630−635.
(14) Shpinkova, L. G.; Carbonari, A. W.; Nikitin, S. M.; Mestnik-filho, J. Influence of Electron Capture After-Effects on the Stability of 111 In (111 Cd) -Complexes with Organic Ligands. *Chem. Phys.* **2002**, *279*, 255−263.
(15) Kurakina, E. S.; Radchenko, V.; Belozub, A. N.; Bonchev, G.; Bozhikov, G. A.; Velichkov, A. I.; Stachura, M.; Karaivanov, D. V.; Magomedbekov, E. P.; Filosofov, D. V. Perturbed Angular Correlation as a Tool to Study Precursors for Radiopharmaceuticals. *Inorg. Chem.* **2020**, *59* (17), 12209−12217.
(16) Hemmingsen, L.; Butz, T. Perturbed Angular Correlations of γ-Rays (PAC) Spectroscopy. *Encyclopedia of Inorganic and Bioinorganic Chemistry* **2011**, 1−15.
(17) Chakraborty, S.; Pallada, S.; Pedersen, J. T.; Jancso, A.; Correia, J. G.; Hemmingsen, L. Nanosecond Dynamics at Protein Metal Sites: An Application of Perturbed Angular Correlation (PAC) of γ - Rays Spectroscopy. *Acc. Chem. Res.* **2017**, *50*, 2225−2232.
(18) Kassis, A. I.; Walicka, M. A. Double-Strand Break Yield Following ^{125}I Decay: Effects of DNA Conformation. *Acta Oncologica* **2000**, *39*, 721−726.
(19) Hofer, K. G.; Bao, S.-P. Low-LET and High-LET Radiation Action of 125 I Decays in DNA: Effect of Cysteamine on Micronucleus Formation and Cell Killing Low-LET and High-LET Radiation Action of 1251 Decays in DNA: Effect of Cysteamine on Micronucleus Formation and Cell Killing. *Radiation Research* **1995**, *141*, 183.
(20) Huclier-Markai, S.; Kerdjoudj, R.; Alliot, C.; Bonraisin, A. C.; Michel, N.; Haddad, F.; Barbet, J. Optimization of Reaction Conditions for the Radiolabeling of DOTA and DOTA-Peptide with 44m/44Sc and Experimental Evidence of the Feasibility of an in Vivo PET Generator. *Nucl. Med. Biol.* **2014**, *41* (S), e36−e43.
(21) Rosch, F.; Knapp, F. F. 40 Radionuclide Generators. In *Handbook of Nuclear Chemistry*; Springer Science + Business Media B.V., 2011; pp 1936−1967 DOI: 10.1007/978-1-4419-0720-2.
(22) Kurakina, E. S.; Wharton, L.; Hoehr, C.; Orvig, C.; Magomedbekov, E. P.; Filosofov, D.; Radchenko, V. Improved Separation Scheme for 44Sc Produced by Irradiation of NatCa Targets with 12.8 MeV Protons. *Nucl. Med. Biol.* **2022**, *104−105*, 22−27.
(23) Mirzadeh, B. S.; Kumar, K.; Gansow, O. A. The Chemical Fate of 212 Bi-DOTA Formed by β^- Decay of 212 Pb (DOTA)2-. *Radiochim. Acta* **1993**, *60*, 1−10.
(24) Bhardwaj, R.; Van Der Meer, A.; Das, S. K.; De Bruin, M.; Gascon, J.; Wolterbeek, H. T.; Denkova, A. G.; Serra-Crespo, P. Separation of Nuclear Isomers for Cancer Therapeutic Radionuclides Based on Nuclear Decay After-Effects. *Sci. Rep* **2017**, *7*, n/a DOI: 10.1038/srep44242.
(25) Filosofov, D.; Kurakina, E.; Radchenko, V. Potent Candidates for Targeted Auger Therapy: Production and Radiochemical Considerations. *Nucl. Med. Biol.* **2021**, *94−95*, 1−19.
(26) Zeevaart, J. R.; Szucs, Z.; Takacs, S.; Jarvis, N. V.; Jansen, D. Recoil and Conversion Electron Considerations of the 166Dy/166Ho in Vivo Generator. *Radiochim. Acta* **2012**, *100* (2), 109−113.
(27) Koning, A.; Hilaire, S.; Goriely, S. *TALYS-1.96/2.0 Simulation of Nuclear Reactions*; 2021. www.LaTeXTemplates.com.
(28) Koning, A.; Verpelli, M. The Medical Isotope Browser: An app for prediction of radioisotope production yields. In *Nuclear Data Section, IAEA, International Symposium on Trends in Radiopharmaceuticals #ISTR2019*. https://www-nds.iaea.org/relnsd/isotopia/isotopia.html.
(29) Szkliniarz, K.; Sitarz, M.; Walczak, R.; Jastrzębski, J.; Bilewicz, A.; Choiński, J.; Jakubowski, A.; Majkowska, A.; Stolarz, A.; Trzcińska, A.; Zipper, W. Production of Medical Sc Radioisotopes with an Alpha Particle Beam. *Applied Radiation and Isotopes* **2016**, *118*, 182−189.
(30) Alliot, C.; Kerdjoudj, R.; Michel, N.; Haddad, F.; Huclier-Markai, S. Cyclotron Production of High Purity 44m,44Sc with Deuterons from 44CaCO3 Targets. *Nucl. Med. Biol.* **2015**, *42* (6), 524−529.

https://doi.org/10.1021/acs.inorgchem.3c01495
Inorg. Chem. XXXX, XXX, XXX−XXX

Inorganic Chemistry

pubs.acs.org/IC

Article

Perturbed Angular Correlation as a Tool to Study Precursors for Radiopharmaceuticals

Elena S. Kurakina,* Valery Radchenko, Andrey N. Belozub, Georgi Bonchev, Gospodin A. Bozhikov, Atanas I. Velichkov, Monika Stachura, Dimitar V. Karaivanov, Eldar P. Magomedbekov, and Dmitry V. Filosofov

Cite This: https://dx.doi.org/10.1021/acs.inorgchem.0c01208

Read Online

ACCESS | Metrics & More | Article Recommendations | Supporting Information

ABSTRACT: One of the key components of radiopharmaceuticals for targeting imaging and therapy is a stable bifunctional chelating system to attach radionuclides to selective delivery systems. After-effects of radioactive decay can cause the release of a radioactive isotope from its chelation agent. Perturbed angular correlation (PAC) of γ-rays has become a unique technique to study the behavior of complexes formed between a chelating agent and radionuclide *in vivo* (in real time) over a relevant range of concentrations (10^{-12} M). In the present work, four radionuclides, ^{111}In, ^{111m}Cd, and $^{152,\ 154}$Eu, were investigated with diethylenetriaminepentaacetic acid (DTPA) at different pH values to determine the stability constants of the complexes as well as the effects of post-decay processes, which play a major role in determining the suitability of these complexes for application as radiopharmaceuticals (e.g., *in vivo* generators). The study provides a convenient parameter for the characterization of radionuclide−chelator systems using the PAC method. PAC is proven to be a suitable tool to study novel chelators and radiopharmaceutical precursors attached to radiometals.

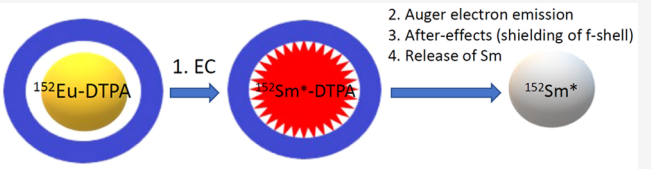

INTRODUCTION

Nowadays, radiopharmaceuticals for targeted imaging and therapy are of frequent application. The radiopharmaceuticals consist of the appropriate targeting vectors and chelators labeled with a radionuclide. Today, the development of new vectors and chelators is one of the main streams of nuclear medicine. However, some of their crucially important characteristics, such as thermodynamic (e.g., stability constant) and kinetic parameters for complexes of new chelators with radionuclides in relevantly low concentrations, are very challenging to determine. This is mainly due to the low concentrations of the radiometals and chelators. However, the common methods of determination are thin layer chromatography and high-performance liquid chromatography, in addition to further animal studies.[1,2] PAC is a useful technique for these purposes, as is presented in a number of works.[3−5] However, it has not become a routine technique, mainly due to uncertainty concerning after-effects, the need for a convenient parameter, and a relatively small choice of the radionuclides suitable for PAC. The aim of the present work is to provide an example of the application of PAC and its suitability for the study of a chelator−radionuclide system. To prove the sufficiency of this approach (introduction of a convenient parameter), stability constants were determined and compared with the literature data using the common chelating agent DTPA.

^{111}In ($T_{1/2}$ = 2.8 d), as one of the common isotopes used in nuclear medicine, is particularly suitable for single photon emission computed tomography (SPECT)[6,7] and for targeted Auger therapy.[8] At the same time, indium-111 is one of the most suitable radionuclides for PAC spectroscopy.[9] Moreover, there are several other elements for which there exist multiple isotopes, where some can be used in targeted imaging and therapy, and others are suitable for PAC. The most attractive example might be the lanthanides, which possess similar chemical properties and are represented by several candidates useful in targeted imaging and therapy (e.g., ^{177}Lu (β^- therapy),[10] $^{152,\ 155,\ 149,\ 161}$Tb,[11−14] and ^{165}Er[15]) and also several candidates suitable as PAC isotopes (e.g., $^{152,\ 154}$Eu[16]). All properties of the selected probes for PAC measurements are presented in Table 1 (see also Figure 1).

The γ−γ perturbed angular correlation technique is based on the angular correlation between two γ-rays, which is perturbed by the hyperfine interaction of the nuclear electric quadrupole moment (Q) with the electric field gradient (EFG) or the nuclear magnetic moment with an extranuclear magnetic field. PAC gives information serving as a "fingerprint" of the local structure.[20−22] As the PAC can be used to measure changes in the local environment of the nucleus, this technique can be

Received: April 23, 2020

Table 1. Properties of the Selected PAC Probes[17−19]

						intermediate state		
parent	daughter	decay	half-life	$\gamma-\gamma$ cascade (keV)	A_{22}	half-life (ns)	spin	quadrupole moment (barn)
^{111}In	^{111}Cd	EC	2.8 d	171−245	−0.178	84.5	5/2+	+0.77
^{111m}Cd	^{111}Cd	IT	49 min	151−245	+0.160	84.5	5/2+	+0.77
^{152}Eu	^{152}Sm	EC	13.5 y	1408−122	+0.225	1.396	2+	−1.67
^{154}Eu	^{154}Gd	β^-	8.6 y	1274−123	+0.251	1.184	2+	−1.82

[a]^{111}In decays into ^{111}Cd* (I = 7/2+) by EC (Figure 1), resulting in the well-known $\gamma-\gamma$ cascade (171−245 keV) with an intermediate state half-life of 84.5 ns and quadrupole moment of Q = +0.77 barn (Table 1), which is suitable for the hyperfine interaction measurements of the nucleus. The (151−245 keV) $\gamma-\gamma$ cascade of ^{111m}Cd goes through the same intermediate state (84.5 ns) via isomeric transition.[18]

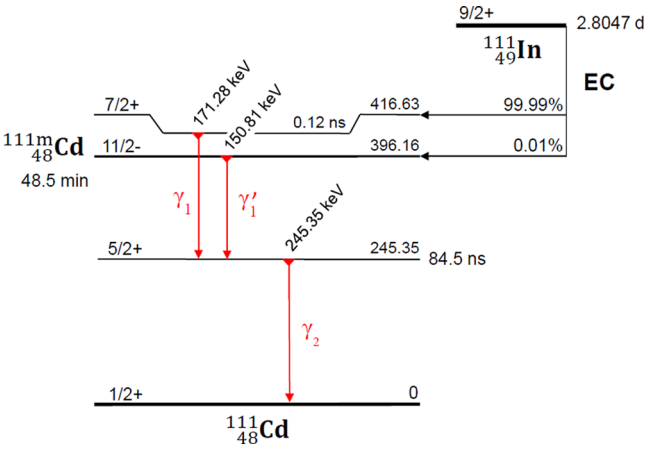

Figure 1. Decay scheme of ^{111}In and ^{111m}Cd.

useful for more detailed investigation of the radionuclides attached to a ligand.[5]

It is known that electron capture (EC) decay creates a hole in one of the inner shells (K, L), which moves toward the outer shells due to Auger-electron and X-ray emissions.[23] The Auger cascade becomes a reason for the daughter to be left in a highly ionized state, which may cause changes at the probe site, which in turn would cause changes in the static and dynamic characteristics of the electric field.[24,25] These processes lead to so-called "after-effects", causing degradation of the complex. After-effects can be described by a few models, i.e., via the (i) fragmentation model, where an electric charge is distributed over the molecule and dissociation occurs due to electrostatic repulsion; (ii) exciton model, where energy of an atomic particle in a molecule after decay is insufficient to cause the breaking of a chemical bond, therefore causing its conversion into exciton energy (vibrational excitation) which migrates over the whole molecule (concentration of this exciton energy on a "weak link" (the weakest bond) can lead to the dissociation of the molecule); (iii) thermal wedge model, where the energy emitted during radioactive decay is absorbed by some volume around the daughter atom and the temperature at this volume is increased, and as a result, the molecules in this vicinity are dissociated; and (vi) auto-radiolysis, where low-energy electron emissions and X-ray photon emissions interact with a local environment of the atom resulting in the production of reactive agents which change the chemical environment of the daughter.[19]

The PAC method has a number of advantages which can be applied in nuclear medicine, i.e., (i) the studying of the system in any aggregated state; (ii) the noninvasive nature of the measurement (for liquids); (iii) the applicability of small activities of a radioisotope; (iv) the capability to measure samples of low concentration (as low as 10^{-12} M); (v) the capability to measure very small sample volumes; and (vi) operation over a wide range of temperatures and pressures.[21,26]

^{154}Eu and ^{152}Eu are the other suitable candidates for PAC (Table 1). They have half-lives of 8.6 and 13.5 years, respectively, which are convenient for the long-term studies. ^{152}Eu decays into ^{152}Sm by EC and ^{154}Eu undergoes β^- decay to excited levels of ^{154}Gd. The cascade measured in the present work is shown in Figure 2 by red lines with intermediate state times of 1.396 and 1.184 ns for ^{152}Eu and ^{154}Eu, respectively.[18,27]

In this work, the effects of decay via various modes (Auger electron or β particle emission) on metal−chelator complexes were studied with PAC spectroscopy using complexes of DTPA with ^{111}In, ^{111m}Cd, and ^{152,154}Eu. From a practical point of view, this study can help in the design of *in vivo* generators (e.g., ^{44m}Sc/^{44g}Sc, ^{212}Pb/^{212}Bi, ^{140}Nd/^{140}Pr, etc.[28−30]) as well as

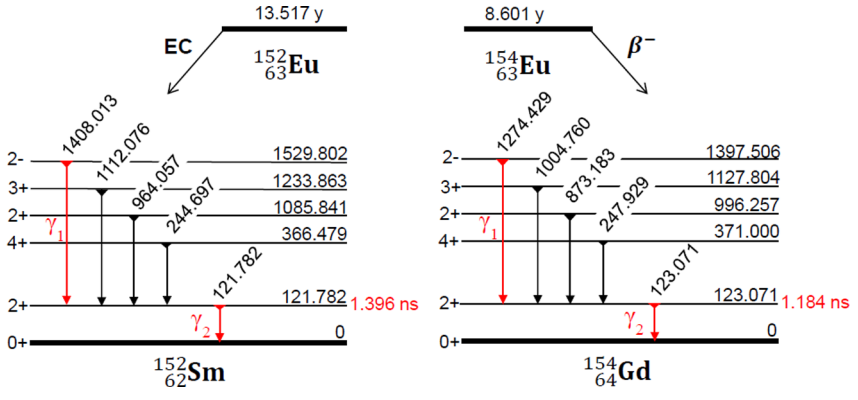

Figure 2. Decay scheme of ^{152}Eu and ^{154}Eu. The energies are given in keV.

https://dx.doi.org/10.1021/acs.inorgchem.0c01208
Inorg. Chem. XXXX, XXX, XXX−XXX

in the development of a better understanding of the effects occurring during and after Auger electrons emission.

EXPERIMENTAL SECTION

Materials. All experiments were performed with doubly distilled water, hydrochloric acid (ultrapure grade) 20-4, GOST 14261-77 (State Standard, Russian Federation), perchloric acid (chemically pure) TU 6-09-2878-84, sodium perchlorate monohydrate (pure) TU 6-09-3605-74 (Reahim, Russian Federation), and sodium hydroxide (analytical grade, Himmed, Russian Federation). The resins used were Dowex 50Wx8 cation-exchange resin (H+, 200−400 mesh, Fluka/Sigma−Aldrich, Germany) and Dowex 50Wx12 (H+, 30−40 μm). DTPA was purchased from Merck, Germany.

To analyze the radionuclides, an Ortec γ-ray spectrometer with an HPGe detector and Samar software was used. The dead time of the detector was always kept below 7%. The pH values were measured using a pH meter with a semi-micro electrode (Thermo Fisher Scientific, Inc.).

Production of Radionuclides. *Production of ^{152}Eu and ^{154}Eu.* A mixture of stable isotopes ^{151}Eu and ^{153}Eu was irradiated in the nuclear reactor (RIAR, Dimitrovgrad, Russian Federation) to produce ^{152}Eu ($T_{1/2}$ = 13.52 y) and ^{154}Eu ($T_{1/2}$ = 8.6 y). The mixture of the isotopes obtained consisted of ^{151}Eu, ^{152}Eu, ^{153}Eu, ^{154}Eu, and ^{155}Eu. Afterward, the isotopes were mass-separated and implanted into an aluminum foil. The radioisotopic purity of the samples was analyzed using γ-spectroscopy. The contamination of ^{152}Eu in ^{154}Eu and ^{154}Eu in ^{152}Eu was ≈0.5% after mass-separation.

Production of ^{111}In and ^{111m}Cd. ^{111}In was produced via the reaction ^{109}Ag(α,2n) → ^{111}In by irradiation of a metallic silver target with α-particles E_a = 30 MeV at the U-200 cyclotron (JINR, Dubna, Russian Federation), according to the method described in ref 31.

^{111m}Cd was produced via an ^{111}In/^{111m}Cd radionuclide generator based on column extraction chromatography using di-2-ethyl-hexyl hydrogen phosphate (HDEHP) as an extractant as described in detail in ref 32.

Preparation of the PAC Samples. Samples for the PAC measurements were prepared by dissolving ^{111}In in HCl (pH = 3). An aliquot of the solution was dried on a Teflon plate at room temperature and taken up with 10^{-4} M DTPA in water, followed by the addition of $HClO_4$, $NaClO_4$, NaOH, and water for ionic strength adjustment. The concentration of ^{111}In in the sample was estimated to be 5×10^{-10} M.

^{111m}Cd was eluted from the generator with 0.2 M of HCl (1.5 mL) and was loaded directly onto a small (50 × 1.25 mm) cation exchange column (Dowex 50Wx8, 200−400 mesh). The column was washed with 0.2 M HCl (0.5 mL) and Cd-111 was eluted with 1 M HCl (100 μL). The eluent was evaporated at 100 °C on a Teflon plate, and a similar procedure as the above, described for indium-111, was applied.

An Eu-containing aluminum foil was dissolved in conc. HCl. The purification of Eu consisted of double separation using a cation-exchange resins Dowex 50Wx8 and Dowex 50 × 12 and HCl solutions. The solution containing ^{152}Eu/^{154}Eu was evaporated on a Teflon plate and taken up with DTPA solution of the same concentration. The constant ionic strength (I = 0.5) of all the samples was maintained by adding NaOH, $NaClO_4$, and $HClO_4$.

The activity of ^{111}In in each sample was no greater than 100 kBq, whereas the activity of Eu samples varied from 50 to 70 kBq. The volumes of these samples were both 500 μL. The volumes of Cd samples were 150 μL, with activities ∼40 kBq. The samples were measured by PAC over 10 h. The pH values were controlled after the PAC measurements. The experiment was carried out at room temperature (25 °C).

PAC Spectroscopy. The PAC spectra were collected using four BaF_2 detectors (50 × 50 mm) arranged with respect to each other at angles of θ = 90° and 180° by counting coincidence $N(\theta, t)$, within a resolution time of at 0.5 ns. The perturbation factor, also called the time-dependent factor $G_{22}(t)$, describing a nuclear spin precession due to a hyperfine interaction, was determined in the usual way from the time-dependent angular anisotropy. It was obtained by combining the delayed coincidence spectra, according to the expression:

$$R(t) = -2\frac{[N(180°, t) - N(90°, t)]}{[N(180°, t) + 2N(90°, t)]} = -A_{22}G_{22}(t)Q_2 \quad (1)$$

where $Q_2 \approx 0.80$ is the geometric correction factor and A_{22} is the the anisotropy coefficient of the cascade.

The block diagram, operation procedure, and software of the PAC spectrometer used in this study are as per ref 33.

In this work, the case of dynamic perturbance is expressed by two equations, 2 and 3, given by[34]

$$G_2(t) = e^{-\lambda_2 t} \text{ (differential model)} \quad (2)$$

where the relaxation constant is expressed by $\lambda_2 = K\omega_Q^2\tau_C$, and the quadrupole frequency is described by $\omega_Q = \left(\frac{2\pi}{4I(2I-1)}\right)\frac{eQV_{zz}}{\hbar}$, where I and Q are the spin and quadrupole moment of the intermediate state and V_{zz} − EFG. The correlation time is $\tau_C = \frac{4}{3}\pi r^3\frac{\eta}{kT}$, where r is the molecule radius and η the viscosity at temperature T.

$$G_2(\infty) = \frac{1}{\tau}\int_0^\infty e^{-\lambda_2 t}e^{1/\tau}d\tau = \frac{1}{1+\lambda_2\tau} \text{ (integral model)} \quad (3)$$

where τ is the lifetime of intermediate state.

The two chemical fractions observed can be expressed by two exponentials (e.g., for ^{111}In−DTPA spectra[9]):

$$G_2(t) = a_1e^{-\lambda_2^{(1)}t} + (1-a_1)e^{-\lambda_2^{(2)}t} \quad (4)$$

Equation 4, with three independent parameters, is inconvenient to use for describing the data of all isotopes. Moreover, eq 3 poorly describes the ^{152,154}Eu spectra, due to the short lifetime of the intermediate state (1−2 ns). Thus, when the condition $|\lambda_2^{(1)} - \lambda_2^{(2)}| \bullet t \leq 1$ is satisfied, eq 5 can be applied to the spectra fitting of ^{111}In, ^{111m}Cd, and both ^{154}Eu and ^{152}Eu:

$$G_2(t) \approx e^{-L_2 t} \quad (5)$$

where L_2 is a generalized integral-differential relaxation parameter. In some cases, where one exponential is observed, $L_2 = \lambda_2$ (see Cd TDPAC spectrum in Figure 3B). The dependence of $G_2(\infty)$ and L_2 on the correlation time τ_C, and therefore on the complex size (r^3), plays a major role in determining the species of the probes in liquids.

Fitting. The stability constant (K) of the complexes is determined by the equation:

$$M^{n+} + Y^{x-} = MY^{n-x}, \qquad K = \frac{[MY^{n-x}]}{[M^{n+}][Y^{x-}]} \quad (6)$$

where M is the metal ion, Y the ligand (DTPA), x = 5 due to DTPA being a pentabasic acid, and n^+ the oxidation number of each metal ion.

The following calculations are presented according to the consideration of both the complexed and free form of the metal ion: MY^{n-x} and M^{n+}. Then, the equation for the calculated PAC parameter is

$$G_2(\infty)^{calc} = G_2(\infty)^{M^{n+}} \times X_{M^{n+}} + G_2(\infty)^{MY^{n-x}} \times X_{MY^{n-x}} \quad (7)$$

where $G_2^{M^{n+}}$ and $G_2^{MY^{n-x}}$ are the PAC parameters for the metal ion form and complex form, respectively; $X_{MY^{n-x}}$ is the mole fraction of the metal complex; and $X_{M^{n+}}$ is the mole fraction of the metal ion which is determined by the equation:

$$X_{M^{n+}} = \frac{[M^{n+}]}{[M^{n+}] + [MY^{n-x}]} \quad (8)$$

As we use L_2 as a generalized relaxation parameter, eq 7 can be rewritten:

$$L_2^{calc} = L_2^{M^{n+}} \times X_{M^{n+}} + L_2^{MY^{n-x}} \times X_{MY^{n-x}} \quad (9)$$

https://dx.doi.org/10.1021/acs.inorgchem.0c01208
Inorg. Chem. XXXX, XXX, XXX−XXX

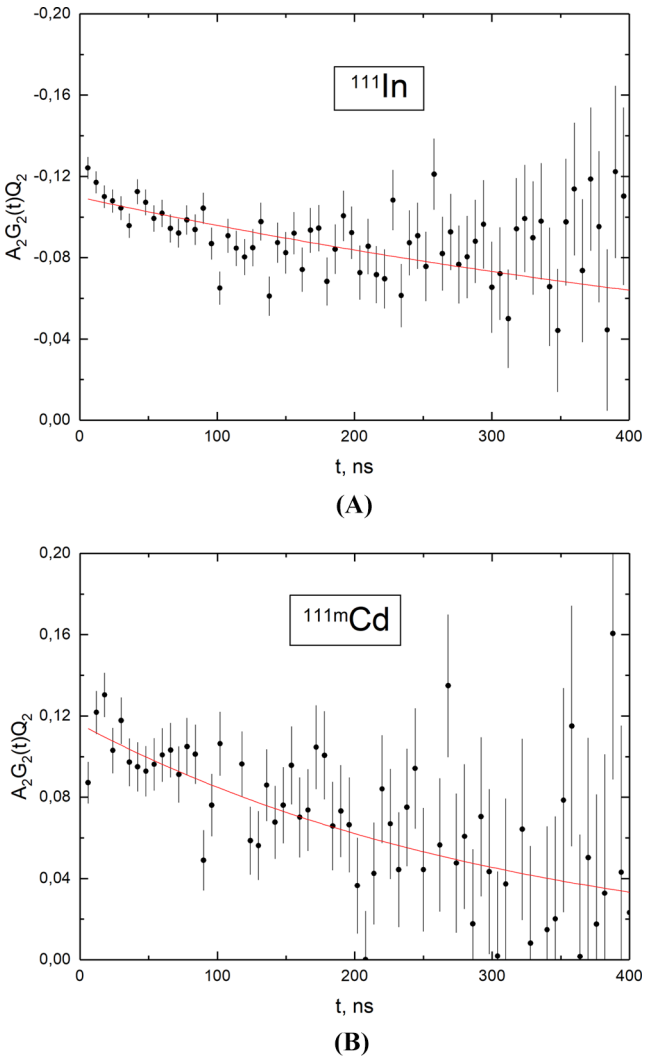

Figure 3. TDPAC spectra of the 171−245 keV (A) and 151−245 keV (B) γ-ray cascades in n.c.a. ^{111}In and ^{111m}Cd, respectively, at C(DTPA) = 10^{-4} M, ionic strength I = 0.5 ($HClO_4$, $NaClO_4$), pH = 3. The fitting functions are shown by red curves using the L_2 parameter.

Then, using eqs 6 and 8:

$$L_2^{calc} = L_2^{M^{n+}}\left(\frac{1}{1 + K[Y^{x-}]}\right) + L_2^{MY^{n-x}}\left(1 - \frac{1}{1 + K[Y^{x-}]}\right) \quad (10)$$

For the DTPA ligand, the equation can be written:

$$[Y^{x-}] = [DTPA^{5-}] = \frac{C_Y}{\frac{[H^+]^5}{K_5K_4K_3K_2K_1} + \frac{[H^+]^4}{K_5K_4K_3K_2} + \frac{[H^+]^3}{K_5K_4K_3} + \frac{[H^+]^2}{K_5K_4} + \frac{[H^+]}{K_5} + 1} \quad (11)$$

where C_Y is the ligand concentration, 10^{-4} M, and K_1−K_5 are the protonation constants for DTPA, i.e., pK_1 = 1.5, pK_2 = 2.64, pK_3 = 4.27, pK_4 = 8.6, and pK_5 = 10.58.[35]

Using the least-squares method, stability constants were found and are presented in Tables 2 and 3.

RESULTS AND DISCUSSION

PAC Measurements of ^{111}In and ^{111m}Cd Complexes. The PAC samples were measured at different pH values, up to pH = 5 (Figures 4A and 5A). The spectra for ^{111}In and ^{111m}Cd with DTPA at different pH values are presented in Figures 3A and 3B and Figures S1−S5. Using eq 3 for the processing of TDPAC spectra and eq 7 for fitting, the dependences for ^{111}In and ^{111m}Cd with DTPA were plotted. At low pH values, indium exists in an aqueous form $[In(H_2O)_x]^{3+}$ (Figure 4A).[36] The transition at pH (0.5∼1.5) corresponds to the complex formation of $[In(DTPA)]^{2-}$. Also observed is a small transition at pH = 2, which may correspond to a transition between ^{111}Cd* forms (between the complex with DTPA and the aqua complex). The complex of Cd with DTPA at pH of lower than 2 is thermodynamically unstable. The initial physicochemical transformations for ^{111}In and ^{111m}Cd complexes over a range of pH are schematically shown in Figures 4B and 5B.

Using literature data,[35] the distribution diagram (Figure 6) for Cd^{2+} complexes with DTPA was plotted. It is shown that at low pH values, acidic complexes of cadmium form. The experimental data on electrophoretic mobility of Cd (Figure 7), presented in ref 37, support this statement. Herein, we assume the formation of $[Cd(HDTPA)]^{2-}$.

The data in Figure 5A shows complex formation at pH ∼ 2. Considering the facts described above, the stability constant of $[Cd(HDTPA)]^{2-}$ was determined (Table 2) using both models for processing TDPAC spectra. Unfortunately, the PAC method applied in this work is unsuitable for the exact determination of the species formed ($[Cd(HDTPA)]^{2-}$ or $[Cd(H_2DTPA)]^{-}$). More likely, it is the $[Cd(HDTPA)]^{2-}$ complex which forms. The obtained value for the $[Cd(HDTPA)]^{2-}$ complex correlates well with that reported in the literature.[35]

Using eq 5, with the L_2 parameter, the TDPAC spectra were processed. Afterward, the data obtained were fitted by eq 9 and plotted in Figures 8 and 9.

The stability constants were determined using the least-squares method and are shown in Table 2. The difference between the values determined via the $G_2(\infty)$ parameter (eq 3) and L_2 is negligible. The uncertainty of the determined stability constants was no greater than 10%.

Table 2. Experimental and Literature Data on the Stability Constant of ^{111}In and ^{111m}Cd Complexes with DTPA

		log K		
		experimental data (present work) processed		literature data
isotope	reaction	via $G_2(\infty)$ parameter	via L_2 parameter	
^{111}In	M + Y ↔ MY	28.90	28.20	28.42[38]
				29.00[39]
^{111m}Cd	M + Y ↔ MY	23.00	22.09	19.30[39]
	M + HY ↔ MHY	13.78	13.70	12.63[a35]

[a]The stability constant was recalculated in terms of different interpretations of the reaction of complex formation used in present work for $[^{111m}Cd(HDTPA)^{2-}]$.

Table 3. Experimental and Literature Data on the Stability Constant of $[^{154}Eu(DTPA)]^{2-}$ Complex

	log K	
	experimental data processed via L_2 parameter	literature data
reaction		
M + Y ↔ MY	23.26	23.17[40]
		22.50[39]

https://dx.doi.org/10.1021/acs.inorgchem.0c01208
Inorg. Chem. XXXX, XXX, XXX−XXX

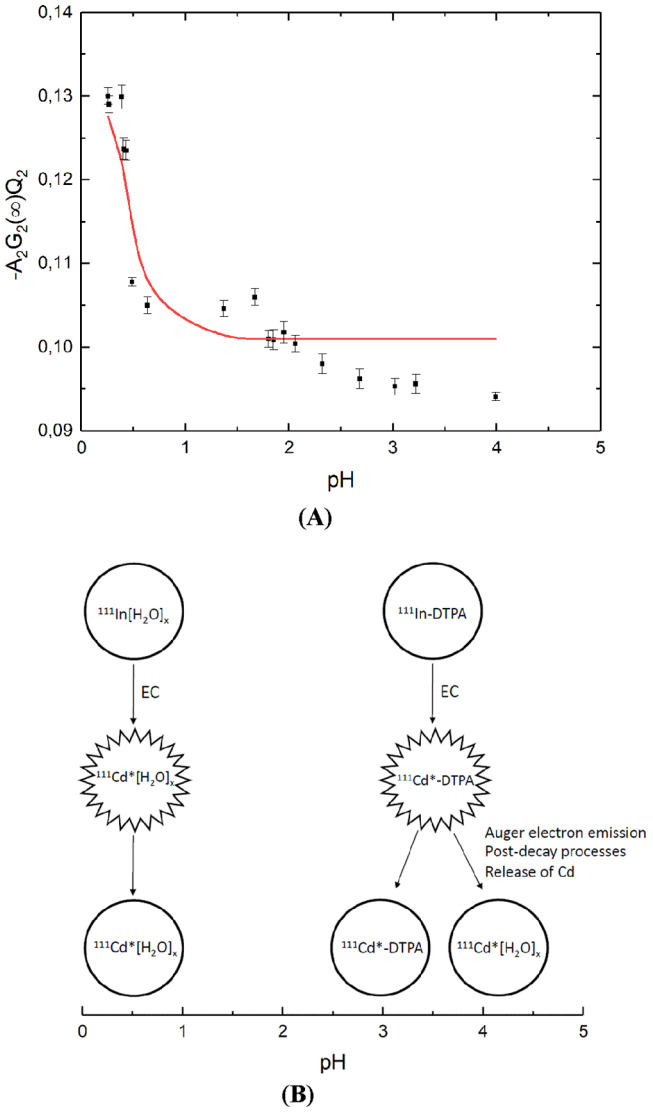

Figure 4. (A) TDPAC parameter versus pH values for In–DTPA complexes at C(DTPA) = 10^{-4} M, ionic strength I = 0.5 ($HClO_4$, $NaClO_4$). (B) The hypothetical route of transformations between the initial physicochemical forms of the mother–daughter pair (^{111}In/^{111}Cd), where ^{111}Cd* denotes the excited levels (I = 7/2+ and/or 5/2+).

PAC Measurements of Eu Complexes. For radionuclides ^{154}Eu and ^{152}Eu, graphs of the differential perturbed factor were plotted (Figure 10 and Figures S6–S11) using eq 2.

For ^{152,154}Eu complexes with DTPA, using the integral model (eq 3) is not sensitive for processing the spectra, due to the short lifetimes of intermediate states (Figure 2) of 1.396 and 1.184 ns for ^{152}Eu and ^{154}Eu, respectively. The resultant dependency depicted in Figure 11A was obtained by using the generalized parameter L_2 (eq 5).

The transition at pH ∼ 1.5 in Figure 11A shows that ^{154}Eu in solution has at least two forms (Figure 11B), including the ^{154}Eu–DTPA complex. Moreover, the ^{154}Eu decay product (β^-)^{154}Gd is not released from the complex. The values obtained experimentally were compared with those found in the literature (Table 3).

The ^{152}Eu complex with DTPA should form at the same pH as the ^{154}Eu–DTPA complex. The dashed line in Figure 12A

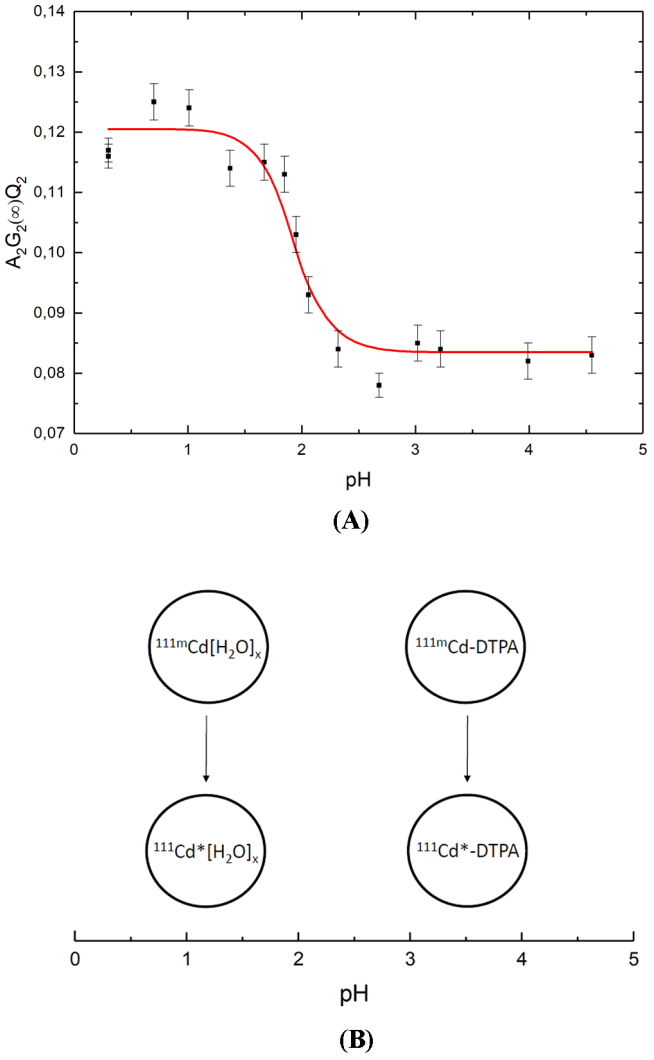

Figure 5. (A) TDPAC parameter versus pH values for Cd–DTPA complexes at C(DTPA) = 10^{-4} M, ionic strength I = 0.5 ($HClO_4$, $NaClO_4$). (B) The hypothetical route of transformations between initial physicochemical forms of the mother–daughter pair (^{111m}Cd/^{111}Cd) is shown, where ^{111}Cd* denotes the excited level (I = 5/2+).

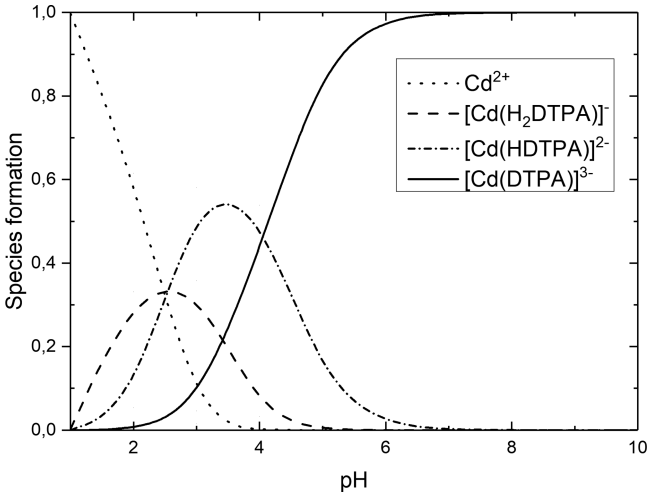

Figure 6. Distribution diagram of Cd^{2+} complexes with C(DTPA) = 10^{-4} M versus pH values.

https://dx.doi.org/10.1021/acs.inorgchem.0c01208
Inorg. Chem. XXXX, XXX, XXX–XXX

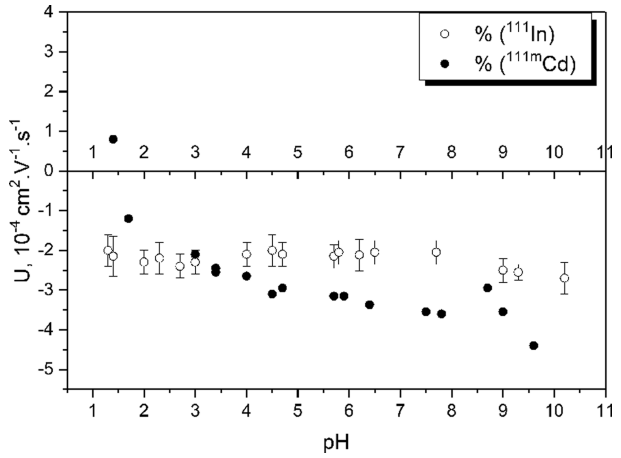

Figure 7. Electrophoretic mobility dependence on pH values for ^{111}In and ^{111m}Cd complexes at C(DTPA) = 3×10^{-5} M, ionic strength I = 0.1. Reproduced from ref 37 with permission.

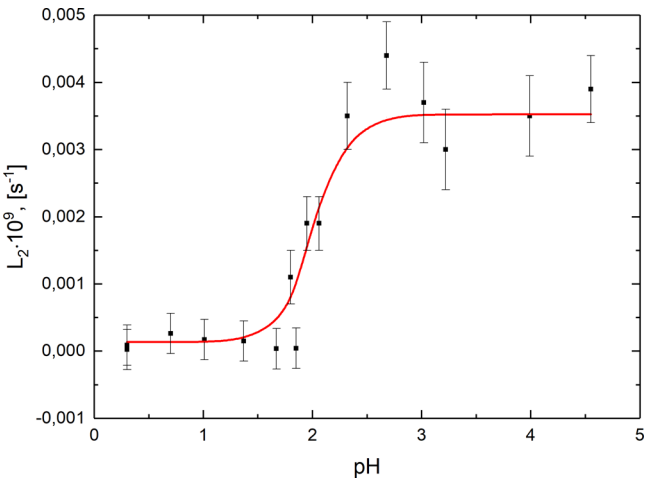

Figure 8. L_2 dependence on the pH value for ^{111m}Cd–HDTPA solution at ionic strength I = 0.5 ($HClO_4$, $NaClO_4$), C(DTPA) = 10^{-4} M.

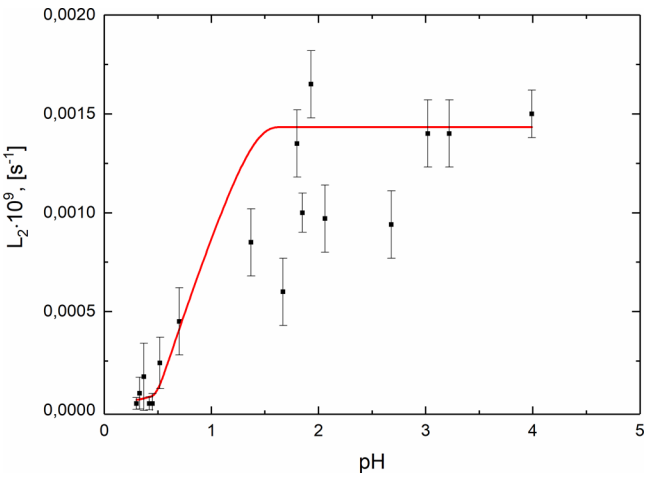

Figure 9. L_2 dependence on the pH value for ^{111}In–DTPA solution at ionic strength I = 0.5 ($HClO_4$, $NaClO_4$), C(DTPA) = 10^{-4} M.

was drawn to show that the pH value corresponded to complex formation. However, in the case of ^{152}Eu, determination of the stability constant becomes difficult, i.e., the daughter ^{152}Eu-

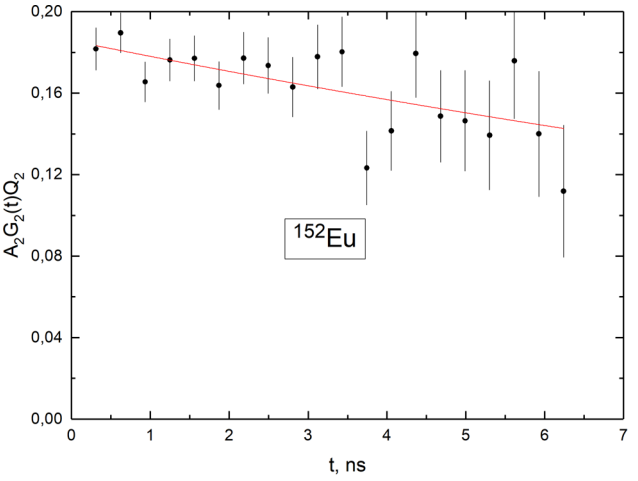

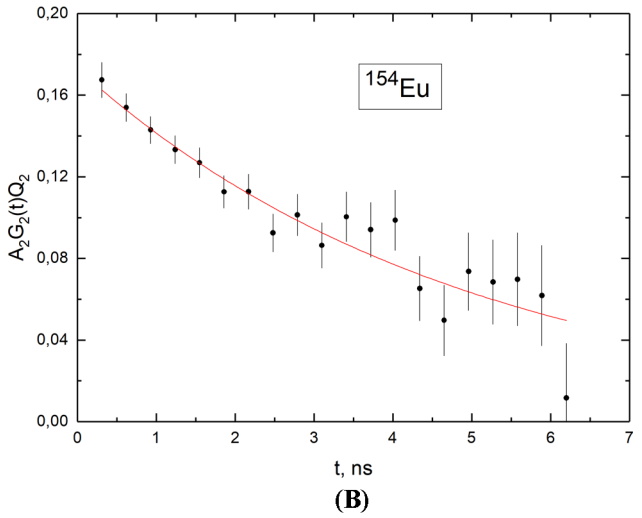

Figure 10. (A) TDPAC spectra for ^{154}Eu and (B) for ^{152}Eu at C(DTPA) = 10^{-4} M, ionic strength I = 0.5 ($HClO_4$, $NaClO_4$, NaOH) with pH = 3. The fitting functions are shown by red curves using the L_2 parameter.

(EC)^{152}Sm leaves the DTPA molecule due to after-effects (Figure 12B). Since Sm is released from the complex, the chemical environment does not cause the former perturbed angular correlation. It is possible that ^{152}Sm reforms a complex with DTPA after initial decomplexation. However, we can definitely assume that this does not happen during the measurement time ≈5 ns. There is a possibility that after-effects lead to the fragmentation of the molecule.

Mechanism of Post-decay Processes. On the one hand, as the atomic number of indium is 49 and that of europium is 63, a total disintegration of the ^{152}Eu–DTPA complex can be caused by the majority of the Auger electrons resulting from one of four mechanisms entailed in the post-decay processes described in the Introduction. On the other hand, another mechanism can be postulated in order to describe the release of Sm from the complex, namely, the relaxation of electron shells. As the electronic shells comprising the xenon core [Kr]4d^{10}5s^{2}5p^6 are first filled, more peripheral electrons are shielded by the filling of Sm the valence electronic f-shells (Figure S12, plotted using ref 41). This may cause an increase in the time spent in high energy shells. Relatively continuous ($\gg 10^{-12}$ s) being of electrons at the excited state (in the

https://dx.doi.org/10.1021/acs.inorgchem.0c01208
Inorg. Chem. XXXX, XXX, XXX–XXX

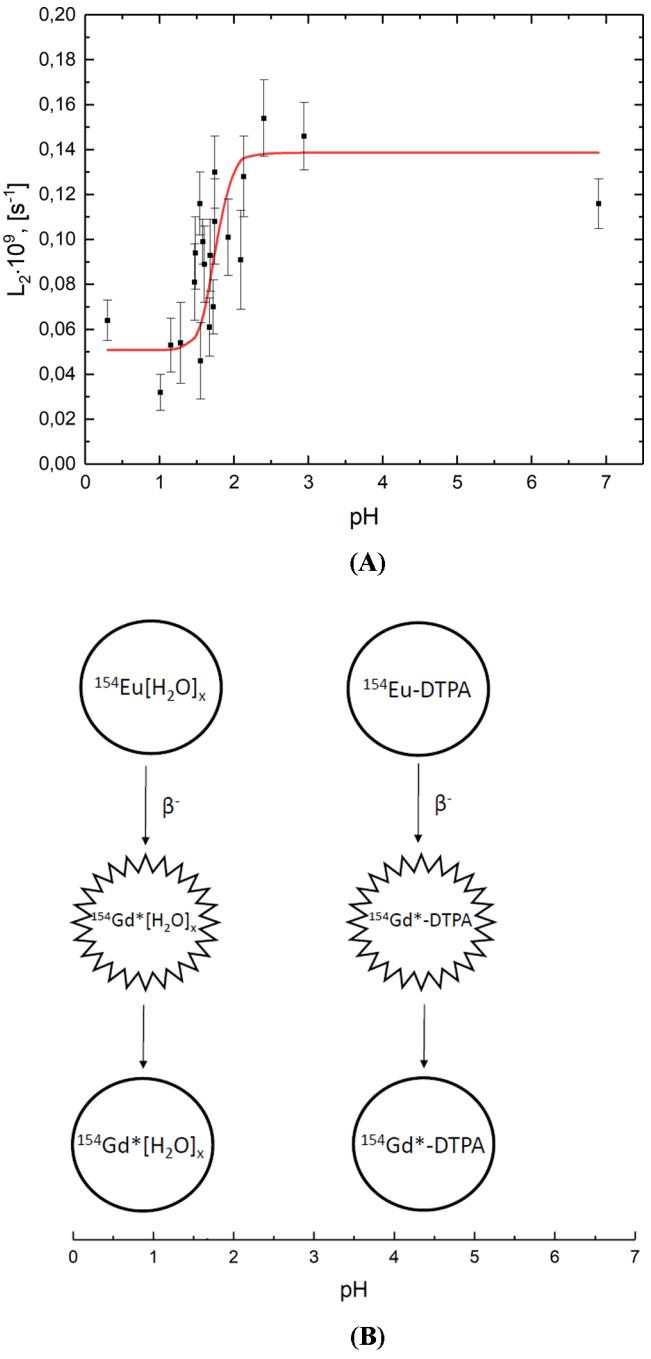

Figure 11. (A) L_2 dependence on the pH value for ^{154}Eu−DTPA complexes at ionic strength I = 0.5 ($HClO_4$, $NaClO_4$, NaOH), C(DTPA) = 10^{-4} M. (B) The hypothetical route of transformations between initial physicochemical forms of the mother−daughter pair ^{154}Eu/^{154}Gd is shown, where ^{154}Gd* denotes the excited levels (I = 2−, 1398 keV, and/or I = 2+, 123 keV).

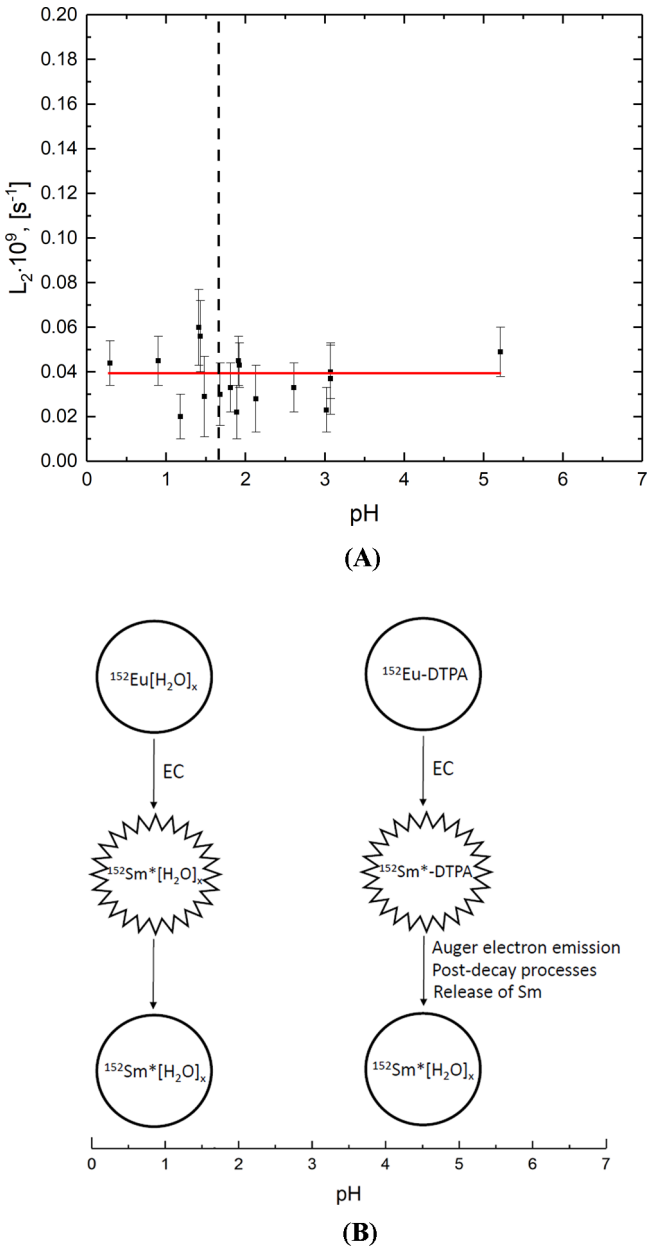

Figure 12. (A) L_2 dependence on the pH value for ^{152}Eu−DTPA complexes at ionic strength I = 0.5 ($HClO_4$, $NaClO_4$, NaOH), C(DTPA) = 10^{-4} M. (B) The hypothetical route of transformations between initial physicochemical forms of the mother−daughter pair ^{152}Eu/^{152}Sm is shown. ^{154}Gd* denotes the excited levels (I = 2−, 1530 keV, and/or I = 2+, 122 keV).

remote shell) can cause complex disintegration. A shielding of the f-shell in lanthanides is usually taken into account when describing its luminescent properties.[42]

However, for ^{111}In−DTPA, despite the after-effect processes, only part of the complexes disintegrates. This makes it possible to determine their stability constant. Figure S13 shows that for the daughter Cd there is no shielding effect as for Sm. In the case of ^{152}Eu, there is total disintegration of the complexes with DTPA, due to post-decay processes via the fifth mechanism described above. This thus makes for considerable difficulty in determining the stability constant. An additional example of one such case is that of ^{140}Nd(EC)^{140}Pr coupled with DOTA, for which there is total complex disintegration as well.[29]

CONCLUSION

An investigation into the hyperfine interactions of the decays of ^{111}In, ^{111m}Cd, ^{154}Eu, and ^{152}Eu in aqueous solution with DTPA over a wide range of pH values was performed. Suggested in the present work, the hyperfine interactions parameter L_2 and an integral parameter $G_2(\infty)$ of perturbed angular correlation are appropriate for stability constant determination. In the case of PAC isotopes with short-lived intermediate states (~1−2 ns), the L_2 parameter effectively

https://dx.doi.org/10.1021/acs.inorgchem.0c01208
Inorg. Chem. XXXX, XXX, XXX−XXX

becomes the only one suitable for the investigation of the distribution of a given radionuclide over the physicochemical species in the solution. The stability constants determined in this work by the L_2 generalized parameter correlate well with literature data, which proves the sufficiency of the method. This approach used can be applied for the study of radiometals in low concentrations (up to 10^{-12} M) attached to novel chelators (radiopharmaceuticals) for purposes of nuclear medicine.

This work presents the influence of after-effects on stability of the isotope−chelator system. In the case of ^{111}In, approximately half (∼50%) of the complexes with the daughter Cd disintegrated. However, the remaining complexes were numerous enough for the determination of a stability constant for In−DTPA. The stability constant determined for the acidic complex of ^{111m}Cd with DTPA also correlates well with the data reported in the literature. For ^{154}Eu, almost all of the complexes with the daughter ^{154}Gd did not disintegrate, allowing for the determination of the stability constant of the ^{154}Eu−DTPA complex. For ^{152}Eu complexes, almost all initial complexes of the daughter ^{152}Sm disintegrated. A potential mechanism for ^{152}Eu−DTPA decomplexation due to a shielding effect of ^{152}Sm was shown.

■ ASSOCIATED CONTENT

Supporting Information

The Supporting Information is available free of charge at https://pubs.acs.org/doi/10.1021/acs.inorgchem.0c01208.

(Figures S1−S11) TDPAC spectra for the selected PAC probes at different pH values; (Figures S12 and S13) charge distribution (ψ^2) in electronic states of a free atom of Sm and Cd, respectively, versus R distance from the nucleus in units of Bohr radius R_B (PDF)

■ AUTHOR INFORMATION

Corresponding Author

Elena S. Kurakina − *Dzhelepov Laboratory of Nuclear Problems, Joint Institute for Nuclear Research, Dubna 141980, Russian Federation; Department of High-Energy Chemistry and Radioecology, D. Mendeleev University of Chemical Technology of Russia, Moscow 125047, Russian Federation;* orcid.org/0000-0001-5126-1663; Phone: +7-49621-62680; Email: kurakina@jinr.ru

Authors

Valery Radchenko − *Life Sciences Division, TRIUMF, Vancouver V6T 2A3, Canada; Department of Chemistry, University of British Columbia, Vancouver V6T 1Z1, Canada*

Andrey N. Belozub − *Dzhelepov Laboratory of Nuclear Problems, Joint Institute for Nuclear Research, Dubna 141980, Russian Federation*

Georgi Bonchev − *Military Medical Academy, Varna 9010, Bulgaria*

Gospodin A. Bozhikov − *Flerov Laboratory of Nuclear Reactions, Joint Institute for Nuclear Research, Dubna 141980, Russian Federation*

Atanas I. Velichkov − *Dzhelepov Laboratory of Nuclear Problems, Joint Institute for Nuclear Research, Dubna 141980, Russian Federation; Institute for Nuclear Research and Nuclear Energy, Bulgarian Academy of Sciences, Sofia BG-1784, Bulgaria*

Monika Stachura − *Life Sciences Division, TRIUMF, Vancouver V6T 2A3, Canada;* orcid.org/0000-0003-1426-689X

Dimitar V. Karaivanov − *Dzhelepov Laboratory of Nuclear Problems, Joint Institute for Nuclear Research, Dubna 141980, Russian Federation; Institute for Nuclear Research and Nuclear Energy, Bulgarian Academy of Sciences, Sofia BG-1784, Bulgaria*

Eldar P. Magomedbekov − *Department of High-Energy Chemistry and Radioecology, D. Mendeleev University of Chemical Technology of Russia, Moscow 125047, Russian Federation*

Dmitry V. Filosofov − *Dzhelepov Laboratory of Nuclear Problems, Joint Institute for Nuclear Research, Dubna 141980, Russian Federation*

Complete contact information is available at: https://pubs.acs.org/10.1021/acs.inorgchem.0c01208

Author Contributions

The manuscript was written through contributions of all authors. All authors have given approval to the final version of the manuscript.

Notes

The authors declare no competing financial interest.

■ ACKNOWLEDGMENTS

This work was supported by the Russian Foundation for Basic Research (15-53-12372 NNIO_a) and NSERC Discovery Grants [RGPIN-2018-04997 (VR)]. TRIUMF receives funding via a contribution agreement with the National Research Council of Canada. We thank Dr. Anvar Inoyatov for valuable discussions on the physics of the Auger processes and Keiran Maskell for revising the language of this manuscript.

■ ABBREVIATIONS USED

PAC, perturbed angular correlation; TDPAC, time-dependent perturbed angular correlation; DTPA, diethylenetriaminepentaacetic acid; SPECT, single photon emission computed tomography; EFG, electric field gradient; EC, electron capture; n.c.a., no carrier added; HDEHP, di-2-ethyl-hexyl hydrogen phosphate; HPGe, high purity germanium.

■ REFERENCES

(1) Ramogida, C. F.; Orvig, C. Tumour Targeting with Radiometals for Diagnosis and Therapy. *Chem. Commun.* **2013**, *49* (42), 4720−4739.

(2) Knapp, F. F. R.; Dash, A. Radiopharmaceuticals for Therapy. *Springer India* **2016**, 1.

(3) Leipert, T. K.; Baldeschwieler, J. D.; Shirley, D. A. Applications of Gamma Ray Angular Correlations to the Study of Biological Macromolecules in Solution. *Nature* **1968**, *220* (5170), 907−909.

(4) Mekata, M.; Hamada, E.; Seguchi, Y.; Sigiura, S.; Kawamura, M. PAC Study Of111In-Bleomycin Complex in Solutions. *Hyperfine Interact.* **1990**, *61* (1−4), 1179−1183.

(5) Bauer, R.; Atke, A.; Danielsen, E.; Marcussen, J.; Olsen, C.E.; Rehfeld, J.; Saermark, T.; Schneider, D.; Vilhardt, H.; Zeppezauer, M. The Potential of Perturbed Angular Correlation of Gamma Rays as a Tool for Dynamic Studies of Peptides/Proteins. *Appl. Radiat. Isot.* **1991**, *42* (11), 1015−1023.

(6) Mariani, G.; Bruselli, L.; Kuwert, T.; Kim, E. E.; Flotats, A.; Israel, O.; Dondi, M.; Watanabe, N. A Review on the Clinical Uses of SPECT/CT. *Eur. J. Nucl. Med. Mol. Imaging* **2010**, *37* (10), 1959−1985.

(7) Lahiri, S.; Maiti, M.; Ghosh, K. Production and Separation of 111In: An Important Radionuclide in Life Sciences: A Mini Review. *J. Radioanal. Nucl. Chem.* **2013**, *297* (3), 309−318.
(8) McLean, J. R.; Blakey, D. H.; Douglas, G. R.; Bayley, J. The Auger Electron Dosimetry of Indium-1 11 in Mammalian Cells in Vitro. *Radiat. Res.* **1989**, *119* (2), 205−218.
(9) Shpinkova, L. G.; Kulakov, V. N.; Sorokin, A. A.; Ryasny, G. K.; Komissarova, B. A.; Nikitin, S. M. Stability of 111In-Ligand Complexes Studied by TDPAC. *Z. Naturforsch., A: Phys. Sci.* **1998**, *53*, 630−635.
(10) Heck, M. M.; Retz, M.; D'Alessandria, C.; Rauscher, I.; Scheidhauer, K.; Maurer, T.; Storz, E.; Janssen, F.; Schottelius, M.; Wester, H.-J.; Gschwend, J. E.; Schwaiger, M.; Tauber, R.; Eiber, M. Systemic Radioligand Therapy with 177Lu-PSMA-I&T in Patients with Metastatic Castration-Resistant Prostate Cancer. *J. Urol.* **2016**, *196*, 382−391.
(11) Kostelnik, T. I.; Orvig, C. Radioactive Main Group and Rare Earth Metals for Imaging and Therapy. *Chem. Rev.* **2019**, *119*, 902−956.
(12) Lehenberger, S.; Barkhausen, C.; Cohrs, S.; Fischer, E.; Grünberg, J.; Hohn, A.; Köster, U.; Schibli, R.; Türler, A.; Zhernosekov, K. The Low-Energy β-and Electron Emitter 161Tb as an Alternative to 177Lu for Targeted Radionuclide Therapy. *Nucl. Med. Biol.* **2011**, *38* (6), 917−924.
(13) Müller, C.; Vermeulen, C.; Köster, U.; Johnston, K.; Türler, A.; Schibli, R.; van der Meulen, N. P. Alpha-PET with Terbium-149: Evidence and Perspectives for Radiotheragnostics. *EJNMMI Radiopharm. Chem.* **2017**, *1* (1), 5.
(14) Baum, R. P.; Singh, A.; Benešová, M.; Vermeulen, C.; Gnesin, S.; Köster, U.; Johnston, K.; Müller, D.; Senftleben, S.; Kulkarni, H. R.; Türler, A.; Schibli, R.; Prior, J. O.; Van Der Meulen, N. P.; Müller, C. Clinical Evaluation of the Radiolanthanide Terbium-152: First-in-Human PET/CT With152Tb-DOTATOC. *Dalt. Trans.* **2017**, *46* (42), 14638−14646.
(15) Sadeghi, M.; Enferadi, M.; Tenreiro, C. Nuclear Model Calculations on the Production of Auger Emitter 165 Er for Targeted Radionuclide Therapy. *J. Mod. Phys.* **2010**, *01*, 217−225.
(16) Nasir, H. M.; Grabowski, Z. W.; Steffen, R. M. Conversion-Electron Particle Parameters in the Decay of Eu 152 and Eu 154 F. *Phys. Rev.* **1967**, *162* (4), 1118−1124.
(17) Nagl, M. A.; Barbosa, M. B.; Vetter, U.; Correia, J. G.; Hofsäss, H. C. Nuclear Instruments and Methods in Physics Research A A New Tool for the Search of Nuclides with Properties Suitable for Nuclear Solid State Physics Based on the Evaluated Nuclear Structure Data Files. *Nucl. Instrum. Methods Phys. Res., Sect. A* **2013**, *726*, 17−30.
(18) Stone, N. J. Table of Nuclear Electric Quadrupole Moments. *At. Data Nucl. Data Tables* **2016**, *111*−*112*, 1−28.
(19) Filosofov, D. V. Radiohimicheskie Aspecty Primeneniya Metoda Vozmushchennyh Uglovyh Gamma-Gamma Korrelyaciy v Issledovaniyah Kondensirovannyh Sred Na Primere 111In i 111mCd. *JINR*; 2005.
(20) Chakraborty, S.; Pallada, S.; Pedersen, J. T.; Jancso, A.; Correia, J. G.; Hemmingsen, L. Nanosecond Dynamics at Protein Metal Sites: An Application of Perturbed Angular Correlation (PAC) of γ - Rays Spectroscopy. *Acc. Chem. Res.* **2017**, *50*, 2225−2232.
(21) Hemmingsen, L.; Butz, T. Perturbed Angular Correlations of γ-Rays (PAC) Spectroscopy. *Encycl. Inorg. Bioinorg. Chem.* **2011**, 1−15.
(22) Jancso, A.; Correia, J. G.; Gottberg, A.; Schell, J.; Stachura, M.; Szunyogh, D.; Pallada, S.; Lupascu, D. C.; Kowalska, M.; Hemmingsen, L. TDPAC and β -NMR Applications in Chemistry and Biochemistry. *J. Phys. G: Nucl. Part. Phys.* **2017**, *44* (6), No. 064003.
(23) Kassis, A. I. Molecular and Cellular Radiobiological Effects of Auger Emitting Radionuclides. *Radiat. Prot. Dosim.* **2011**, *143* (2−4), 241−247.
(24) Butz, T. Analytic Perturbation Functions for Static Interactions in Perturbed Angular Correlations of γ-Rays. *Hyperfine Interact.* **1989**, *52* (3), 189−228.
(25) Shpinkova, L. G.; Carbonari, A. W.; Nikitin, S. M.; Mestnik-filho, J. Influence of Electron Capture After-Effects on the Stability of 111 In (111 Cd) -Complexes with Organic Ligands. *Chem. Phys.* **2002**, *279*, 255−263.
(26) Filosofov, D. V.; Novgorodov, A. F.; Kochetov, O. I.; Korolev, N. A.; Lebedev, N. A. Investigation of the DTPA Complex Formations of Indium and Cadmium by a $\gamma\gamma$ - Perturbed Angular Correlation Method. *Jahresbericht, Inst. für Kernchemie* **2004**, *3* (2002).
(27) Bauer, R. W.; Deutsch, M. Magnetic Moments of the First Excited 2+ States in Sm 152, Gd 154, and Gd 156. *Phys. Rev.* **1962**, *128* (2), 751−760.
(28) Huclier-Markai, S.; Alliot, C.; Rousseau, J.; Chouin, N.; Fani, M.; Bouziotis, P.; Maina, T.; Cutler, C. S.; Barbet, J. Promising Prospects of 44mSc/44Sc as an in Vivo Generator: Biological Evaluation and PET Images. *Nucl. Med. Biol.* **2014**, *41* (7), 631.
(29) Zhernosekov, K. P.; Filosofov, D. V.; Qaim, S. M.; Rosch, F. A 140Nd/140Pr Radionuclide Generator Based on Physico-Chemical Transitions in 140Pr Complexes after Electron Capture Decay of 140Nd-DOTA. *Radiochim. Acta* **2007**, *95* (6), 319−327.
(30) Rösch, F.; Knapp, F. F. 40 Radionuclide Generators. *Handbook of Nuclear Chemistry* **2011**, 1935−1976.
(31) Akselrod, Z.; Filossofov, D.; Buša, J.; Bušova, T.; Kochetov, O.; Lebedev, N.; et al. 111Cd Time Differential Perturbed Angular Correlation Studies of High Specific Activity m In-Aqueous Solutions. *Z. Naturforsch., A: Phys. Sci.* **2000**, *55*, 151−154.
(32) Filosofov, D. V.; Korolev, N. A.; Lebedev, N. A.; Starodub, G. Y.; Novgorodov, A. F. A 111In −111mCd Radionuclide Generator. *Radiochemistry* **2002**, *44* (6), 576−581.
(33) Brudanin, V. B.; Filossofov, D. V.; Kochetov, O. I.; Korolev, N. A.; Milanov, M.; Ostrovskiy, I. V.; Pavlov, V. N.; Salamatin, A. V.; Timkin, V. V.; Velichkov, A. I.; Fomicheva, L. N.; Tsvyaschenko, A. V.; Akselrod, Z. Z. PAC Spectrometer for Condensed Matter Investigation. *Nucl. Instrum. Methods Phys. Res., Sect. A* **2005**, *547* (2−3), 389−399.
(34) Abragam, A.; Pound, R. V. Influence of Electric and Magnetic Fields on THz Radiation. *Phys. Rev.* **1953**, *92* (4), 943−962.
(35) Hyvönen, H. Studies on Metal Complex Formation of Environmentally Friendly Aminopolycarboxylate Chelating Agents. Thesis, University of Helsinki, 2008.
(36) Baes, C. F.; Mesmer, R. E. *The Hydrolysis of Cations*; Robert, E., Ed.; Krieger Publishing Company: Malabar, 1986.
(37) Bozhikov, G. A. Aparaturno-Metodicheskiy Kompleks Gorizontal'nogo Zonnogo Electroforeza v Svobodnom Electrolite: Issledovanie Electroforeticheskih Podvizhnostey, Kompleksoobrazovaniya, Diffuzionnyh i Kineticheskih Harakteristik 237Pu(VI), 111In(III), and 111mCd(II). *MUCTR*; 2004.
(38) Byegård, J.; Skarnemark, G.; Skålberg, M. The Stability of Some Metal EDTA, DTPA and DOTA Complexes: Application as Tracers in Groundwater Studies. *J. Radioanal. Nucl. Chem.* **1999**, *241* (2), 281−290.
(39) Anderegg, G.; Arnaud-Neu, F.; Delgado, R.; Felcman, J.; Popov, K. Critical Evaluation of Stability Constants of Metal Complexes of Complexones for Biomedical and Environmental Applications* (IUPAC Technical Report). *Pure Appl. Chem.* **2005**, *77* (8), 1445−1495.
(40) Galaktionov, Y. P.; Astakhov, K. V. Spectrophotometric Investigation of Complexes of Samarium(III) and Europium(III) with Diethylenetriaminepentaacetic Acid. *Russ. J. Inorg. Chem.* **1963**, *724* (8), 1395−1306.
(41) Herman, F.; Skillman, S. *Atomic Structure Calculations*; Prentice-Hall: Englewood Cliffs, 1963.
(42) Werts, M. H. V. Making Sense of Lanthanide Luminescence. *Sci. Prog.* **2005**, *88* (2), 101−131.

https://dx.doi.org/10.1021/acs.inorgchem.0c01208
Inorg. Chem. XXXX, XXX, XXX−XXX

Available online at www.sciencedirect.com
SCIENCE DIRECT®
ELSEVIER
Nuclear Instruments and Methods in Physics Research A 547 (2005) 389–399
NUCLEAR INSTRUMENTS & METHODS IN PHYSICS RESEARCH Section A
www.elsevier.com/locate/nima

PAC spectrometer for condensed matter investigation

V.B. Brudanin[a], D.V. Filossofov[a], O.I. Kochetov[a], N.A. Korolev[a], M. Milanov[a], I.V. Ostrovskiy[a,*], V.N. Pavlov[a], A.V. Salamatin[a], V.V. Timkin[a], A.I. Velichkov[a], L.N. Fomicheva[b], A.V. Tsvyaschenko[b], Z.Z. Akselrod[c,*]

[a]*Joint Institute for Nuclear Research, Joliot-Curie 6, Dubna 141980 (Moscow region), Russian Federation*
[b]*Institute for High Pressure Physics, Troitsk, Russian Federation*
[c]*Skobeltsyn Institute of Nuclear Physics, Moscow State University, Moscow, Russian Federation*

Received 5 March 2005; accepted 5 April 2005
Available online 10 May 2005

Abstract

A four-detector spectrometer of perturbed angular $\gamma\gamma$ correlations is developed for investigation of hyperfine interactions in condensed matter. It allows measurements with practically any type of detectors. A unique circuit design involving a specially developed Master PAC unit combined with a computer allows a substantially higher efficiency, reduced set-up time and simpler operation in comparison with traditional PAC spectrometers. A cryostat and a high-temperature oven allow measurements in the temperature range from 120 to 1300 K. An encased electromagnet makes it possible to generate a magnetic field up to 2 T on a sample. The measurement system includes a press with a specially designed high-pressure chamber allowing on-line PAC measurements in samples under pressure up to 60 GPa.

PACS: 29.30

Keywords: TDPAC spectrometer; Delayed coincidence; Hyperfine interactions; High pressure

1. Introduction

Hyperfine interaction (HFI) physics deals with a wide range of phenomena where interaction of atomic nuclei with electric and magnetic field generated by electrons in free atoms and in condensed matter is manifested. This allows the electron structure of solids, chemical compounds, and biological objects to be studied. The HFI parameters are quite sensitive to details of the electron wave functions for atoms and ions, which makes it possible to gain unique information unobtainable by other methods.

The HFI Hamiltonian may be written down as a series

$$H_{\mathrm{HFI}} = H(E_0) + H(H_1) + H(H_2) + \ldots,$$

*Corresponding author. Tel.: +7 9263 842501.
E-mail address: ostrov@nusun.jinr.ru (I.V. Ostrovskiy).
*Deceased.

0168-9002/$ - see front matter © 2005 Elsevier B.V. All rights reserved.
doi:10.1016/j.nima.2005.04.002

where E_0 is the electric monopole interaction, M_1 is the magnetic dipole interaction, E_2 is the electric quadrupole interaction. Each term of the series is a product of one of the nuclear moments by the corresponding component of the extranuclear electromagnetic field. As the interaction energy rapidly decreases with increasing multipolarity, the dipole/quadrupole interactions alone are usually dealt with. Thus, knowing the magnetic dipole moment and the electric quadrupole moment of the probe nucleus, we may determine the electromagnetic fields of the probe nucleus surroundings.

The main methods used to study HFI are the nuclear orientation method, nuclear magnetic resonance method, Mössbauer effect, and method of perturbed angular correlations (PAC) of nuclear radiation cascades.

One of the major advantages of the PAC method is that it allows experiments to be carried out with samples in any aggregate state, in a wide range of pressures, temperatures, and external electromagnetic fields, with extremely small concentrations of probe nuclei (probe radionuclides) down to 10^{-15} M. As a result, it is possible to investigate a wide range of objects from gaseous substances to biological samples measured in vivo.

The PAC method requires spectrometers that provide data taking with a good statistical accuracy within reasonable measurement time. The efficiency of PAC spectrometers is mainly increased by increasing the number of detectors to four or six, as a rule.

To decrease the load of the accumulation equipment in the PAC spectrometers, only signals passed through the preliminary energy selection are applied to the time-to-amplitude converter (TAC) [1–3]. Since the energy selection requires time, either fast analogue signals are delayed [2], which may result in worse time resolution, or only the fast component of scintillation (BaF_2) is used [3], which worsens the energy resolution. Sometimes trade-off decisions are taken, e.g. partial collection of the slow component (BaF_2) is carried out with a small time signal delay [1]. Note that in all above-mentioned spectrometers the energy selection of gamma-quanta is carried out by hardware. In addition, the above detectors are made to work only with a particular type of detectors.

PAC spectrometers were designed and constructed by groups of physics engaged in solving nuclear-physics problems. Recently, PAC methods have found wide use in other sciences, such as solid state physics, chemistry, medicine, etc. To make PAC widely used, it is necessary to have spectrometers which do not require sophisticated set-up procedures and which allow a wide range of radioactive isotopes to be used as probes. Development of electronic and computer circuitry and components makes it possible to develop such spectrometers.

We have developed a four-detector spectrometer which can be used with different types of detectors and with all radionuclides suitable for PAC measurements. Preliminary selection for reducing the load of the equipment is done by time, and the energy selection is carried out by using the accumulation program and codes corresponding the total detector charge collection. Special devices are built into the spectrometer to increase the measurement accuracy and to make set-up (operation) easier. This spectrometer is used to carry out investigations in solid state physics [4] and physical chemistry [5].

2. Block diagram and operation of the spectrometer

The block diagram of the PAC spectrometer is displayed in Fig. 1.

Detectors of the spectrometer (DET1–DET4) are cylinder-shaped BaF_2 or NaI(Tl) crystals, 40×40 mm in size, optically connected to the XP2020Q photomultiplier.

Time referencing is by the anode signal of the detector, the CANBERRA 2126 constant fraction discriminator (CFD) is used. The dynode output of the photomultiplier is connected to the shaping spectrometric amplifier (Ampl).

The hardware and software of the spectrometer provide two modes of operation:

- basic mode, in which 12 time spectra (TS) and four energy spectra are recorded,
- set-up mode, in which energy windows may be set up and operation of detector sections may be controlled.

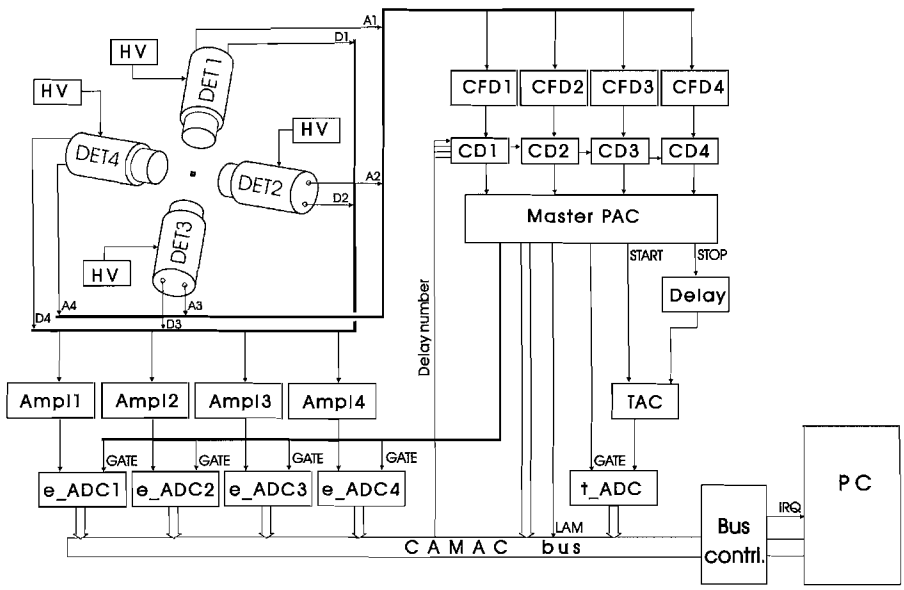

Fig. 1. Block diagram of the four-detector spectrometer.

During the experiment (basic mode), the Master PAC unit provides selection of two events coinciding in time for any pair of the detectors. The coincidence time range is set by the switch on the front panel of the unit. In the case of coincidences, the Master PAC produces GATE signals turning on the recording instruments while at the START and STOP outputs information pulses are generated. The time interval between them is equal to the interval between signals from the detectors. The time selection in the Master PAC reduces the accidental signal load of the recording instruments by 2–3 orders of magnitude.

The TAC unit (ORTEC 467 time-to-amplitude converter) receives START signals directly from the Master PAC and STOP signals through the cable delay (DELAY) and generates pulses with an amplitude proportional to the START–DELAY/STOP time interval. Positions of switches on the Master PAC and TAC and the DELAY value determine the time interval measurement range. Signals from the TAC and the amplifiers Ampl1–Ampl4 arrive at the analogue-to-digital converters, time t_ADC and energy e_ADC1–e_ADC4 ones, respectively. Master PAC pulses GATE trigger the ADC and LAM-IRQ signals launch the data recording procedure in the PC.

The data recording procedure involves the "hardware interruption" mechanism. The data reading program itself is a resident, i.e. it is permanently stored in the main memory of the computer. The resident procedure and "hardware interruptions" ensure a high rate of the PC response to the LAM-IRQ signal and comfortable display of accumulated data. After the procedure is started in the PC and conversion is completed in the ADC, the data arrive at the computer through the controller "Bus contrl." Then the data transfer energy selection begins and the measuring instruments are set ready for recording the next events while processing of the last event is still on; that is, the instrumentation and the PC operate in parallel in the "pipeline" mode. This organization allows the dead time to be reduced by 20–30%.

In the Master PAC, fast time selection is effected at high input loads, in the computer energy selection-sorting is effected by e_ADC codes. Before the experiment, two energy windows are set in the program for each detector, $\Delta E\gamma_1$ corresponding to the γ-quantum populating the intermediate level and $\Delta E\gamma_2$ corresponding to the γ-quantum de-exciting it. The code of each e_ADC is compared with the windows $\Delta E\gamma_1$ and $\Delta E\gamma_2$ set for it. If the code of one of the time-coincident

e_ADCs falls within the window $\Delta E\gamma_1$ and code of the other e_ADC falls within its preset window $\Delta E\gamma_2$, the event is considered useful. The operation of a pair of detectors (six variants for four detectors) and the result of the energy selection (two variants) form 12 TS to which the t_ADC code will be added.

The codes from the e_ADC are used not only for selection of t_ADC codes but also for accumulation of four energy spectra, i.e. the code of each triggered e_ADC is recorded in the corresponding energy spectrum. The shape of these spectra is used to check the operation stability of the detectors during the experiment and may later be used to normalize TS.

The spectrometer makes it possible to carry out experiments in the multidimensional analysis mode. In this case, ADC codes for each event may be stored on an event-by-event basis, i.e. files are formed where each event consisting of the codes of two e_ADC and one t_ADC is successively written. After these files are written, TS of interest may be formed by optimizing boundaries of energy windows and other parameters.

In a spectrometer like this, the number of detectors can be easily varied. There are no problems with increasing the number of energy windows for any detector and with adding pressure, temperatures detectors and others.

Checking and setting-up are particularly troublesome procedures in PAC spectrometers. To cope with most problems arising in the set-up mode, additional procedures in the program and a special mode of operation of the Master PAC are provided.

When the programmed set-up/test procedure is started by a command from the computer, the Master PAC is switched to the test mode. In this case, e_ADCs are triggered by each detector signal. After conversion the code of an e_ADC is stored in the computer. Energy spectra are constructed for each detector. On the basis of their shape,

- operation of the detectors is appraised,
- energy ranges of detector operation are selected by varying the high voltage of the photomultiplier (HV unit) and the amplification factor (Ampl unit),
- CFD thresholds are set,
- boundaries of the energy windows $\Delta E\gamma_1$ and $\Delta E\gamma_2$ are set.

All settings are made without an oscilloscope and without reconnection of units. The spectrometer can be periodically switched to the test mode during data taking without interrupting measurements.

Energy selection of events in the computer, unlike the traditional one with the use of differential discriminators, allowed the operation of the spectrometer to be much simpler, the data taking control to be improved, the energy selection to be optimized, and the spectrometer set-up time to be reduced.

3. Master PAC

The only specialized unit of the spectrometer is the Master PAC. As mentioned in the previous section, the Master PAC may operate in two modes, basic and set-up. The desirable mode is selected by the PC command.

Basic mode functions:

- determination of signals from any two detectors which coincided within the preset time range (for four detectors there are six variants),
- generation of the START and STOP pulses with the interval between them equal to the interval between the CFD signals,
- triggering of ADCs and launching the procedure of reading data into the computer,
- transmission of the numbers of the detectors whose signals appear at the START and STOP outputs to the computer.

Depending on the time interval between the signals from the detectors, two versions of the basic mode of operation are possible.

One is when operation of one of the detectors is not followed within the present time interval by operation of the other three detectors for they did not detect radiation, i.e. there are no coincidences. In this case, the Master PAC returns to the initial state as fast as possible for receiving next signals.

This initialization time is less than 100 ns (i.e. considerably smaller than initialization in TAC). With the event rate 1,00,000 events/s at all inputs the counting errors do not exceed 1%.

The other is when two detectors detected radiation simultaneously or one after the other within the preset time interval, i.e. coincidence is detected. Interaction of spectrometer units in this case is described in the previous section. While conversion of the analogue signals to code and their transfer to the computer take place, the Master PAC inputs are closed. For our spectrometer this time varies from 10 to 20 μs. After the data transfer is completed, computer sends the Reset signal. By this signal all spectrometer units are initialized and the Master PAC inputs switch to the open state. The number of coincidences for a four-detector PAC spectrometer do not normally exceed 2000 events/s. At such a load the dead time of the spectrometer is no larger than 4%, and the total dead time, with no-coincidence cases (1%) taken into account, will be less than 5%.

In the set-up mode, the Master PAC supplies GATE signals to the e_ADC each time there appears a signal from the CDF (irrespective of coincidences).

Setting up of the Master PAC itself consists in setting the coincidence time, which is done by the "Time of coincidence" switch on its front panel. There are eight options: 100, 200, 300, 400, 500, 600, 700, and 800 ns.

4. Software for the γγ-PAC spectrometer

The operation of the spectrometer is controlled by the IBM-compatible computer which is a part of the spectrometer. Most of the software is in PASCAL. Parts of the programs critical for their execution are in ASSEMBLER. Now a version of the accumulation program with on-line visualization is developed for working under the Linux operating system with using ROOT 3.10 environment.

The program allows accumulation of four energy spectra and 12 TS (Fig. 2). To each of the 12 TS there corresponds its own combination of the triggered detectors and the energy windows $\Delta E\gamma_1$ and $\Delta E\gamma_2$. The program regularly saves the data on a disc without interrupting measurements.

5. Suppression of interchannel interference

Interchannel interference (pick-up) is a common problem of multichannel spectrometers. In our case, this interference manifests itself as wave-like structures in the spectra of delayed coincidences. Fig. 3 shows a spectrum of accidental coincidences from two detectors measured with a ^{137}Cs source. A wave-like structure is seen in the spectrum.

It was decided to solve this problem by using the statistical level-off method ("sliding scale" method) developed by Gatti [6]. An additional unit CD (see Fig. 1) with a few cable delays (four in our case) is installed in each of the four channels of the spectrometer. The delays vary from 1 to 20 ns, which corresponds to the pick-up "period". The delay duration is changed by the PC command.

During measurements, the program periodically (e.g. once a minute) changes the combination of delays in the units. On detection of an event, the time ADC code changes by a value corresponding to the given combination of delays. Thus, the spurious effect is "leveled off" while the useful signal remains as it is. Fig. 4 shows two TS measured with the (^{137}Cs + ^{60}Co) source without (a) and with (b) the use of the "sliding scale" method. The interference is seen to be appreciably suppressed while the peak of prompt coincidences is not smeared out.

6. PAC measurement at high pressure

The main advantages of the PAC method for studying materials under high pressure are

- the possibility of using isotopes with a sufficiently high γ-radiation energy, which considerably simplifies technical support of the experiment,
- a small (0.3–0.5 mm^3) volume of samples.

A many-stage high-pressure apparatus of the "matryoshka" type [7] allows a pressure up

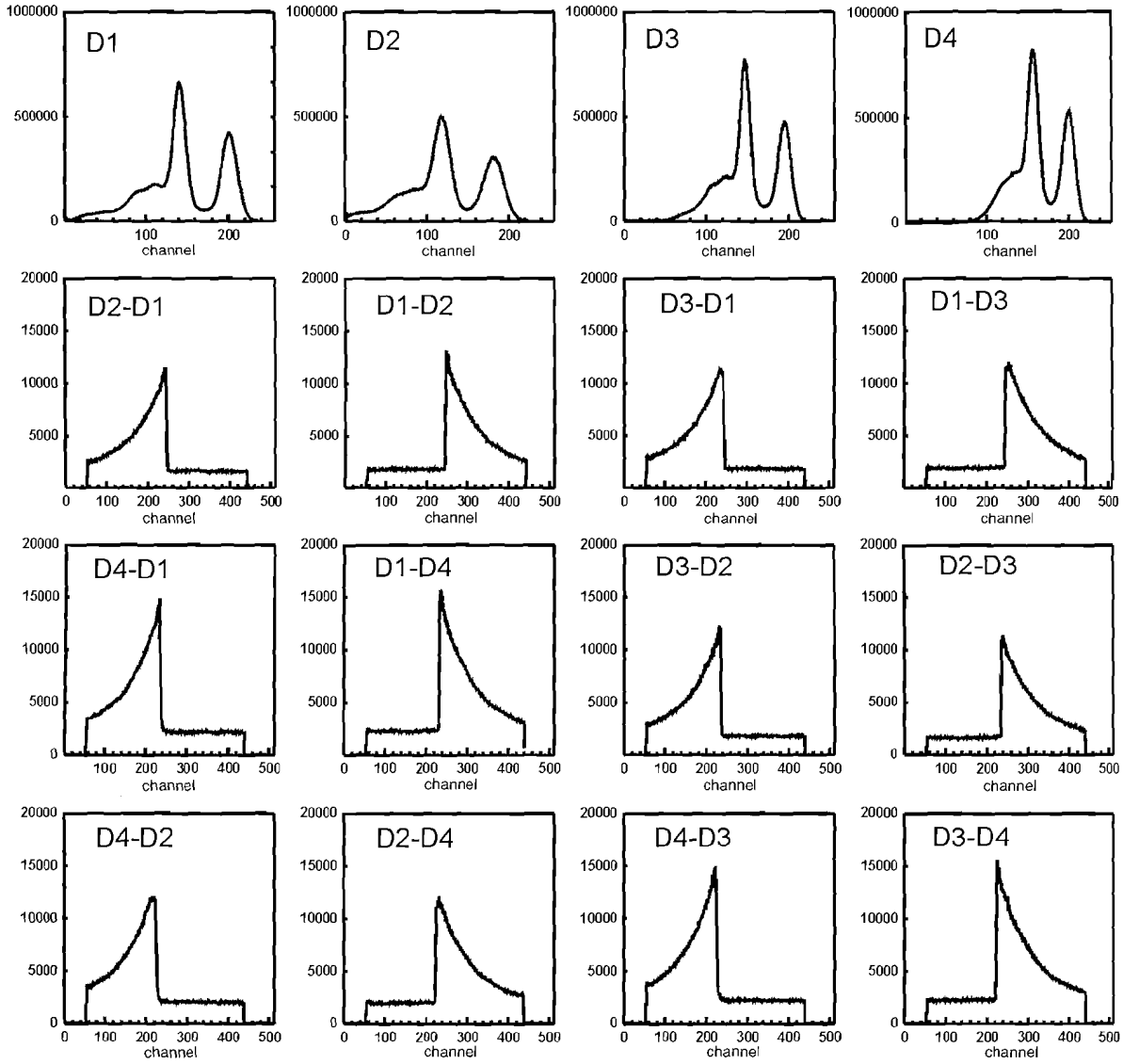

Fig. 2. Four energy spectra and 12 time spectra obtained with ^{111}In.

to 60 GPa to be generated in a volume sufficient for PAC measurements in a sample under pressure at the temperature of liquid nitrogen and higher.

To carry out under-pressure PAC measurements, the four-detector spectrometer is equipped with a small-size hydraulic four-arm press of capacity up to 300 t, which makes it possible to use the many-stage high-pressure apparatus (Fig. 5). A "toroid"-type chamber [8] is used as the first stage. Its holes 10 and 15 mm in diameter allow generation of pressure up to 10 and 8 Gpa, respectively. Bridgman anvils are used as the second stage. They are made either of carbonado (sintered artificial diamonds) or of sintered natural diamonds, which allows pressures about 60 GPa to be attained.

Resistance transitions of reference substances or residual quartz density-against-pressure curves were used to calibrate the apparatus [7].

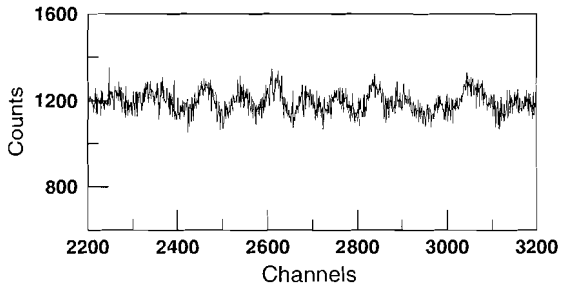

Fig. 3. Spectrum of accidental coincidences measured with a ^{137}Cs source.

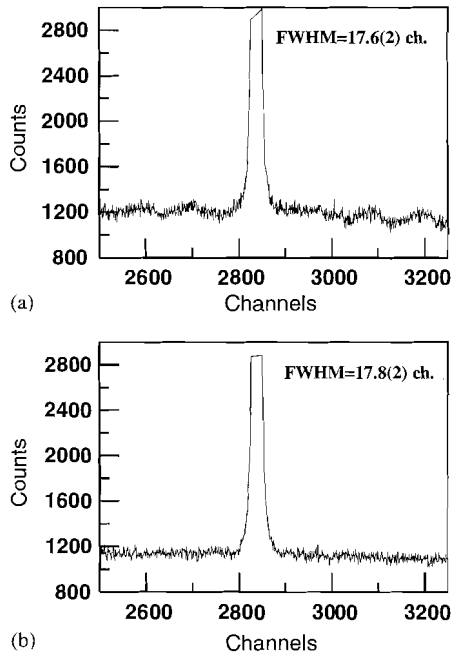

Fig. 4. Time spectra measured with the (^{137}Cs + ^{60}Co) source.

Quartz and catlinite (Ca and Al oxide) or pyrophyllite were used as a medium transferring and maintaining pressure.

7. Thermostatting system

The spectrometer is equipped with a thermostat and a high-temperature oven to measure temperature dependence of the HFI parameters.

The thermostat chamber (Fig. 6) is tightly fixed on the upper end of the evacuated siphon with vacuum insulation. The siphon enters the Dewar vessel with liquid nitrogen through the air-tight seal in its neck. The pressure in the Dewar vessel is a few millibars higher than the atmospheric pressure. Cold nitrogen vapour moves over the siphon from the vapour region through the heat exchanger at the bottom of the Dewar vessel to the experimental chamber. The cold nitrogen vapour is heated to the required temperature by the electric heater inside the isothermal unit. A thermocouple and commercial electronic devices intended for controlling industrial processes are used to control and stabilize temperature. Then the heated gas uniformly cools the experimental ampoule on all sides and passes to atmosphere over the spiral groove between the foam plastic plug and the body of the experimental chamber. The thermostat makes it possible to cover the temperature range from 120 to 350 K and to maintain the temperature with an error of 0.5 K.

The main element of the high-temperature oven (Fig. 7) is the refractory block with four cone-shaped windows to let radioactive radiation from the sources under study pass to the detectors and a vertical channel to accommodate the heater. The block is made of foam chamotte brick. The cone-shaped space of the windows is insulated with Goodfellow refractory wool of non-woven aluminium oxide fibres. The wool is kept in the windows by a thin capton film. The electric tantalum-wire heater of the oven is wrapped on an aluminium oxide pipe inserted with its closed end up in the channel of the block. The rest of the oven space inside the steel body is filled with foam chamotte crumb. Temperature is stabilized and controlled in the range up to 1300 K by a computer through the above-mentioned electronic devices (Figs. 8 and 9).

8. Construction of the anisotropy function

The procedure for construction of the anisotropy function from the TS is as follows.

1. For all TS, "zero" channels are determined from the independent measurement of the spectra of prompt coincidences with ^{60}Co. Six spectra are rotated with respect to their "zero"

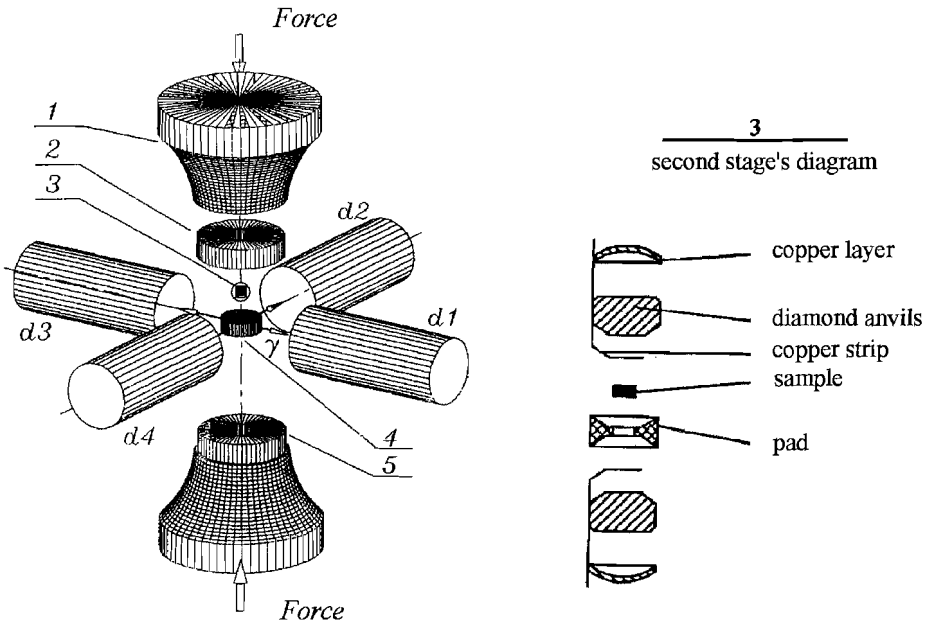

Fig. 5. Schematic view of the apparatus for high-pressure PAC measurements: 1—support transferring force from the press; 2, 5—first stage of the high-pressure chamber, upper and lower parts; 3—second state of the high-pressure chamber and a sample (right: schematic view of the second stage assembly); 4—catlinite cell transferring and maintaining pressure.

and then all spectra are adjusted by the "zero" channels.

2. The TS are normalized to the number of counts in the windows $\Delta E\gamma_1$ and $\Delta E\gamma_2$. The normalization coefficient K_i for the ith TS is

$$K_i = \frac{SS_i}{\min\{SS_i\}}, \tag{1}$$

where $SS_i = S_{\text{start}} \cdot S_{\text{stop}}$; S_{start}, S_{stop} are the numbers of events in the windows of energy spectra corresponding to the "start" and "stop" γ-quanta for a particular TS.
A spectrum is normalized:

$$n_i^\theta(t) = \frac{N_i^\theta(t)}{K_i}, \tag{2}$$

$N_i^\theta(t)$, $n_i^\theta(t)$ are the numbers of events in the ith TS for the angle θ (90° and 180°) before and after normalization.

3. The background from accidental coincidences is taken into account:

$$C_i^\theta(t) = n_i^\theta(t) - F_i^\theta(t), \tag{3}$$

$C_i^\theta(t)$ is the number of true coincidences, $F_i^\theta(t)$ is background from accidental coincidences.

4. TS are multiplied channel by channel:

$$X_{90}(t) = \left[\prod_{i=1}^{8} C_i^{90}(t)\right]^{1/8}, \tag{4a}$$

$$X_{180}(t) = \left[\prod_{i=1}^{4} C_i^{180}(t)\right]^{1/4}. \tag{4b}$$

5. The anisotropy function is calculated:

$$R(t) = 2\frac{X^{180}(t) - X^{90}(t)}{X^{180}(t) + 2X^{90}(t)}. \tag{5}$$

6. The statistical error $\sigma_{R(t)}$ is calculated:

$$\sigma_{R(t)} = 6\frac{X^{180}(t)X^{90}(t)}{(X^{180}(t) + 2X^{90}(t))^2} \times \left[\sum_\theta \frac{1}{N_\theta^2}\sum_{t=1}^{N_\theta}\frac{C_i^\theta(t) + 2F_i^\theta(t)}{C_i^\theta(t)^2}\right]^{1/2}. \tag{6}$$

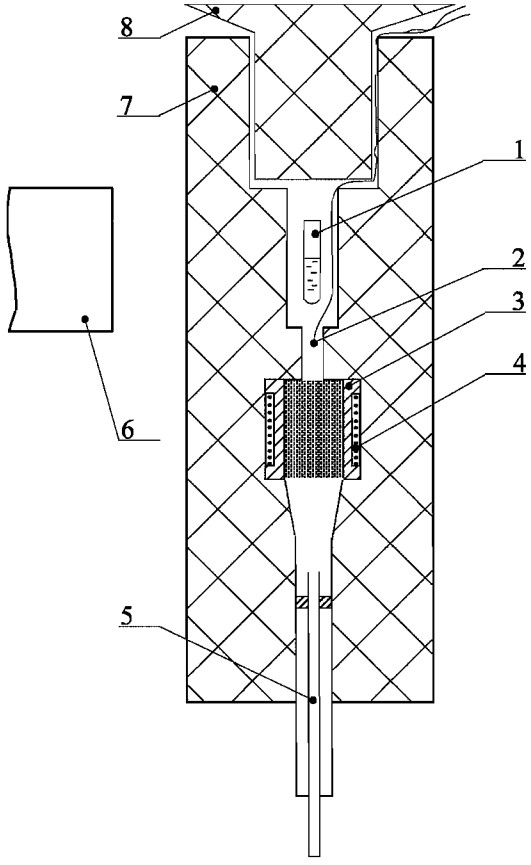

Fig. 6. Head part of the thermostat: 1—capsule with a sample to be studied; 2—thermocouple; 3—isothermic heat exchanger of sintered large-grain copper powder; 4—heater; 5—evacuated siphon; 6—detector; 7—foam plastic heat insulation; 8—foam plastic plug.

The channel division value in the TS for further calculations is determined from the independent measurement with a calibrated delay introduced before time-to-amplitude conversion.

9. Experimental results and conclusion

A four-detector spectrometer of perturbed angular $\gamma\gamma$ correlations is developed with the following characteristics:

- time range 1–800 ns;
- time resolution (^{60}Co 1173–1332 keV) 200 ps with BaF_2, 2.0 ns with NaI(Tl);

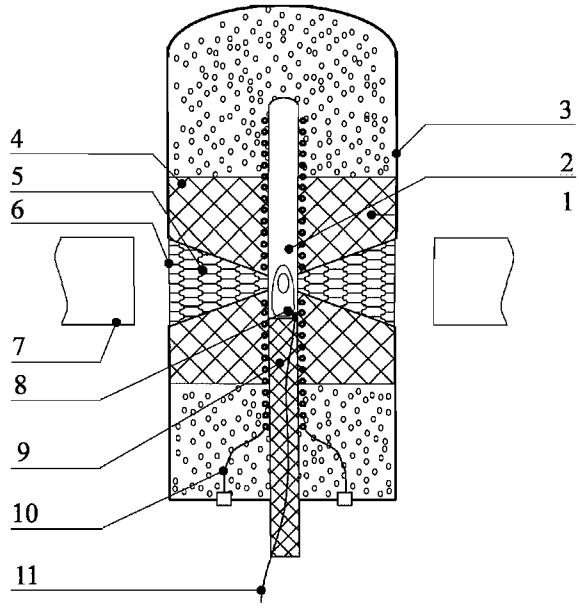

Fig. 7. High-temperature oven: 1—refractory block; 2—aluminium oxide pipe; 3—stainless-steel body; 4—chopped foam firebrick; 5—refractory wool of thin aluminium oxide fibres; 6—thin capton foil; 7—detector; 8—refractory air-tight capsule with a sample; 9—heat plug; 10—heater; 11—thermocouple.

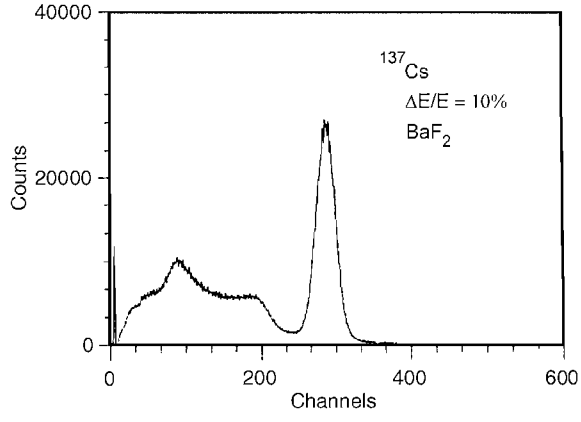

Fig. 8. ^{137}Cs energy spectrum.

- energy resolution (^{137}Cs 662 keV) 10% with BaF_2, 8% with NaI(Tl).

A wide range of investigations in solid state physics and physical chemistry were carried out

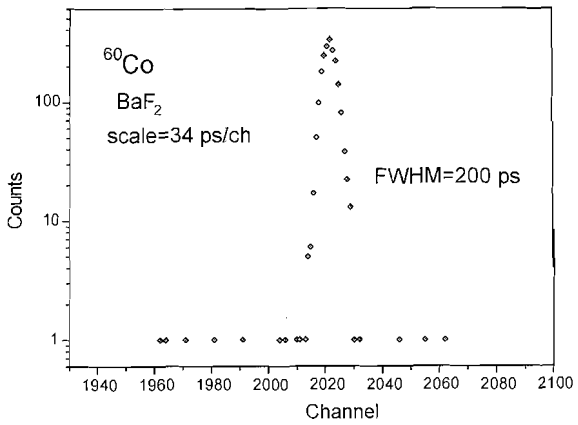

Fig. 9. Spectrum of prompt coincidences with the ^{60}Co source.

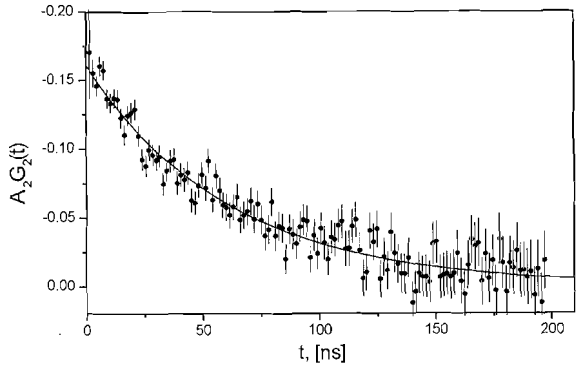

Fig. 10. Dynamic character of PAC (^{111}In(EC)^{111}Cd) in ice.

with the PAC spectrometer, in particular PAC investigations in frozen aqueous solutions with the use of ^{111}In(EC)^{111}Cd. One of the measured anisotropy spectra is shown in Fig. 10.

These measurements revealed the mechanism for the dynamic character of PAC in ice. Fluctuation of the electric field gradient in this system was attributed to mobility of ion and orientation defects [5].

The angular correlation anisotropy spectrum for ^{111}Cd nuclei in $LaRu_2$ (Fig. 11) is processed by the DEPACK program [9]. The HFI parameters ($\nu_Q = 242(3)$ MHz, $V_{zz} = (1.2 \pm 0.2) \times 10^{18}$ V/cm^2) derived from this spectrum are in good agreement with the results derived from the spectra measured with a three-detector spectrometer of the Institute of Nuclear Physics, Moscow State University [10].

Temperature dependence of the EFG on ^{111}Cd nuclei at boron sites was measured in the superconductor MgB_2 synthesized at a pressure of 8 GPa. The experimental and calculated EFG values were in good agreement [4].

The measuring complex described in the paper will allow on-line studies of variation in the electric field gradient on ^{111}Cd impurity nuclei with valence of rare-earth ions in Laves cubic phases.

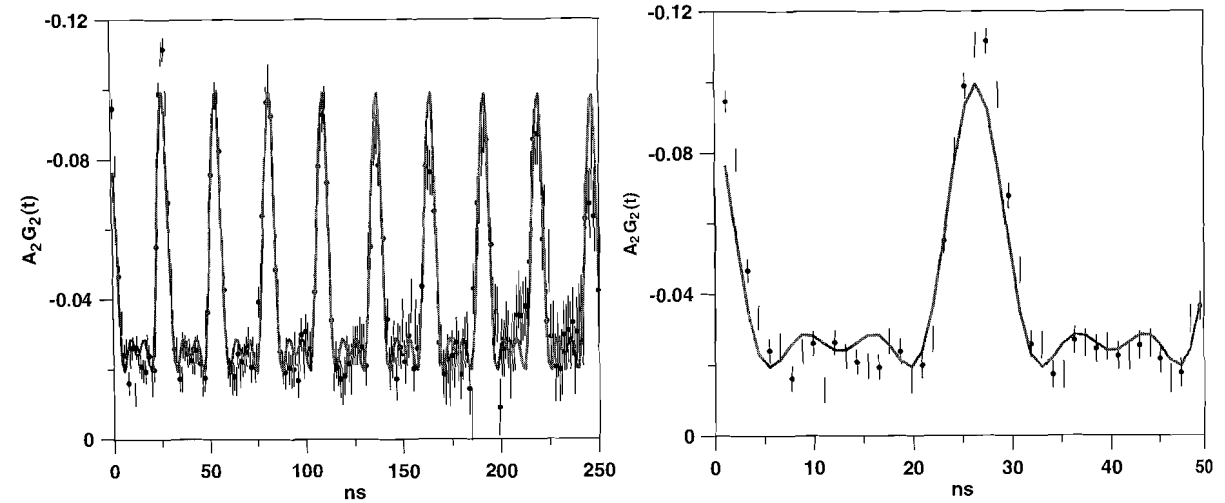

Fig. 11. Angular correlation anisotropy spectrum for ^{111}Cd nuclei in $LaRu_2$.

Acknowledgements

The authors are grateful to A.F.Novgorodov (Joint Institute for Nuclear Researches, Dubna, Russia) for support and Michal Rams (Institute of Physics, Jagellonian University, Cracow, Poland) for allotting a software package for processing of anisotropy spectra.

Financial support received from the Russian Foundation for Basic Research (Projects 03-03-32120, 04-02-16061) during the final period of the work is acknowledged.

References

[1] A. Baudry, et al., Nucl. Instr. and Meth. A 260 (1987) 160.
[2] T. Butz, et al., Nucl. Instr. and Meth. A 284 (1989) 417.
[3] A. Bartos, et al., Nucl. Instr. and Meth. A 330 (1993) 132.
[4] A.V. Tsvyashchenko, L.N. Fomicheva, M.V. Magnitskaya, E.N. Shirani, V.B. Brudanin, D.V. Filossofov, O.I. Kochetov, N.A. Lebedev, A.F. Novgorodov, A.V. Salamatin, N.A. Korolev, A.I. Velichkov, V.V. Timkin, A.P. Menushenkov, A.V. Kuznetsov, V.M. Shabanov, Z.Z. Akselrod, Solid State Commun. 119 (3) (2001) 153.
[5] Z.Z. Akselrod, A.I. Velichkov, N.A. Korolev, O.I. Kochetov, N.A. Lebedev, M. Milanov, A.F. Novgorodov, V.V. Timkin, D.V. Filossofov, E.N. Shirani, Izv. Akad. Nauk RF Ser. Fiz. 65 (7) (2001) 1077.
[6] E. Gatti, V. Svelto, C. Cottini, Nucl. Instr. and Meth. 24 (1963) 241.
[7] Ya.R. Bilyalov, A.A. Kaurov, A.V. Tsvyashchenko, Rev. Sci. Instrum. 63 (4) (1992) 2311.
[8] L.G. Khvostantsev, L.F. Vereschagin, A.P. Novikov, High Temp. High Pressures 9 (1977) 637.
[9] Bengt Lingren, Hyperfine Interact. (C) 1 (1996) 613.
[10] A.V. Tsvyashchenko, L.N. Fomicheva, A.A. Sorokin, G.K. Ryasny, B.A. Komissarova, L.G. Shpinkova, K.V. Klementev, A.V. Kuznetsov, A.P. Menushnkov, V.N. Trofimov, A.E. Primenko, R. Cortes, Phys. Rev. B 65 (2002) 1745XX.

Radiochim. Acta **95**, 319–327 (2007) / **DOI** 10.1524/ract.2007.95.6.319

A ^{140}Nd/^{140}Pr radionuclide generator based on physico-chemical transitions in ^{140}Pr complexes after electron capture decay of ^{140}Nd-DOTA

By K. P. Zhernosekov[1], D. V. Filosofov[2], S. M. Qaim[3] and F. Rösch[1,*]

[1] Institut für Kernchemie, Johannes Gutenberg-Universität, 55128 Mainz, Germany
[2] Joint Institute of Nuclear Research, Laboratory of Nuclear Problems, 141980 Dubna, Russian Federation
[3] Institut für Nuklearchemie, Forschungszentrum Jülich GmbH, 52425 Jülich, Germany

(Received July 1, 2006; accepted in revised form January 2, 2007)

Radionuclide generator / Radiolanthanides / Hot atom chemistry / Radiochemical separation / Positron emission tomography

Summary. ^{140}Nd was produced by irradiations of CeO_2 and Pr_2O_3 targets leading to ^{nat}Ce(^{3}He,*xn*)^{140}Nd and ^{141}Pr(*p*,2*n*)^{140}Nd nuclear reactions. The practical yield of ^{140}Nd at EOB in the former reaction over the energy range of $E_{^3\mathrm{He}} = 33.5 \rightarrow 0$ MeV amounted to 3.5 MBq/μA h and in the latter reaction over the energy range of $E_\mathrm{p} = 18.6 \rightarrow 16.2$ MeV to 15.5 MBq/μA h. These values correspond to about 41% and 60% of the respective theoretical values. Successful separations of the radionuclide were performed by means of cation-exchange chromatography resulting in decontamination factors of $\geq 10^8$ and $\geq 7 \times 10^5$ for the cerium and praseodymium target materials, respectively. With the no-carrier-added ^{140}Nd obtained, an efficient ^{140}Nd/^{140}Pr radionuclide generator system was developed and evaluated. The principle of the radiochemical separation is based on physico-chemical transitions (hot-atom effects) of the daughter ^{140}Pr following the electron decay process of ^{140}Nd. The parent radionuclide ^{140}Nd(III) is quantitatively adsorbed on a solid phase matrix in the form of ^{140}Nd-DOTA-conjugated complexes. The daughter nuclide ^{140}Pr is generated in an ionic species and is easily separated using low volumes of various aqueous eluents. The elution yield is at least 93%, if an optimized eluent, such as DTPA solution is applied. The system remains stable at least over three half-lives of ^{140}Nd, with high radiolytic stability and low ^{140}Nd breakthrough. This radionuclide generator system ^{140}Nd ($T_{1/2} = 3.37$ d) provides the short-lived positron-emitting radiolanthanide ^{140}Pr ($T_{1/2} = 3.4$ min) for molecular imaging using positron emission tomography (PET).

1. Introduction

A radionuclide generator is a concept based on a nuclear genetic relationship, resulting in a chemical system which permits continuous isolation of a short-lived daughter radionuclide from its long-lived radioactive mother nuclide. Radionuclide generators provide an alternative and often more convenient source of radionuclides compared to direct production routes at rather complex facilities such as accelerators and nuclear reactors.

There are several radiolanthanide generator pairs of interest [1]. Commonly used radionuclide generator systems are based on conventional separation methods (*e.g.* cation-exchange, extraction chromatography, liquid-liquid extraction, *etc.*), and entail sufficient chemical differences between mother and daughter radionuclides as an essential requirement. If parent/daughter radionuclides are $_Z$Ln/$_{Z\pm1}$Ln due to the chemical similarity of the two adjacent members of the lanthanide series, however, those radiochemical techniques may not be applicable. Therefore alternative and in principle new radiochemical concepts have to be developed in order to realize the generator systems of radiolanthanides.

^{140}Nd (EC = 100%, $T_{1/2} = 3.37$ d) produces a short-lived intermediate positron emitter ^{140}Pr ($\beta^+ = 49\%$, $E_\mathrm{max} = 2.4$ MeV, $T_{1/2} = 3.4$ min) which decays to stable ^{140}Ce. The pair ^{140}Nd/^{140}Pr shows potential as a radionuclide generator or as an *in vivo* generator system for PET [2, 3].To develop further the short-lived positron emitter ^{140}Pr for clinical application, a ^{140}Nd/^{140}Pr radionuclide generator system needs to be designed. For application of the system in the form of an *in vivo* generator (*i.e.* direct labelling of biomolecules with the long-lived ^{140}Nd which, after targeting and accumulation at the specific disease sites, generates ^{140}Pr *in situ*), a consideration of the chemical effects following nuclear transitions is required.

The physico-chemical processes occurring after the primary radioactive decay, such as electron capture (EC) and/or Auger electron emission or X-ray emission, can cause changes in the chemical state of the generated daughter nucleus. In the case of electron capture or internal conversion these "post-effects" are known to provide the possibility of separation of different chemical forms of the parent and daughter radionuclides [4–6]. Attempts to separate neighbouring lanthanides have been reported for several cases as well [7, 8]. An initial prototype of continuous separation (a radionuclide generator system) of type $_Z$Ln/$_{Z\pm1}$Ln was reported for the ^{140}Nd/^{140}Pr pair [7]. In that work the parent radionuclide ^{140}Nd was adsorbed in the form of a DTPA (diethylene triaminepentaacetic acid) complex

*Author for correspondence (E-mail: frank.roesch@uni-mainz.de).

on an anion-exchanger (Dowex 1, Wofatit SBW). The generated daughter radionuclide ^{140}Pr, stabilised in a cationic form, was eluted with 10^{-6} M solution of a carrier (stable lanthanide). This approach provided $30 \pm 15\%$ yield of the daughter radionuclide. The breakthrough of the parent ^{140}Nd was in the range of 0.2%–0.3%.

In the present work we report on a quantitative evaluation of "post-effects" for ^{140}Pr(III) formed following electron capture decay of ^{140}Nd-DOTA (DOTA = 1,4,7,10-tetraazacyclododecane-1,4,7,10-tetraacetic acid). Furthermore an efficient ^{140}Nd/^{140}Pr radionuclide generator system, based on physico-chemical transitions in this type of complex, is described.

First, the chemical fate of ^{140}Pr is studied by separation of the different chemical forms of the parent and the daughter radionuclides. The daughter ^{140}Pr is released from its chemical micro-environment. DOTA is well known to offer excellent thermodynamic stability and kinetic inertness, particularly for complexes with trivalent metals such as lanthanides [9]. Rapid formation of ^{140}Pr-DOTA complex is inhibited by the kinetic inertness of DOTA. The same is true for the radionuclide exchange. Thus, the fraction of "free" ^{140}Pr, *i.e.* non ^{140}Pr-DOTA, can be effectively separated from the ^{140}Nd-DOTA complex. The other point to realise in the ^{140}Nd/^{140}Pr radionuclide generator system is (a) to synthesise and (b) to stabilise the parent radionuclide ^{140}Nd in form of a ^{140}Nd-DOTA complex on a solid phase. Due to the high thermodynamic stability and kinetic inertness of ^{140}Nd-DOTA type complexes (as mentioned above), the release of the long-lived parent radionuclide ^{140}Nd is inhibited at room temperature. ^{140}Nd-DOTA or ^{140}Nd-DOTA-conjugated compounds are adsorbed on selected resins/cartridges. This immobilises ^{140}Nd and allows an effective continuous separation of ^{140}Pr, *i.e.* representing a ^{140}Nd/^{140}Pr radionuclide generator system.

2. Experimental

2.1 Reagents and materials

Only analytical-reagent grade chemicals and Milli-Q water (18.2 MΩ cm) were used. Cation-exchange resins Bio-Rad AG 50W-X8, 200–400 mesh and minus 400 mesh, and Aminex A6 were used to prepare chromatography columns. DOTA-DPhe^1-Tyr^3-octreotide (DOTATOC) was kindly provided by Novartis Pharma AG. For preparation of a ^{140}Nd/^{140}Pr radionuclide generator, a C-18 cartridge, Phenomenex Strata-X Tube, 30 mg, was used.

Complex formation yields were controlled by TLC on aluminium sheets, silica gel 60, and 0.1 M Na_3Citrate as eluent. Measurement of the radionuclidic composition was done by γ-ray spectrometry using an HPGe detector.

2.2 Production of ^{140}Nd

2.2.1 ^{nat}Ce(^{3}He,*xn*)^{140}Nd

^{140}Nd was produced by irradiation of natural cerium oxide target with ^{3}He-particles of 36 MeV primary energy at the CV 28 cyclotron of the Forschungszentrum Jülich as described earlier [2]. The target consisted of 500 mg CeO_2 (99.999%, Sigma Aldrich) and was compressed to a pellet of 13 mm diameter. The pellet was placed in the groove of a target holder and covered by a 25 μm thick Cu foil. The target holder was cooled by a stream of water flowing at the back. An average beam current of 2.6 μA and an irradiation period of 4 hours were applied. A defocussed and wobbled beam was used. The beam current was measured by a charge integrator.

2.2.2 ^{141}Pr(*p*, 2*n*)^{140}Nd

In addition, ^{140}Nd was produced by irradiation of praseodymium oxide with protons of 19 MeV primary energy at the CV 28 cyclotron of the Forschungszentrum Jülich. The target consisting of 200 mg Pr_2O_3 (99.999%, Sigma Aldrich) was compressed into a pellet and irradiated in a similar way as in the case of the ^{3}He-particle irradiation of Ce_2O_3. The beam current used was 3 μA and the irradiation time 4 hours.

2.3 Radiochemical isolation of ^{140}Nd from target materials

2.3.1 Chemical separation of n.c.a. ^{140}Nd(III) from macro amounts of Ce(III)

The irradiated Ce_2O_3 target contained about 35 MBq of ^{140}Nd. The activity of the co-produced praseodymium and cerium radionuclides was low, but enough for subsequent γ-ray spectrometric analysis of the distribution of elements. Radiochemical separation was performed using cation-exchange chromatography, according to a Ce(III)/Nd(III) scheme, *i.e.* not according to the Ce(IV)/Nd(III) separation as used earlier [2]. The irradiated CeO_2 (500 mg, 2.9 mmol) was dissolved in concentrated HCl. The Ce(IV) was completely reduced to Ce(III) in the presence of I^- ions. The target material was boiled with ∼ 40 ml of concentrated HCl with addition of 0.5–1 g KI for 1–1.5 h. After complete dissolution of the target material, the volume was adjusted to 110 ml with H_2O and filtered on a standard glass filter.

The solution was loaded on a primary chromatography column of 400 × 20 mm dimensions, filled with Bio-Rad AG 50W-X8, 200–400 mesh, in hydrogen form. The resin was washed with about 600 ml of 0.5 M NH_4Cl to convert the cation-exchanger to the NH_4^+-form. The lanthanides were eluted selectively using α-hydroxyisobutyric acid (α-HIBA) solutions of varying concentration at pH 4.75. In order to evaluate the optimum separation condition a gradient elution was applied. Starting with 0.26 M α-HIBA, the concentration was increased for each 60 ml eluent (see Fig. 1). The eluate was fractionated in 30 ml portions. Alternatively, the primary chromatography column was loaded with the dissolved target, the resin was washed with 0.5 M NH_4Cl, and 120 ml of 0.20 M α-HIBA were applied. The chromatographic separation in this case was performed by isocratic elution (Fig. 2). ^{140}Nd(III) was selectively eluted with 0.30 M α-HIBA solution, while Ce(III) was washed out of the resin at a concentration of 0.40 M. Next, the ^{140}Nd available was converted to the chloride form. The pH of the ^{140}Nd(III) solution (150–180 ml, 0.30 M α-HIBA) was adjusted to ∼ 1 by addition of concentrated HCl. The solution was loaded on a cation-exchange chromatography column of 90 × 8 mm dimensions, filled with Bio-Rad AG 50W-X8,

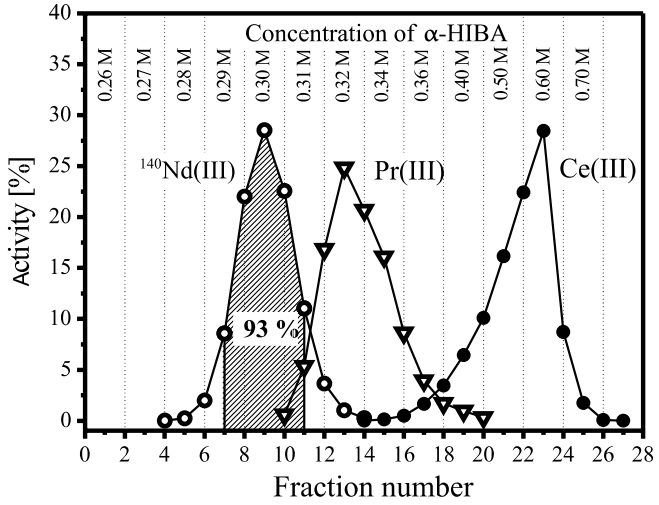

Fig. 1. ^{140}Nd(III)/Ce(III) separation. Profiles of a gradient elution on the primary chromatography column (400 × 20 mm, AG 50W-X8, 200–400 mesh). Each fraction contained 30 ml of eluted volume.

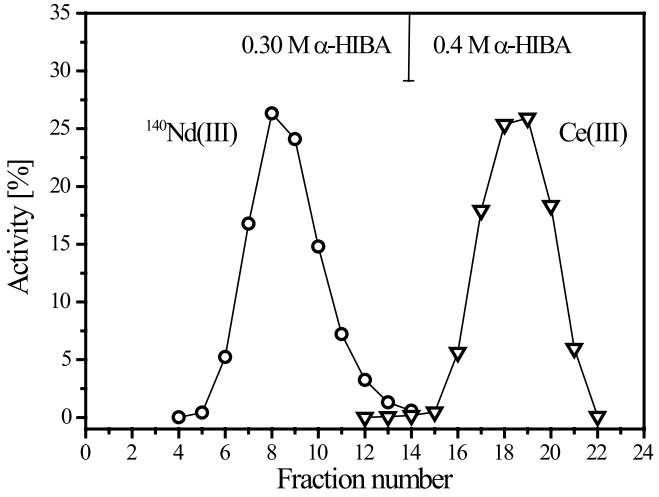

Fig. 2. ^{140}Nd(III)/Ce(III) separation. Profiles of an isocratic elution on the primary chromatography column (400 × 20 mm, AG 50W-X8, 200–400 mesh). Each fraction contained 30 ml of eluted volume.

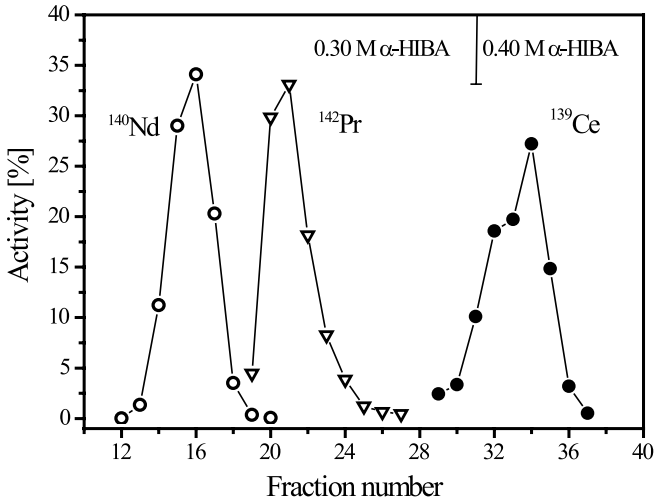

Fig. 3. ^{140}Nd(III)/Ce(III) separation. Profiles of isocratic elution on the small chromatography column (100 × 2 mm, Aminex A6). Each fraction contained 2 drops (∼ 60 µl) of eluted volume. The fractions 13 to 18 were collected to obtain pure ^{140}Nd.

200–400 mesh, hydrogen form. The resin was washed with 1 M HCl. ^{140}Nd(III) was eluted with about 20 ml of 4 M HCl. After evaporation the activity was collected in ∼ 1 ml of 0.1 M HCl.

The final purification of ^{140}Nd(III) was performed on a small Aminex A6 column (100 × 2 mm). The activity was loaded on the resin in hydrogen form from the 0.1 M HCl solution. The resin was washed with 0.5 M NH_4Cl and 0.20 M α-HIBA. ^{140}Nd(III) was selectively eluted with 0.30 M α-HIBA in a 60 µl fraction. The co-produced praseodymium radioisotopes are separated as well. The remaining Ce(III) was washed out again with 0.40 M α-HIBA. An example of the elution profile is shown in Fig. 3.

2.3.2 Chemical separation of n.c.a. ^{140}Nd(III) from macro amounts of Pr(III)

Following ^{141}Pr(p, 2n) production, about 200 MBq of ^{140}Nd were available. As no Pr radioisotope was co-produced in adequate amount, ^{142}Pr ($T_{1/2}$ = 19.13 h) was separately produced for γ-ray spectrometric analysis of the distribution of elements. Praseodymium chloride (5 mg) was irradiated at the TRIGA II reactor in Mainz at a neutron flux of 4×10^{12} cm^{-2} s^{-1} for 3 h, resulting in 93 MBq of ^{142}Pr. Radiochemical separation was performed using cation-exchange chromatography.

The cyclotron irradiated target material (200 mg Pr_2O_3, 0.6 mmol) was dissolved in 5 ml of concentrated HCl by heating (50–60 °C) for 20–30 min. After addition of $^{142/141}PrCl_3$ and 5 mmol of NH_4Cl, the mixture was evaporated under argon atmosphere. The dried residue was dissolved in 20 ml of H_2O. Due to the remaining HCl, the pH of the solution was 1–2. The mixture was passed through a standard glass filter.

The primary chromatography column was of 390 × 16 mm (V_{fr} ∼ 80 ml) dimensions, filled with Bio-Rad AG 50W-X8, 200–400 mesh. In contrast to the protocol used for separating ^{140}Nd from Ce(III), the resin was prepared in the NH_4^+-form. After loading the column with the dissolved target solution, it was washed with 120 ml of 0.20 M

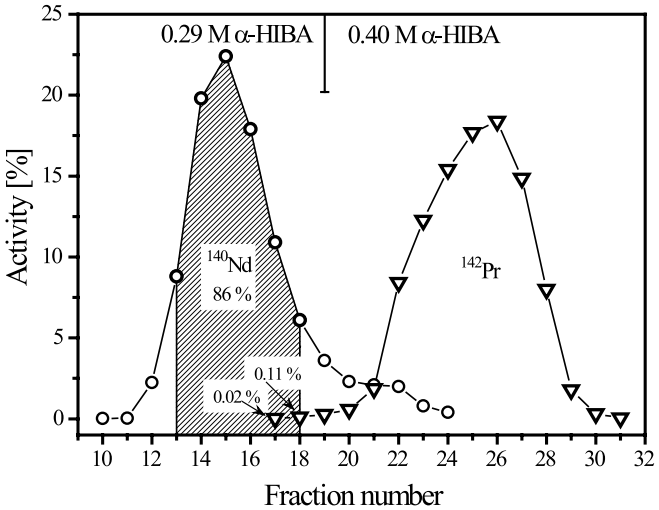

Fig. 4. ^{140}Nd(III)/Pr(III) separation. Profiles of an isocratic elution on the primary chromatography column (390 × 16.1 mm, AG 50W-X8, 200–400 mesh). Each fraction contained 12 ml of eluted volume.

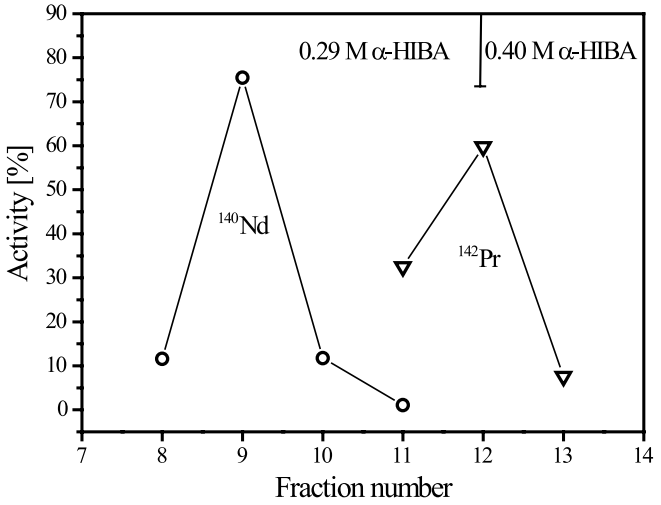

Fig. 5. ^{140}Nd(III)/Pr(III) separation. Profiles of isocratic elution on the small chromatography column (100 × 2 mm, Aminex A6). Each fraction contained 3 drops (∼ 90 µl) of eluted volume. The fractions 8 to 10 were collected to obtain pure ^{140}Nd.

α-HIBA solution. The chromatographic separation was performed by isocratic elution (Fig. 4). Each fraction contained 12 ml of the eluate. ^{140}Nd(III) was selectively eluted with 0.29 M α-HIBA solution whereas Pr(III) was washed out at an α-HIBA concentration of 0.40 M. The ^{140}Nd(III) available was converted to its chloride form using a medium chromatography column 90 × 5 mm, filled with Bio-Rad AG 50W-X8, 200–400 mesh, hydrogen form, as described above (see Sect. 2.3.1). The ^{140}Nd activity was obtained in 1 ml of a 0.25 M HCl solution.

Final purification of ^{140}Nd(III) was performed on a small Aminex A6 column (100 × 2 mm). The activity was loaded on the resin in hydrogen form from the 0.25 M HCl solution. Thereafter the resin was washed with 0.5 M NH_4Cl and 0.20 M α-HIBA. The ^{140}Nd(III) was selectively eluted with 0.29 M α-HIBA whereas Pr(III) was washed out at the concentration 0.40 M α-HIBA (Fig. 5).

2.4 Investigation of the chemical fate of ^{140}Pr in aqueous solutions

After the final purification on the small cation-exchange chromatography column (Figs. 3, 5), the ^{140}Nd activity was obtained in a small volume of the 0.29–0.30 M α-HIBA eluate. It was diluted with 300 µl of H_2O and taken directly for preparation of the ^{140}Nd-DOTA complex. About 1–3 nmol of DOTA was added to the ^{140}Nd solution and the mixture was heated at ∼ 100 °C for about 30 min. The complex formation yield was controlled by TLC (aluminium sheets silica gel 60; 0.1 M Na_3Citrate eluent). The procedure was repeated (if needed) until the labelling yield was ≃ 90%. This procedure allowed preparation of the ^{140}Nd-DOTA complex without excess of the free ligand DOTA. The separation of ^{140}Nd-DOTA from ≃ 10% of uncomplexed ^{140}Nd(III) was performed on a micro-chromatography column, prepared using 50 mg of Bio-Rad AG 50W-X8 cation exchanger, minus 400 mesh. Reaction mixtures were passed through the column in NH_4^+-form. Free ^{140}Nd(III) was quantitatively adsorbed on the resin while the ^{140}Nd-DOTA complex (1 : 1 stoichiometry without excess of the ligand) was obtained in the eluate. The α-HIBA content in the mixture was negligible.

In order to determine the release of ^{140}Pr(III) from the DOTA complex, ^{140}Nd/^{140}Pr-DOTA (1 : 1 stoichiometry) aqueous solutions with activities of 1–2 MBq ^{140}Nd were passed through the micro-chromatography column at room temperature. The column was additionally washed with 300 µl of water. The procedure could be performed within 10–15 s only. Free stabilized ^{140}Pr(III) was quantitatively adsorbed on the resin, while ^{140}Nd-DOTA passed through the column with the eluate. The accumulation of ^{140}Pr in the eluted ^{140}Nd fraction was studied by HPGe detector γ-ray spectrometry, using the intense 511 keV annihilation peak associated with the positron decay of ^{140}Pr. A series of 25 s measurements were performed until an equilibrium in the ^{140}Nd/^{140}Pr generator system was achieved.

2.5 ^{140}Nd/^{140}Pr radionuclide generator

The ^{140}Nd-DOTATOC complex was prepared in aqueous solution containing 1 to 100 µg of DOTATOC (mainly depending on the specific activity of ^{140}Nd) as described above. With ∼ 95% reaction yield the mixture represented 95% of the ^{140}Nd-DOTATOC complex at 1 : 1 stoichiometry and 5% of free ^{140}Nd(III) without excess of the ligand DOTATOC. For preparation of a ^{140}Nd/^{140}Pr radionuclide generator system, about 2.15 MBq of the ^{140}Nd-DOTATOC was loaded on a C-18 cartridge, Phenomenex Strata-X tubes, 30 mg. ^{140}Nd-DOTATOC was adsorbed quantitatively on the solid phase. The cartridge was washed with 5 ml of 10^{-3} M DTPA, pH 6.2, in order to remove the 5% free ^{140}Nd(III). The cartridge itself became the column of the radionuclide generator system. It could be operated with standard single-use syringes. As eluent system, aqueous solutions of 10^{-7}–10^{-3} M DTPA, 10^{-3}–10^{-1} M citrate and 10^{-3} M NTA (pH ∼ 6.0) were examined. The cartridge was eluted with 1 ml each of these mixtures. The procedure could be performed within about 10 s only. Between successive elutions, the generator was washed with water and kept in pure water.

3. Results and discussion

3.1 ^{140}Nd production

^{140}Nd ($T_{1/2} = 3.37$ d) can be produced by (i) irradiation of ^{141}Pr with protons (^{141}Pr(p,2n)^{140}Nd) or deuterons (^{141}Pr(d,3n)^{140}Nd) and (ii) ^{3}He- or ^{4}He-induced nuclear reactions on ^{140}Ce such as ^{140}Ce(^{3}He,3n)^{140}Nd or ^{140}Ce (^{4}He,4n)^{140}Nd. In both cases elements of natural isotopic composition, *viz.* ^{nat}Ce (0.19% ^{136}Ce; 0.25% ^{138}Ce; 88.5% ^{140}Ce; 11.08% ^{142}Ce) and ^{nat}Pr (100% ^{141}Pr) can be used as target material.

A detailed study of the nuclear reactions ^{nat}Ce(^{3}He,xn)^{140}Nd and ^{141}Pr(p,2n)^{140}Nd was published recently [10]. The yields of ^{140}Nd calculated from the excitation functions were found to be 12 MBq/µA h if cerium is irradiated with ^{3}He particles ($E = 35 \rightarrow 20$ MeV) and 210 MBq/µA h when Pr is irradiated with protons ($E = 30 \rightarrow 15$ MeV).

Table 1. Possible nuclear processes and their products (with $T_{1/2} > 1$ h) in the interactions of 36 MeV ^{3}He-particles with ^{nat}Ce and of 19 MeV protons with ^{141}Pr.

Radionuclide[a]	$T_{1/2}$	Nuclear processes on targets	
		^{nat}Ce	^{141}Pr
^{141}Nd	2.5 h	^{140}Ce(^{3}He,2n) ^{142}Ce(^{3}He,4n)	^{141}Pr(p,n)
^{140}Nd	3.37 d	^{140}Ce(^{3}He,3n) ^{138}Ce(^{3}He,n)	^{141}Pr(p,2n)
^{139m}Nd	5.5 h	^{140}Ce(^{3}He,4n) ^{138}Ce(^{3}He,2n)	
^{139}Pr	4.5 h	^{140}Ce(^{3}He,p3n) ^{138}Ce(^{3}He,pn)	^{141}Pr(p,t)
^{142}Pr	19.1 h	^{140}Ce(^{3}He,p) ^{142}Ce(^{3}He,p2n)	
^{143}Pr	13.6 d	^{142}Ce(^{3}He,pn)	
^{139}Ce	137.6 d	^{138}Ce(^{3}He,2p) ^{140}Ce(^{3}He,α)	^{139}Pr(EC,β^+)
^{141}Ce	32.5 d	^{140}Ce(^{3}He,2p) ^{142}Ce(^{3}He,α)	
^{143}Ce	33.0 h	^{142}Ce(^{3}He,2p)	

a: Decay data takes from the *Table of Radioactive Isotopes* (E. Browne and R. B. Firestone), Wiley, 1986 [11].

The radionuclides, co-produced with ^{140}Nd in the interactions of ^{3}He-particles with ^{nat}Ce and of protons with ^{141}Pr, are listed in Table 1. The corresponding nuclear reactions are also given. Due to the higher energy of the ^{3}He-particles used (36 MeV) and the four stable isotopes in ^{nat}Ce, the number of possible reaction channels is high. In the case of ^{nat}Pr the energy of protons used was only 19 MeV and the target is monoisotopic; the number of possible reactions was therefore low. The radionuclides detected in the cerium target about 40 hours after the end of irradiation are listed in Table 2. Their estimated activities are also given.

The radionuclide ^{140}Nd can be achieved in high radionuclidic purity *via* both routes due to the absence of any long-lived co-produced Nd-isotope. The longest-lived ^{139m}Nd (EC, $T_{1/2} = 5.5$ h) will be present only in negligible amounts at the end of the target processing (1–2 days after EOB). However, for *in vivo* application of ^{140}Nd, the relatively long-lived ^{143}Pr (β^-, $E_{max} = 0.9$ MeV, $T_{1/2} = 13.57$ d) might be a critical contaminant associated with the ^{nat}Ce(^{3}He,xn) route. Thus, a special purification of ^{140}Nd from praseodymium should be taken into consideration, although the basic radiochemical separation strategy aims at the isolation of ^{140}Nd from macro-amounts of cerium.

3.1.1 Chemical separation of n.c.a. ^{140}Nd(III) from macro amounts of Ce(III)

As mentioned in Sect. 2.3.1, ^{140}Nd(III) was effectively eluted from the cation-exchanger in 0.29–0.30 M α-HIBA solution, whereas Ce(III) was obtained in α-HIBA solutions with concentrations above 0.40 M. After these steps about 90% of ^{140}Nd(III) could be obtained with an estimated amount of Ce(III) of ~ 41 μg, thus leading to a reduction by a factor of $\sim 10^4$ (*i.e.* 406 mg $\rightarrow \sim 41$ μg). The separation efficacy of the Nd(III)/Pr(III) pair, on the other hand, was poorer (Fig. 1). Praseodymium was washed out already in the range of the concentration 0.31–0.32 M α-HIBA. Nevertheless, the content of Pr(III) was reduced by a factor of around 20. The second purification step *via* the small chromatographic column yielded additional decontamination factors $> 10^4$ and $\sim 10^2$ for Ce(III) and Pr(III), respectively. An example of the elution profile is shown in Fig. 3.

The present two-step route of purification of ^{140}Nd(III) from macro amounts of Ce(III) provided an overall decontamination factor $> 10^8$, *i.e.* resulting in ≤ 4 ng of cerium remaining. The praseodymium amount was reduced down to 0.05%. The complete radiochemical procedure lasted 1–2 days with an overall yield of ^{140}Nd of about 90%.

Table 2. Radionuclides detected in the ^{nat}Ce target irradiated with 36 MeV ^{3}He-particles.

Radionuclide	$T_{1/2}$	Activity[a] [kBq]	E_γ used for quantification [keV]	I_γ (%)
^{140}Nd	3.37 d	12 500–15 600[b]	1596.5	0.5
^{139m}Nd	5.5 h	400–2100	113.9 738.2 982.2	34.0 30.0 22.4
^{142}Pr	19.1 h	2100–2300	1575.7	3.7
^{139}Ce	137.6 d	33–95	165.8	79.9
^{141}Ce	32.5 d	99–113	145.4	48.4
^{143}Ce	33.0 h	170–180	293.3 722.0	42.0 5.1

a: Measured about 40 hours after the end of irradiation;
b: The uncertainly in the estimated radioactivity is rather high since the intensity of the 1596.5 keV γ-ray used is very low. This γ-ray is emitted by the daughter ^{140}Pr ($T_{1/2} = 3.4$ min) which is in transient equilibrium with the parent ^{140}Nd.

3.1.2 Chemical separation of n.c.a. ^{140}Nd(III) from macro amounts of Pr(III)

After processing the ^{140}Nd(III)/Pr(III) lanthanide pair on the primary chromatography column (Fig. 4) about 85% of ^{140}Nd(III) could be obtained with an estimated amount of 121 μg of Pr(III), *i.e.* reduced by a factor of $\sim 7 \times 10^2$ (85 mg → 121 μg). The estimated decontamination factor of ^{140}Nd(III) from Pr(III) after the final purification step (Fig. 5) was $> 10^3$. The activity of ^{142}Pr detected in the eluate after processing on the small column corresponded only to about 8 μg of the metal. Therefore, the separation n.c.a. ^{140}Nd(III)/macroscopic Pr(III) lanthanide pair is performed by a two-step route. An overall decontamination factor of $> 7 \times 10^5$ could be achieved, *i.e.* ≤ 0.1 μg of praseodymium remained in ^{140}Nd. The complete radiochemical procedure lasted 1–2 days and the overall yield of ^{140}Nd was about 90%.

3.1.3 Comparison of production routes

Radiochemistry

The isolation of ^{140}Nd(III) by means of cation-exchange chromatography from the target lanthanide material is evidently more efficient if CeO_2 is irradiated (decontamination factor $\geq 10^8$). An efficient purification of ^{140}Nd could also be performed from macro amounts of Pr(III), but the decontamination factor of $\geq 7 \times 10^5$ is evidently lower due to the direct neighbouring existence of n.c.a. ^{140}Nd and macroscopic Pr ($\Delta Z = 1$) in the Periodic Table of Elements. For the system n.c.a. ^{140}Nd/macroscopic Ce, the ΔZ value is 2. In both cases the amount of the target material remaining in the separated product was below 1 nmol. The time needed for the two procedures was the same.

Processing of the praseodymium target was performed under optimized conditions. The dissolved target was loaded on to the cation-exchanger directly in NH_4^+-form. This approach avoids erosion of the loading zone and reduces time of processing and volume of radioactive liquid waste.

Radionuclide production yield

As mentioned above, the theoretical yield of ^{140}Nd *via* the ^{141}Pr(p,2n) reaction at 30 MeV is by a factor of about 18 higher than that *via* the ^{nat}Ce(^{3}He,xn) reaction at 33.5 MeV. However, since the proton energy available at the CV 28 was only 19 MeV, the expected yield of ^{140}Nd *via* the (p,2n) reaction over the energy range ($E = 18.6 \rightarrow 16.2$ MeV) was about 30 MBq/μA h [10], *i.e.* by a factor of about 3 higher than *via* the (^{3}He, xn) reaction. The practically achieved ^{140}Nd yields at EOB were about 3.5 MBq/μA h and 15.5 MBq/μA h in the ^{nat}Ce(^{3}He,xn) and ^{141}Pr(p,2n) processes, respectively. Considering the chemical compositions of the target materials and the projectile energies effective in those targets, the practical yield values correspond to about 41% and 60% of the respective theoretical values [10]. The relatively low experimental values are possibly due to the use of wobbled and defocussed beam as well as due to radiation damage. These factors appear to be more pronounced in the case of ^{3}He-particle. In view of the much higher ^{140}Nd overall yield and an efficient isolation possibility, the ^{141}Pr(p,2n)^{140}Nd production route seems to be superior even at 19 MeV compared to the ^{nat}Ce(^{3}He,xn)^{140}Nd route. ^{140}Nd can be produced with high specific activity and chemical/radiochemical purity for preparation of metallo-radiopharmaceuticals.

3.2 Chemical fate of ^{140}Pr in aqueous solutions

The chemical fate of ^{140}Pr in aqueous solutions was studied by separation of the different chemical forms of the parent and the daughter radionuclides. The principle of the ^{140}Pr release is illustrated in Fig. 6. Due to post-effects following the electron capture decay of the parent ^{140}Nd, ^{140}Pr is formed in a different chemical form (*i.e.* not as ^{140}Pr-DOTA species). It is therefore chemically separable from its parent radionuclide.

After absorption of ^{140}Nd-DOTA on the micro-chromatography column, ^{140}Pr is generated from ^{140}Nd. The accumulation of this ^{140}Pr generated in the eluted ^{140}Nd-DOTA fractions was studied.

The occurrence of ^{140}Pr activity $A_{^{140}\mathrm{Pr}}$ in the ^{140}Nd-DOTA eluate may be described as follows:

$$A_{^{140}\mathrm{Pr}} = \zeta + (A_{^{140}\mathrm{Nd}} - \zeta)(1 - \exp(-\lambda_{^{140}\mathrm{Pr}} t)) \qquad (1)$$

where ζ is the breakthrough of ^{140}Pr through the column, $A_{^{140}\mathrm{Nd}}$ the initial activity of ^{140}Nd in the system, $\lambda_{^{140}\mathrm{Pr}}$ the decay constant of ^{140}Pr (3.4×10^{-3} s^{-1}). While the lanthanide

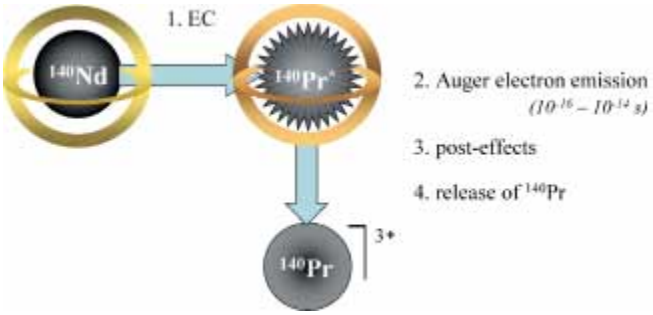

Fig. 6. A simplified scheme of ^{140}Pr release from the initial complex after electron capture decay of the parent^{140}Nd.

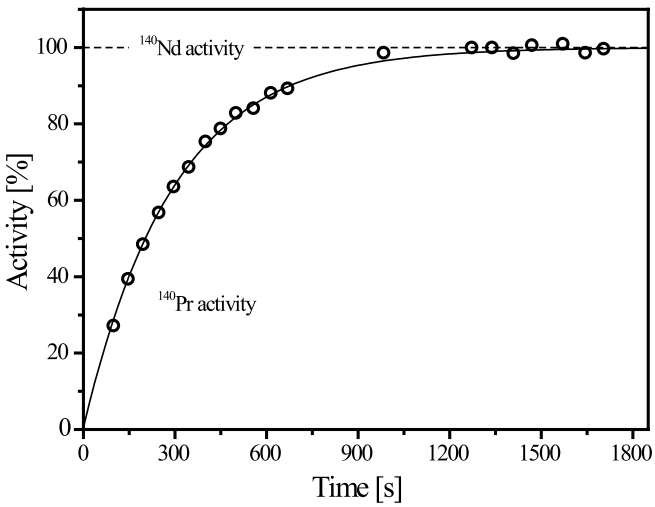

Fig. 7. Accumulation of ^{140}Pr-activity in the ^{140}Nd-DOTA eluate after separation of ^{140}Pr(III) on the micro-chromatography column in aqueous solution. The solid line represents the fitting of the experimental data with Eq. (1).

exchange is inhibited by the kinetic inertness of the ^{140}Nd-DOTA complex, ζ reflects the fraction of the generated radionuclide ^{140}Pr retained in the form of a DOTA complex (first retention). An example of data treatment is presented in Fig. 7. Fitting the experimental data (solid line in Fig. 7) with Eq. (1) leads to $\zeta = 0.2(2)\,\%$, ($R^2 = 0.9981$). The estimated inaccuracy in the experimental performance is 3%–5% and is due to non-instantaneous elution of the micro-chromatography column.

The main result of the study is that in aqueous medium not less than 95% of ^{140}Pr formed after the decay of ^{140}Nd is stabilized in a cationic form, *i.e.* not as ^{140}Pr-DOTA species, and escapes from the DOTA complex.

3.3 ^{140}Nd/^{140}Pr radionuclide generator

Isolating ^{140}Pr from ^{140}Nd-DOTA by means of cation exchange chromatography shows the principle of the hot atom chemistry-based separation strategy. It is, however, not an applicable radionuclide generator design, as the radionuclide generator mother nuclide is mobilised rather than immobilised. Consequently, further research was directed to an approach of chemically stable binding of ^{140}Nd-DOTA on a stationary solid phase with subsequent elution of the ^{140}Pr released in an aqueous phase.

From our experience, DOTA-conjugated peptides (for instance DOTATOC) can be adsorbed on a solid reversed phase from aqueous solutions with a high distribution coefficient, while free lanthanide cations or simple lanthanide complexes can be eluted. A simplified illustration of the generator concept is shown in Fig. 8 (left side). The peptide is bound to the C18 cartridge. Due to the high thermodynamic stability and kinetic inertness of Ln-DOTA type complexes, the release of the longer-lived parent radionuclide ^{140}Nd is inhibited. Post-effects, on the other hand, lead to a release of the shorter-lived daughter radionuclide ^{140}Pr. The generator column (Fig. 8 right side) could be operated with standard single-used syringes. Elution with 1 ml of the eluate could be performed within about 10 seconds only.

3.3.1 Elution yield

After elution of the generator column, *i.e.* the C18 cartridge (Fig. 8, right side), the decay of ^{140}Pr obtained in the eluates was studied. The decrease of ^{140}Pr activity in the eluate may be described as follows:

$$A_{^{140}\mathrm{Pr}} = (\xi A_{\mathrm{act}\,^{140}\mathrm{Nd}}) \exp(-\lambda_{^{140}\mathrm{Pr}} t) \qquad (2)$$

where $A_{\mathrm{act}\,^{140}\mathrm{Nd}}$ is the actual (at elution time) activity of ^{140}Nd, adsorbed on the column and ξ is the fraction of the eluted ^{140}Pr. The ξ-value represents the elution yield of the radionuclide generator. An example of data treatment after elution with 1 ml of 10^{-3} M DTPA is presented in Fig. 9. Fitting of the experimental data (solid line in Fig. 9) with Eq. (2) leads to $\xi = 0.97(7)$ (which is 97.5(7) % elution yield), ($R^2 = 0.9997$). An inaccuracy in the experimental performance is expected to be not more than 3%–5%.

The elution yield of ^{140}Pr in DTPA, citrate and NTA solutions is presented in Fig. 10 as a function of the ligand concentration. Not less than 93% of ^{140}Pr activity could be obtained in 1 ml of 10^{-3} M DTPA eluate. The elution yield decreased with decreasing ligand concentration and

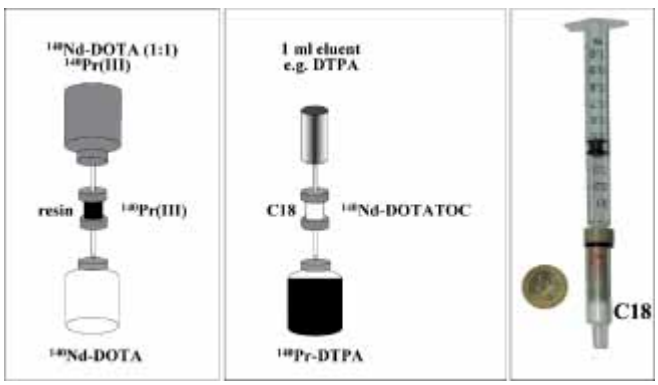

Fig. 8. A simplified illustration of the ^{140}Nd/^{140}Pr radionuclide generator concept (left side); the generator design (right side).

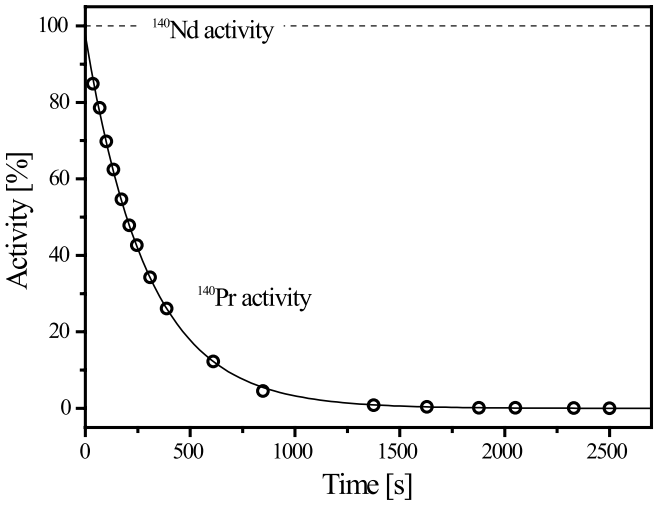

Fig. 9. The decay of ^{140}Pr after an elution of the generator (2 MBq of ^{140}Nd initial activity) with 1 ml of 10^{-3} M DTPA solution. The solid line represents the fitting of the experimental data with Eq. (2).

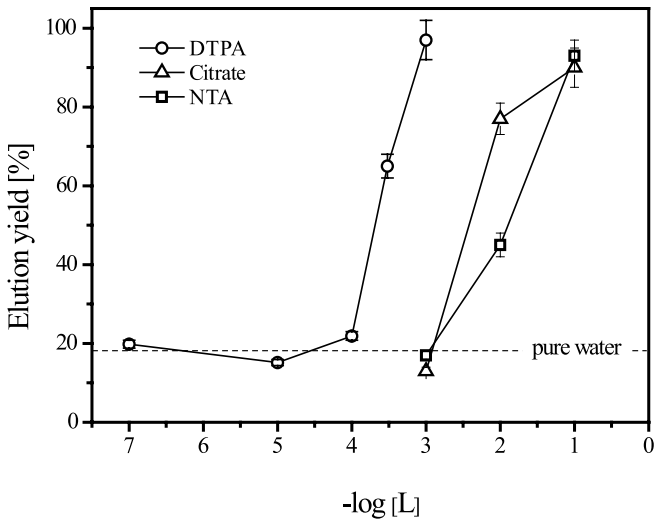

Fig. 10. Elution yield of ^{140}Pr in 1 ml of aqueous solutions of DTPA (circles); citrate (triangles); NTA (squares) as a function of ligand concentration.

was around 20% at a concentration $\leq 10^{-4}$ M DTPA. The elution capacity of citrate and NTA was evidently poorer. About 90% of ^{140}Pr could be eluted only at 0.1 M concentration of citrate and NTA solutions. This obviously is due to lower complex stability of the trivalent Pr(III) lanthanide with citrate and NTA ligands. About 20% of ^{140}Pr(III) could be eluted with 1 ml of pure water.

3.3.2 Breakthrough of ^{140}Nd and radionuclide generator stability

The stability of the system was evaluated for the generator with 2 MBq initial activity. Aqueous solutions of DTPA of 10^{-3} M concentration were used as eluents. The breakthrough of ^{140}Nd in the eluate was measured for at least 10 half-lives of ^{140}Pr after the corresponding radionuclide generator elution. A constant level of ^{140}Pr was observed, as generated by the percentage of co-eluted ^{140}Nd.

In order to evaluate the breakthrough of ^{140}Nd in the form of ^{140}Nd-DOTATOC complex, the generator was eluted at first with 6 ml of 10^{-3} M DTPA solution. It allowed removal of all possible uncomplexed form of ^{140}Nd(III). Immediately there after the column was washed with 1 ml of the eluent. In this eluate ^{140}Nd was observed in an amount of $1.5(5) \times 10^{-3}$% of the actual generator activity. This fraction was referred to as "stable breakthrough" of ^{140}Nd-DOTATOC, following an elution with 1 ml of 10^{-3} M DTPA solution.

The overall breakthrough of the parent radionuclide, however, was found to increase with the increasing time between successive elutions. It is mainly because of radiolytic decomposition of the initial chemical form of the parent radionuclide (^{140}Nd-DOTATOC) and reflects the integral radiation dose adsorbed in the system. The fixed form of the parent radionuclide, if decomposed, provides the free form of ^{140}Nd which will be obtained in the eluate along with the daughter ^{140}Pr. Therefore, in the presented system the radiolytic stability can play a key role and has to be quantitatively estimated.

To link the breakthrough fraction, caused by the radiolytic instability of the system, with the period of time between elutions (and therefore with integral adsorbed dose) a coefficient K_r [h^{-1}] (Fig. 11) was calculated according to:

$$K_r = (A_{br} - A_{act\,^{140}Nd}\,1.5 \times 10^{-5})/A_{act\,^{140}Nd}\,t \qquad (3)$$

where A_{br} is the breakthrough of ^{140}Nd in the eluate, t [h] the period of time passed from the last elution. The value ($A_{act\,^{140}Nd}\,1.5 \times 10^{-5}$) considers the constant fraction of ^{140}Nd washed out in the form of ^{140}Nd-DOTATOC complex. K_r decreased proportionally to the decay of ^{140}Nd (solid line in Fig. 11). It reflects a lower integral radiation dose received from decreasing ^{140}Nd activity in the system.

By normalization of K_r to the actual activity of ^{140}Nd $A_{act\,^{140}Nd}$ [MBq], the coefficient K_r^* [MBq^{-1} h^{-1}] (Fig. 11) could be obtained. K_r^* allows a quantitative evaluation of the radiolytic stability of the system. Thus for different actual activity of ^{140}Nd and time between successive elutions, the breakthrough fraction caused by radiolytic decomposition can be estimated.

The mean K_r^* value (solid line in Fig. 12) was derived to be $4.9(9) \times 10^{-6}$ [MBq^{-1} h^{-1}]. Thus for a system with

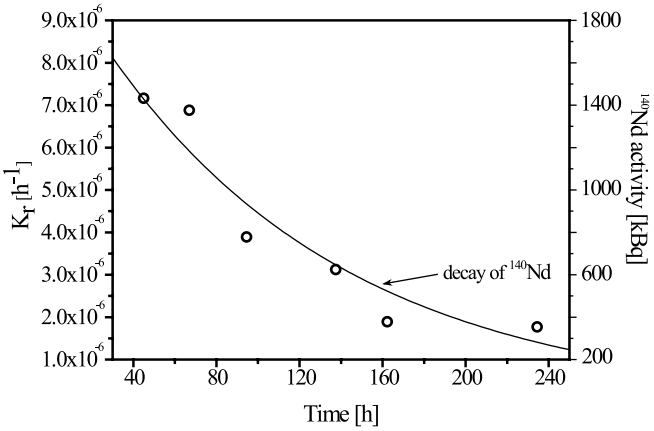

Fig. 11. Coefficient K_r [h^{-1}] (Eq. (3)) as a function of time (observed from the moment of the generator loading); the solid line reflects the decay of ^{140}Nd.

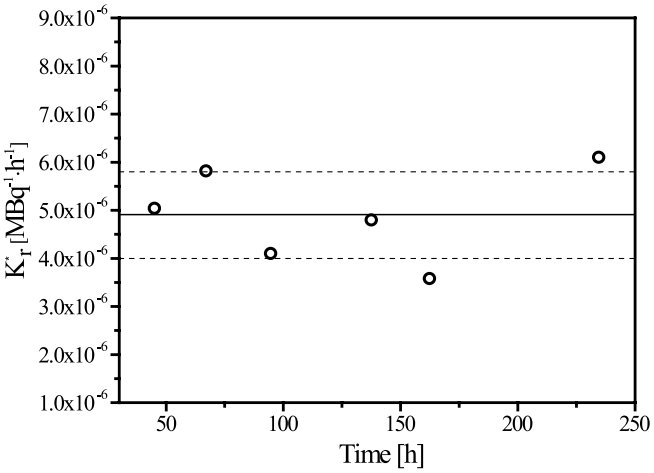

Fig. 12. K_r [h^{-1}] normalized to the actual activity of ^{140}Nd [MBq]; the solid line represents the mean K_r^* value of 4.9×10^{-6} [MBq^{-1} h^{-1}] and the dotted lines give one standard deviation.

an actual ^{140}Nd activity of about 100 MBq and 0.5 h time lapse after the last elution (time enough for accumulation of ^{140}Pr activity), a breakthrough of about 25 kBq of ^{140}Nd ($\sim$ 0.025%) could be expected.

The presented generator design shows high elution yield and high chemical and radiochemical stability. The activity of the generated daughter nuclide allows for *in vivo* PET investigations and can be provided by a safe and simple operation in a clinical environment. The developed radionuclide generator represents the first adequate system, which allows rapid and efficient continuous separation of two neighbouring lanthanides. The system is applicable to ^{140}Nd/^{140}Pr but also for pair such as ^{134}Ce/^{134}La. It combines hot-atom chemistry, in particular post-effects of nuclear transformation, with chemical consequences relevant for lanthanide speciation. Together with the adequate thermodynamic and kinetic stabilities of the macrocyclic chelator DOTA, the concept allows an efficient radiochemical separation.

In the present study, DOTA was selected as the chelate for ^{140}Nd. However, there are other chelates with adequate thermodynamic and kinetic parameters relevant for trivalent lanthanides. In order to design a radiochemical radionuclide generator design, the ^{140}Nd-DOTA complex was adsorbed

on a solid resin *via* an octreotide modification of the DOTA structure, because the octapeptide octreotide strongly binds to reversed phase C18 matrices. Octreoide was selected mainly because of the commercial availability of DOTA-DPhe[1]-octreotide derivatives such as DOTATOC. Other peptides may be used as well for fixing the ^{140}Nd-DOTA moiety to C18 cartridges. Alternatively, the strong adsorption of this ^{140}Nd-DOTA moiety can be arranged by functionalising the DOTA structure in a variety of different ways, providing strong binding on different solid phases. Finally, complex structures may be modified in order to regulate parameters like lipophilicity, for example, allowing liquid/liquid separation systems between organic and aqueous solutions.

Potential directions for ^{140}Nd/^{140}Pr radionuclide generator applications could be PET studies with simple ^{140}Pr complexes, such as ^{140}Pr-DTPA. This complex can be useful as a PET tracer, comparable to several DTPA based Gd complexes as used for MRT or ^{99m}Tc-DTPA in SPECT imaging. Another potentially important application could be as ^{140}Pr-phosphonate complexes for visualisation of skeletal metastases. The radiolanthanide labelled ^{153}Sm-EDTMP (1,2-diaminoethanetetrakis methylenephosphonic acid) for example, has useful pharmacological properties and is used clinically as a radiotherapeutic agent for bone cancer treatment. The phosphonate complexes such as EDTMP are structure analogues to the aminopolycarboxylates (DTPA, NTA), providing also high thermodynamic stability of their complexes. Use of EDTMP as an eluent for the presented ^{140}Nd/^{140}Pr radionuclide generator system could provide further potentially useful ^{140}Pr-complexes for repetitive intravenous injections.

4. Conclusions

The radionuclide ^{140}Nd was produced in quantities between 35 and 200 MBq *via* the nuclear processes ^{nat}Ce(^{3}He, xn) and ^{141}Pr(p, $2n$) at a medium-sized cyclotron. Even at a nominal proton energy of 18.6 MeV the yield *via* the latter process was about four times higher than *via* the former route at 33.5 MeV. Chemical isolation of ^{140}Nd(III) from macro amounts of Ce(III) and Pr(III) could be performed by cation-exchange chromatography (two purification steps only) with overall decontamination factor from the respective target material of $\sim 10^8$ and 7×10^5. ^{140}Nd can be successfully used for preparation of metallo-radiopharmaceuticals with high specific activities.

An efficient ^{140}Nd/^{140}Pr radionuclide generator system has been developed. It combines an aspect of hot atom chemistry, in particular post-effects of nuclear transformation, with chemical consequences relevant to lanthanide speciation. Together with the adequate thermodynamic and kinetic stabilities of the macrocyclic chelator DOTA, the concept allows for an efficient radiochemical separation. The presented generator design shows high elution yield and high chemical and radiochemical stability. The activity of the generated daughter nuclide is enough for *in vivo* PET investigations and it can be provided by safe and simple operation in a clinical environment. The developed radionuclide generator represents the first satisfactory system, for rapid, efficient and continuous separation of two neighbouring lanthanides. The system is applicable to ^{140}Nd/^{140}Pr but also to a pair such as ^{134}Ce/^{134}La.

By virtue of very high elution yield and high chemical and radiochemical stability, the system is able to provide the short-lived positron-emitting radiolanthanide ^{140}Pr for PET investigations. The design resulted in small eluate volumes and could allow safe repetitive injections of, *e.g.*, ^{140}Pr-DTPA.

The potential use of ^{140}Nd/^{140}Pr as an *in vivo* radionuclide generator, however, needs to be studied in more detail. The generation of ^{140}Pr may result in a different chemical form of ^{140}Pr as compared to the initially applied ^{140}Nd-labelled compound. This might disturb imaging qualities. Thus, in contrast to the desired parameters of DOTA ligands, *in vivo* generator systems should utilize chemical forms of ^{140}Nd, which prevent release of ^{140}Pr.

Acknowledgment. The authors would like to acknowledge support *via* the COST D18 action and the Deutsche Forschungsgemeinschaft (grant DFG Ro 985/10-1,2). Acknowledgement is made to the operators of the compact cyclotron CV 28 at Jülich for performing the irradiations and Mr. S. Spellerberg for experimental assistance.

References

1. Rösch, F., Knapp, F. F.: Radionuclide Generators. In: *Handbook of Nuclear Chemistry*. (Vértes, A., Nagy, S., Klencsár, Z., eds.) Kluwer, Amsterdam (2003), vol. 4, p. 81.
2. Rösch, F., Brockmann, J., Lebedev, N. A., Qaim, S. M.: Production and radiochemical separation of the Auger electron emitter ^{140}Nd. Acta Oncol. **39**, 727 (2000).
3. Rösch, F., Forssell-Aronsson, E.: Radiolanthanides in Nuclear Medicine. In: *Metals Ions in Biological Systems*. (Sigel, A., Sigel, H., eds.) New York – Basel (2004), vol. 42, p. 77.
4. Segrè, E., Halford, R. S., Seaborg, G. T.: Chemical separation of nuclear isomers. Phys. Rev. **55**, 321 (1939).
5. Stenström, T., Jung, B.: Rapid chemical separation of isomeric states of lanthanides. Radiochim. Acta **4**, 3 (1965).
6. Mirzadeh, S., Kumar, K., Gansow, O. A.: The chemical fate of ^{212}Bi-DOTA formed by β-decay of ^{212}Pb(DOTA). Radiochim. Acta **60**, 1 (1993).
7. Beyer, G. J., Grosse-Ruyken, H., Khalkin, W. A.: Eine Methode zur Trennung genetisch verknüpfter isobarer und isomerer Nuklidpaare der Seltenen Erden. J. Inorg. Nucl. Chem. **31**, 1865 (1969).
8. Qaim, S. M.: Measurement of (n, p) reaction cross sections at 14.7 MeV using high-pressure liquid chromatography in the region of Rare Earths. Radiochem. Radioanal. Lett. **25**, 335 (1976).
9. Caravan, P., Ellison, J. J., McMurry, T. J. Lauffer, R. B.: Gadolinium chelators as MRI contrast agents: structure, dynamics, and applications. Chem. Rev. **99**, 2293 (1999).
10. Hilgers, K., Shubin, Y. N., Coenen, H. H., Qaim, S. M.: Experimental measurements and nuclear model calculation on the excitation functions of ^{nat}Ce(^{3}He, xn) and ^{141}Pr(p, xn) reactions with special reference to production of the therapeutic radionuclide ^{140}Nd. Radiochim. Acta **93**, 553 (2005).
11. Browne, E., Firestone, R. B.: *Table of Radioactive Isotopes*. (Shirley, V. S., ed.) John Wiley & Sons, New York (1986).